Phil. Trans. R. Soc. Lond. A **316**, 85–189 (1985) [85]
Printed in Great Britain

A RADIOMETRIC DETERMINATION OF THE STEFAN–BOLTZMANN CONSTANT AND THERMODYNAMIC TEMPERATURES BETWEEN −40 °C AND +100 °C

By T. J. QUINN† and J. E. MARTIN
National Physical Laboratory, Teddington, Middlesex TW11 0LW, U.K.

(*Communicated by Alan H. Cook, F.R.S.* – *Received* 11 *October* 1984)

CONTENTS

† Present address: Bureau International des Poids et Mesures, Pavillon de Breteuil, F92310 Sèvres, France.

Vol. 316. A 1536 6 [Published 26 November 1985

The total radiant exitance of a black body at the temperature of the triple point of water, T_{tp} (273.16 K), and at a series of other temperatures in the range from about 233 K (−40 °C) to 373 K (100 °C), has been measured by using a cryogenic radiometer. From the measurements at T_{tp} a value for the Stefan–Boltzmann constant σ has been calculated:

$$\sigma = (5.669\,67 \pm 0.000\,76) \times 10^{-8}\ \mathrm{W\ m^{-2}\ K^{-4}}.$$

This is the first radiometric determination of σ having an uncertainty comparable with that calculated directly from fundamental physical constants. This measured value differs from the calculated one by 13 parts in 10^5, which is less than the combined standard deviations of the measured and calculated values.

From the measurements of exitance at the other temperatures, values of the corresponding thermodynamic temperature T have been calculated by using Stefan's fourth-power law. Since the temperature of the radiating black body was also measured by platinum resistance thermometers calibrated on IPTS-68, values of $(T - T_{68})$ were obtained. These range from about $-(5 \pm 1.6)$ mK at 20 °C to $-(28 \pm 2.5)$ mK at 100 °C and $+(5 \pm 1.5)$ mK at −40 °C. The results confirm to

within a few millikelvins the departure of T_{68} from T above 0 °C already discovered by gas thermometry and show that similar departures, but of opposite sign, exist down to the lowest temperature measured, −40 °C. The uncertainties associated with these new values of T and $(T-T_{68})$ are similar to those of the best gas thermometry.

1. Introduction

(*a*) *Aims of the work*

This is an account of work done at the National Physical Laboratory between 1972 and 1983 on the measurement, by using a cryogenic radiometer, of the total radiative power of a black body at temperatures between −40 °C and +100 °C. The first aim of the work was to determine the Stefan–Boltzmann constant, σ, with an uncertainty of about 1 part in 10^4. The second aim was to make radiometric measurements of thermodynamic temperature, T, in the range 233 K (−40 °C) to about 373 K (100 °C), with an uncertainty of about 1 mK.

The total radiant exitance $M(T)$ of a black body at a temperature T is given by

$$M(T) = 2\pi^5 k^4 T^4/15h^3c^2, \tag{1}$$

which is usually written

$$M(T) = \sigma T^4, \tag{2}$$

where σ is known as the Stefan–Boltzmann constant.

The present recommended value for σ is that calculated from the fundamental physical constants appearing in (1), namely:

the speed of light, $c = 299\,792\,458$ m s^{-1} exactly, which stems from the 1983 definition of the metre;

the Planck constant, $h = 6.626\,078 \times 10^{-34}$ J s, which has an uncertainty of 1 part in 10^6;

the Boltzmann constant, $k = 1.380\,653 \times 10^{-23}$ J K^{-1}, which has an uncertainty of 8.5 parts in 10^6 and which is given by the ratio of the gas constant R to the Avogadro constant N_A, where $R = 8.314\,48$ J K^{-1} mol^{-1} with an uncertainty of 8.4 parts in 10^6 and $N_A = 6.022\,136 \times 10^{23}$ mol^{-1} with an uncertainty of 1.5 parts in 10^6.

The values and uncertainties of the constants h, R and N_A are taken from the 1985 Least Squares Adjustment of the Fundamental Constants (Taylor & Cohen 1985) and lead to the following value for the Stefan–Boltzmann constant:

$$\sigma = 5.670\,42 \times 10^{-8} \text{ W m}^{-2} \text{ K}^{-4} \tag{3}$$

with an uncertainty of 34 parts in 10^6. This uncertainty is given, as are all uncertainties in this paper, at the level of one standard deviation (see also §1 (*e*)). The main contributions to the uncertainty in σ come from that in R and, to a lesser extent, in N_A. The value for R recommended in Taylor & Cohen (1985) is that of Colclough *et al.* (1979), obtained from measurements of the speed of sound in argon at the temperature of the triple point of water. The uncertainty in this determination of R is about one third of that of the previous value, which was based upon measurements of the density of oxygen. There has, therefore, been a substantial reduction in the uncertainty in the value of σ, from 120 to 34 parts in 10^6, due to this new acoustic determination of R.

A radiometric determination of σ having an uncertainty of 100 parts in 10^6, or 0.01 %, is equivalent to a determination of the Boltzmann constant, k, to 25 parts in 10^6. Such an uncertainty is comparable with that obtained by calculating k with the best values of R and

N_A. A radiometric determination of k to 25 parts in 10^6 would, however, provide the first accurate direct value of k not dependent upon the properties of gases.

A direct radiometric determination of σ requires a measurement of the total exitance of a black body at a known thermodynamic temperature. For such a measurement to be independent, the black body can only be at the temperature of the triple point of water, whose thermodynamic value is defined as 273.16 K exactly.

In measuring the total exitance of a black body at the triple point of water, $M(T_{tp})$, it is necessary for purely practical reasons to make the measurements over a small solid angle rather than over a complete hemisphere (2π sr). The geometrical throughput, g, of the system must, therefore, also be measured

$$M(T_{tp}) = M'(T_{tp})/g = \sigma T_{tp}^4, \tag{4}$$

where $M'(T_{tp})$ is the measured quantity. The design of the system permitting an accurate measurement of g, and the details of the measurement procedure itself, provide two of the main topics of this paper.

The second, but by no means subsidiary, aim of the work was to measure thermodynamic temperatures in a range whose lower limit would be set by the decreasing amount of radiant energy available, below 0 °C, and whose upper limit would be the temperature, of about 230 °C, at which the black coating on the black body begins to decompose. In fact, it was found that accurate measurements could be made between about −40 and + 100 °C, the upper limit being set by practical reasons related to the rate at which the liquid helium used boiled off from the cryostat. From (4) we can write, provided that g is independent of temperature,

$$\frac{M(T)}{M(T_{tp})} = \frac{M'(T)}{M'(T_{tp})} = \left(\frac{T}{T_{tp}}\right)^4. \tag{5}$$

Thus values of T may be determined from measurements of ratios of $M'(T)/M'(T_{tp})$.

It will be shown later that there are a number of small temperature-dependent corrections in (4) and (5), which must be evaluated for the determination of both σ and T. From (5) we find that to determine T with an accuracy of 1 mK, it is necessary to measure the ratio $M'(T)/M'(T_{tp})$ with an accuracy of 1 part in 10^5 for $T = 373$ K and 1.7 parts in 10^5 for $T = 233$ K. The design and practical realization of a black-body radiator and a detector that are adequate for such measurements form the other main topics of this paper.

All present values of thermodynamic temperature between *ca.* 20 K (the boiling point of hydrogen (with reference to a pressure of 101 325 Pa, which applies to all boiling points quoted in this paper)) and *ca.* 1337 K (the freezing point of gold) are based upon the results of gas thermometry, largely obtained over the past twenty years. A detailed history of the development of modern thermometry is given in Quinn (1983) but, briefly, the reason why further, independent measurements of T are required is the following. Until 1960, when the kelvin was re-defined as 1/273.16 of the temperature of the triple point of water, all measurements of temperature were based upon the so-called 'fundamental interval' of 100 °C between the freezing and boiling points of water. Interpolation within and extrapolation outside this fundamental interval were made by using gas thermometers calibrated at 0 and 100 °C. Gas thermometers, however, are cumbersome instruments that are difficult to use at high accuracy and, in general, are less reproducible than the best resistance thermometers. This was well appreciated by Callendar (1899) who wrote: 'It is impossible for those who have never worked with a gas thermometer to realize the extent of its short-comings!' In 1927, to meet the growing

needs of science and international trade, the 7th Conférence Générale des Poids et Mesures (CGPM) adopted the International Temperature Scale of 1927 (ITS-27). This was drawn up to allow science and industry to use a common practical temperature scale based upon a set of fixed points whose temperature had been determined by gas thermometry and by using the platinum resistance thermometer (-190 to 660 °C), platinum/rhodium thermocouple (660 to 1063 °C) and optical pyrometer (above 1063 °C) as interpolating instruments. The ITS-27 was succeeded by the International Practical Temperature Scale of 1948. This was modified at the time of the re-definition of the kelvin in 1960 and replaced by the International Practical Temperature Scale of 1968 (IPTS-68), which in turn has been slightly modified in its 1975 Edition. In all of these practical scales, the principles of the ITS-27 have been maintained, namely, that the scale is based upon a set of fixed points of temperature, whose numerical values are chosen to be as close to thermodynamic temperatures as possible at the time the scale is defined, and specified interpolating instruments and methods chosen to give International Practical Temperatures, T_{68}, which are as close as possible to thermodynamic temperatures.

The IPTS-68 was the first International Practical Temperature Scale to be based upon the 1960 definition of the kelvin and was not, therefore, based upon the fundamental interval of 100 °C between the ice and the steam points. One of the consequences of the new definition of the kelvin was that the steam point ceased to have an exact, defined, thermodynamic value of 100 °C, and instead its temperature became subject to experimental determination. Nevertheless, in IPTS-68 the boiling point of water was taken to be exactly 100 °C because at the time the scale was drawn up, the most recent gas thermometry (Preston Thomas & Kirby 1968) had given a value of (100.000 ± 0.005) °C. However, in 1976 the first results of new gas thermometry at the National Bureau of Standards (NBS), Washington, by Guildner & Edsinger (1976) appeared, which showed substantial differences between T_{68} and T in the range of Celsius temperature from 0 to 460 °C. The difference amounted to 25 mK at 100 °C and 80 mK at 460 °C. These differences were about five times the uncertainties that had been assigned to the fixed points of the IPTS-68 in this range and implied serious, unsuspected, errors in earlier gas thermometry. Indeed, Guildner & Edsinger showed quite clearly that significant errors in gas thermometry were inevitable unless (as had not been done in the past) very specific steps were taken to overcome the effects of sorption of condensable gases at the walls of the gas bulb. The implication of these differences is that the gas thermometry of the 1930s was wrong in giving a value of -273.15 °C for the absolute zero of temperature. The correct value, consistent with a fundamental interval of exactly 100 °C, would have been -273.22 °C and this would have led to the adoption of 273.23 K rather than 273.16 K for the thermodynamic temperature of the triple point of water.

The differences between T and T_{68} discovered by Guildner & Edsinger (1976) are such as would require significant changes in numerical values of the International Practical Temperature in the next version of the IPTS, now in preparation. Not the least of these changes would, of course, be that the normal boiling point of water would no longer have a temperature of 100 °C but one closer to 99.97 °C. All of this calls for an independent verification of the results of the new gas thermometry by a method that is not subject to the same sources of error. Hence the need for the present work, one of whose aims is to measure T up to at least 100 °C with an uncertainty equal to that of the gas thermometry of Guildner & Edsinger, namely a few millikelvins.

(*b*) *Outline of the method*

A cut-away drawing of the system is shown in figure 1. The principle of operation is as follows: the black-body radiator at a temperature T between about 233 K (−40 °C) and 373 K (100 °C) irradiates an aperture system at liquid-helium temperatures, which allows a beam of thermal radiation to enter a second black body held initially at a temperature of 2 K. The absorbing black body, which we call the calorimeter, is arranged so that it acts as a heat-flow calorimeter. The radiant power absorbed in the calorimeter leads to a rise in its temperature until the radiant power absorbed is balanced by the heat flow along a poorly conducting heat link to a heat sink maintained at a very stable temperature near 2 K. The temperature rise of the calorimeter, about 3 K for a radiating black-body temperature of 273 K, is monitored by a germanium resistance thermometer attached to the calorimeter. When equilibrium has been reached a shutter at liquid-helium temperature is closed, cutting off radiation from the radiator. At the same time, sufficient electrical power is supplied to a heater on the calorimeter to maintain its temperature. Provided that a number of conditions are met, this electrical power is a very precise measure of the thermal radiative power. In particular, it is necessary to take special precautions to avoid the effects of diffraction and scattering, the whole apparatus must be at a pressure below about 1 μPa (*ca.* 8×10^{-9} Torr) to avoid significant energy transfer by gas molecules and the emissivity of the radiator and absorptivity of the calorimeter must be known.

The main body of measurements was made by using an aperture geometry that allowed about 1.3 mW of radiant power to enter the calorimeter for a radiator temperature of 273 K. The sensitivity and stability of the overall system was such that the relative standard deviation of a single measurement of radiant power was about 1 part in 10^5, i.e. between 7 nW and 45 nW for radiator temperatures between 233 and 373 K. As a check on various sources of uncertainty, a subsidiary set of measurements was made by using a smaller pair of apertures. These allowed only about 200 μW of power to enter the calorimeter with a radiator temperature of 273 K.

For the determination of the Stefan–Boltzmann constant, the radiator was set at a series of temperatures within the range 271–275 K and the radiant power $M'(T)$ was measured at each temperature. Since in this range T_{68} does not differ significantly from T, the temperature T was established from the readings of eight capsule-type platinum resistance thermometers, calibrated on IPTS-68, attached to the radiator. From each measured value of $M'(T)$ a value of $M'(T_{tp})$ was calculated and used, with the measured value of g, to obtain a value for σ.

For the measurement of thermodynamic temperatures, a similar measurement procedure was followed except that it was necessary to determine the ratio $M'(T)/M'(T_{tp})$. With the radiator set to a nominal temperature T_{68}, a series of ten values of $M'(T)$ and the corresponding values of T_{68} were first obtained. The radiator was then cooled to close to 273.16 K for a series of ten values of $M'(T_{tp})$. The average of these values of $M'(T_{tp})$ with each individual value of $M'(T)$ was used to calculate a value for T and by comparison with the corresponding value of T_{68}, the difference $T - T_{68}$ was found. This procedure was repeated at fifteen different temperatures within the range −40 to +100 °C.

(*c*) *Previous thermal-radiation measurements of* σ *and* T

We were strongly influenced in the design of the equipment by two important pieces of work, each in its own way a landmark in metrology. The first was the work of Ginnings & Reilly

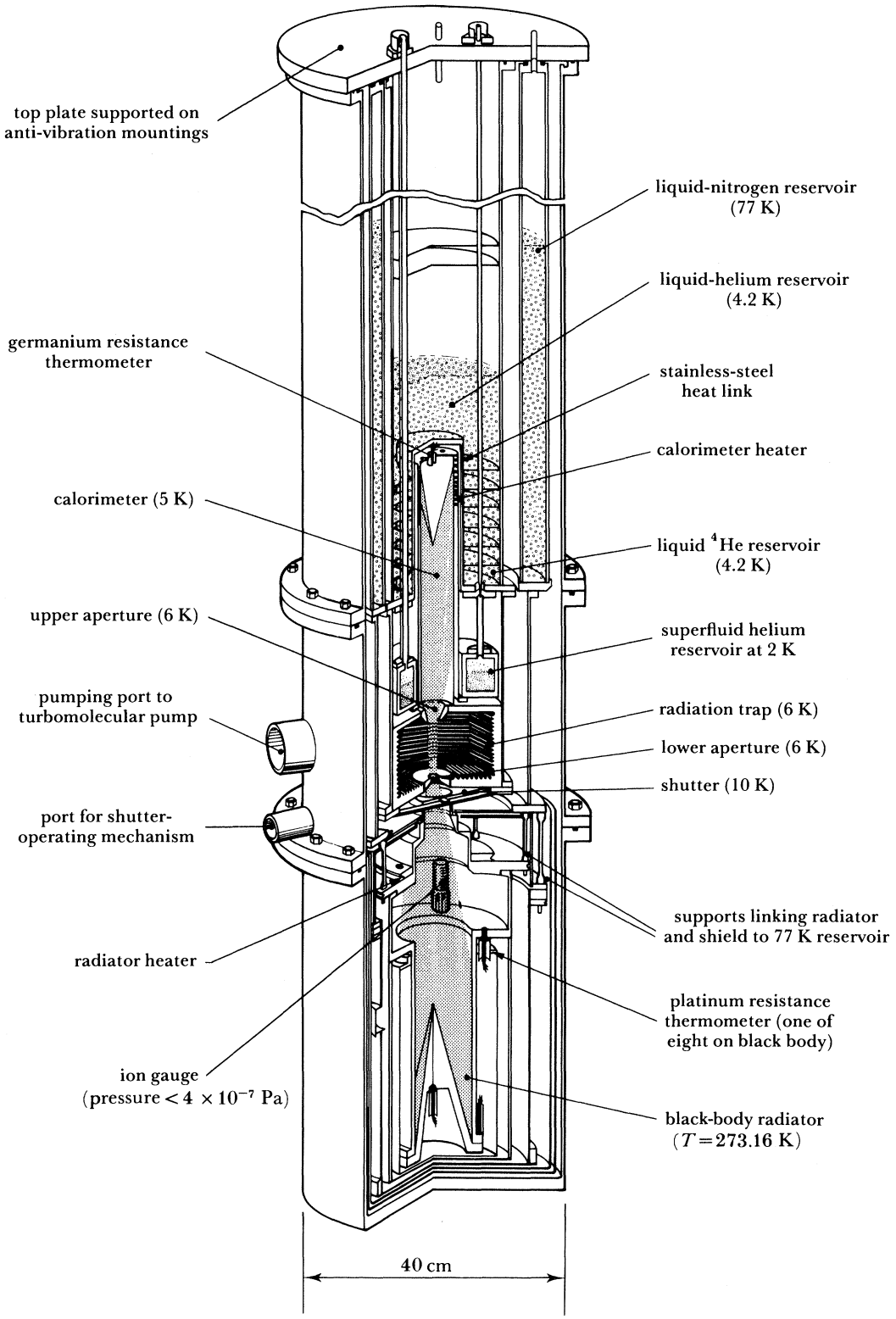

FIGURE 1. Cut-away drawing of the apparatus. The temperatures indicated are typical of those found when the radiator is at a temperature near 273 K.

(1972) who, in the late 1960s, built a cryogenic radiometer at the NBS by using a low-temperature black body as a heat-flow calorimeter in an attempt to measure the thermodynamic temperature of the boiling point of water. Although not succeeding in this aim – largely for reasons related to diffraction and scattering effects – they demonstrated the potential of cryogenic radiometry. Although our design differs in many important respects from theirs, notably in the measures taken to reduce diffraction and scattering, the use of superconducting heater leads, and in the fact that the linear dimensions of the critical components are some five times larger than theirs, the general principle of operation is the same.

The second piece of work that influenced our design was that of Blevin & Brown (1971) who used a room-temperature radiometer and a radiator at the freezing point of gold to determine the Stefan–Boltzmann constant. Not only did they make the first direct measurement to give a value within about 0.1 % of the calculated value, but in so doing they unequivocally showed how diffraction can lead to errors of the order of 1 % and how, in principle, such errors can be avoided (Blevin 1970). Our design in this respect is based upon their work.

There were four main souces of uncertainty in the result of Blevin & Brown (1971) evaluated by them at the 99 % confidence level, each one of which had a magnitude of about $\pm 0.06\,\%$. The major sources of uncertainty were related to the radiator, a black-body cavity held close to the temperature of freezing gold ($T_{68} = 1337.58$ K). The uncertainty in the thermodynamic temperature, taken to be ± 0.2 K, led to an uncertainty in σ of $\pm 0.06\,\%$; the difficulty in measuring the temperature by means of Pt–10 %Rh/Pt (all alloy percentages are quoted by mass) thermocouples led to another $\pm 0.06\,\%$ and various other source-dependent uncertainties amounted to a further $\pm 0.05\,\%$. The other principal sources of uncertainty were diffraction ($\pm 0.06\,\%$) and non-uniformity of response over the detector ($\pm 0.05\,\%$). The overall uncertainty was $\pm 0.13\,\%$. Their value differed from that calculated from fundamental constants by 0.1 %. This difference could be explained by the IPTS-68 value of the gold point being too high by about 0.3 K. Such a conclusion would tend to be supported by recent spectral radiation thermometry in the range 460 °C to the gold point (Coates & Andrews 1982; Jung 1984).

Before the result of Blevin & Brown (1971) there had been many experimental determinations of σ, all of which had resulted in values significantly above that calculated from fundamental constants. The closest was that of Kendall (1968), which was 0.4 % higher and had an uncertainty of $\pm 0.4\,\%$. Before that, the average difference was 1.5 %. Blevin & Brown reviewed all of these measurements and concluded that this previously puzzling systematic difference between the calculated and measured value for σ could be explained by radiometric errors alone and had no more fundamental significance.

(*d*) *Diffraction, scattering and the overall size of the system*

The problem of diffraction and its solution, in principle, as suggested by Blevin & Brown (1971) is illustrated in figure 2. In figure 2*a*, R is a point source of radiation, A_1 is an aperture in a thin screen and C is a detector whose diameter just equals that of the geometrical beam. As a result of diffraction at the edges of A_1, the radiant flux reaching C will be less than that calculated according to geometrical optics. To account for all of the radiant flux passing through A_1, the detector C would have to be of infinite diameter. Alternatively, as illustrated in figure 2*b*, the detector could be concave and arranged so that it subtended a solid angle of 2π sr at A_1. If the direction of rays is now reversed, so that C becomes an extended source

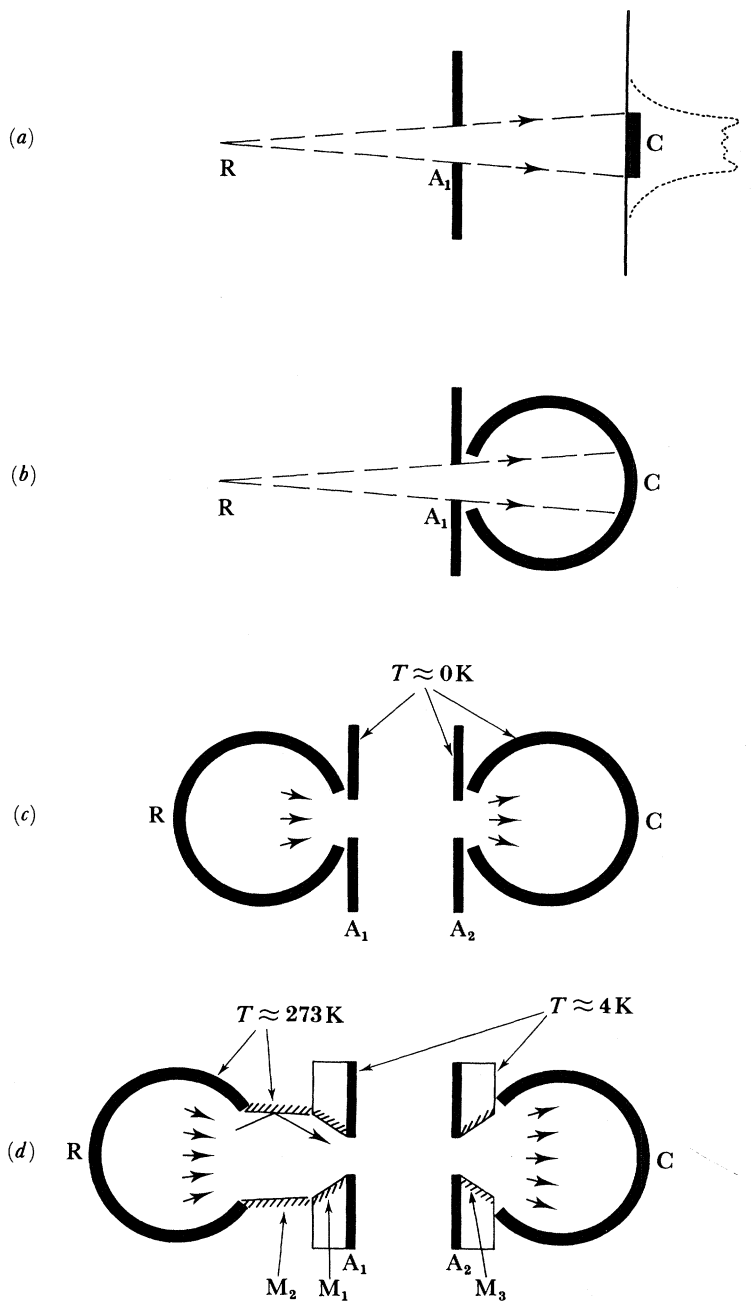

FIGURE 2. Sketch illustrating the argument concerning diffraction losses in an optical system (see text).

of radiation, in figure 2*a* the irradiance at R is less than it would be according to geometrical optics by the same factor as was the radiant flux intercepted by C under the previous conditions. For the irradiance at R to be that predicted by geometrical optics, the source C must subtend a solid angle of 2π sr at A_1, as in figure 2*b*.

Figure 2*c* illustrates an ideal diffraction-free system for the determination of σ. A radiator R subtends 2π sr at an aperture A_1 and a detector C subtends a solid angle of 2π sr at a second aperture A_2. R is a black body at a temperature of 273.16 K; A_1, A_2, and the space between

them are at temperatures close to absolute zero and the detector C is a black body also at low temperatures. Because it is not possible in practice to have a radiator at 273 K in the immediate proximity of an aperture in a thin screen at liquid-helium temperatures, the arrangement of figure 2*d* is used. Between the radiator and the aperture A_1 a mirror system is placed. Part of this mirror system is formed by the conical entrance to the aperture M_1 and hence is at 4.2 K, and the remainder M_2 is attached to the radiator and is at the same temperature as the radiator. Provided that the mirror surfaces are perfect reflectors, the radiant flux leaving A_1 in the direction of A_2 will be identical to that in the ideal system of figure 2*c*. Similarly, a mirror surface M_3, which is the conical exit of aperture A_2, ensures that all of the radiation passing through A_2 reaches the detector C. Diffraction losses occur only to the extent that M_1, M_2 and M_3 are not perfect mirrors and, as we shall see, these losses can be calculated with a sufficient accuracy.

Scattering, that is to say radiant flux passing through A_2 that is not in the direct beam from A_1, occurs if the space between A_1 and A_2 does not behave as a black-body absorber of radiant flux coming from A_1. This also can be calculated and a small correction made. The inner surfaces of A_1 and A_2 must be non-reflecting as well as being close to absolute zero in temperature.

The two factors that were decisive in fixing the overall dimensions of the system have not yet been mentioned. These were: first, the wide spectral range of the thermal radiation emitted by a black body at 273 K, and second the need to measure the cross-sectional area and distance between the apertures to better than 1 part in 10^4. Less than 0.01 % of the total radiant power is outside the wavelength range 3–400 μm, but 0.6 % is in the range beyond 100 μm. It is essential that all the dimensions of the radiating and absorbing black bodies and also those of the apertures be very large compared with the wavelengths of the radiation in question. This calls for aperture diameters to be of the order of centimetres rather than millimetres. In consequence, to obtain good black-body conditions with apertures of this size, the principal dimension of the radiating and absorbing black bodies must be of the order of a metre (in fact about half a metre was found to be sufficient). To be able to measure the diameters of the apertures and the distance between them with an accuracy sufficient to calculate the throughput g to 1 part in 10^4, we considered that a minimum aperture diameter of 1 cm was necessary. We finally chose 1.8 and 2.6 cm for the diameters of the principal pair of apertures and 1.0 and 1.8 cm for the subsidiary pair as being diameters suitable for measurement. The distance between the apertures, 10 cm, was chosen to allow sufficient radiation to pass into the calorimeter, while at the same time keeping the solid angle of the beam small enough to allow an efficient design of radiator and calorimeter. The dimensions of the rest of the apparatus, the capacities of the liquid-nitrogen and liquid-helium reservoirs and the design of the pumping system were all set by these initial decisions on the sizes of the apertures.

(*e*) *The evaluation of uncertainties*

The question of uncertainties is central to the whole of this paper. The results of metrological work such as this have little value unless accompanied by a proper evaluation of the associated uncertainties. A final overall uncertainty should be given, but sufficient information is also required on the origin of each of the contributing uncertainties to allow the reader, and in due course those whose task it is to evaluate the results of metrological work, to make their own evaluation of the overall uncertainty if needed.

In estimating and combining our uncertainties, we have followed the principles endorsed by the Comité International des Poids et Mesures following the recommendations, in 1980,

of a Working Group made up of the representatives of national standards laboratories and international organizations (Giacomo 1981; BIPM Rapport no. 80/3 1980). Briefly, uncertainties are considered under two headings: type A uncertainties, evaluated by applying statistical methods to the results of a series of repeated observations and type B uncertainties, evaluated by other means. Type A uncertainties are calculated at the level of one standard deviation and an attempt is made to estimate type B uncertainties also at the same level (of one standard deviation). To obtain an overall uncertainty, all of the type A and type B uncertainties may be combined in quadrature, but with due account being taken of correlations between individual uncertainties.

In this introductory section we have outlined some of the more important considerations that influenced us in the design of the experiment. In the sections that follow, each of the principal components is dealt with in more detail and the associated uncertainties evaluated. We discuss first the black-body radiator and black-body calorimeter – the detector – and the evaluation of the thermal-radiation transfer function, which takes into account the emissivity of the radiator, absorptivity of the calorimeter and the vignetting effects of the apertures. We then describe the apertures, their construction and measurement, the effects of finite edge thickness and the calculation of g. This leads on to the problem of the radiation trap, i.e. the space between the apertures, which must absorb almost completely the superfluous thermal radiation, about 98% of that passing through the lower aperture. This is followed by the calculation of the residual losses, due to diffraction, from imperfect reflection at the mirror surfaces. We then describe the whole electrical measurement and control system, the vacuum system and the general mechanical and cryogenic arrangements. Finally, we come to the results, the summation of uncertainties and a discussion of the implications of the results, particularly when compared with those from other work.

2. The black-body radiator

(a) *Fundamental considerations*

The black body was designed to provide a beam of thermal radiation having a well characterized spectral distribution that would pass through the pair of apertures and be absorbed by the black-body calorimeter. To achieve our aims, the effective temperature of the black body must be known to within about 1 mK, this in the presence of temperature gradients, which can amount to as much as 20 mK over the length of the black body, and variations in the apparent emissivity over the internal walls of the radiator due to the presence of the aperture. This very strict temperature requirement posed a number of problems. While some of these were of a practical nature, others were more fundamental and concerned the limitations inherent in the Planck and Stefan–Boltzmann formulas when applied to real situations. These will be dealt with first.

The total radiation energy U inside a closed cavity of volume V whose walls are at a given temperature T is generally considered to be given by the Stefan–Boltzmann formula

$$U = 8\pi^5 k^4 V T^4 / 15 c^3 h^3. \tag{6}$$

This results from the integration over all frequencies of the Planck formula

$$U = \frac{8\pi k^4 V T^4}{c^3 h^3} \int_0^\infty \frac{x^3}{e^x - 1}\, dx, \tag{7}$$

where $x = h\nu/kT$.

It has always been recognized that there is a difficulty in the practical application of the Planck and Stefan–Boltzmann formulas stemming from the assumption that all wavelengths of the radiation are infinitesimal compared with the dimensions of the cavity. In a closed cavity whose walls are at a high temperature such that an overwhelming proportion of the radiant energy is at wavelengths that are, indeed, infinitesimal compared with the dimensions, no particular problem arises. At very low temperatures, on the other hand, where the spectral radiant energy is far from negligible at wavelengths of a few millimetres, the predictions of the Stefan–Boltzmann formula for a cavity whose dimensions are of the order of a few centimetres, for example, are unlikely to be correct at the level of 1 part in 10^5. The question for this work was, therefore, the following: how large must a cavity at 233 K be for the Stefan–Boltzmann formula to represent correctly the total radiant energy density to better than 1 part in 10^5? A subsidiary question was how large must the aperture be for the energy passing through to differ by less than 1 part in 10^5 from that incident on the aperture? This second question is quite different from that concerned with the effect of size of aperture on the emissivity of the cavity, which is a purely geometrical one.

The condition that all wavelengths must be small compared with the dimensions of the cavity is only one of a number of restrictions on the Planck and Stefan–Boltzmann formulas, but for this work it is the most important one. Others are related to the shape of the cavity, the radii of curvature of edges, the effects within a few wavelengths' distance from the walls and the losses at the walls themselves. It was shown by Weyl (1913) that the restrictions on shape, namely that the cavity must be a rectangular parallelepiped, cease to apply in the limit of high frequencies. Only in the last fifteen years, however, have detailed calculations been made of the eigenfrequency distribution for finite cavities of particular shapes such as cubes, spheres, hemispheres, cones and cylinders.

The renewed theoretical interest in this area stems from the link between the problem of black-body radiation in finite cavities and similar problems, concerned, for example, with coherent and partially coherent radiation, the density of states and quantum-size effects in the statistical mechanics of finite non-interacting systems, and thermal radiation transfer between closely spaced surfaces at very low temperatures. A general review of these subjects can be found in the monograph by Baltes & Hilf (1976) and, for the particular problem of black-body radiation in finite cavities, in Baltes (1973, 1976) and Case & Chiu (1970).

In the limit of high temperatures and large volumes, for which the product $TV^{\frac{1}{3}}$ tends to infinity, the total radiation is accurately described by the Stefan–Boltzmann formula. At very low temperatures or in small cavities such that $TV^{\frac{1}{3}} \approx 1$ cm K, the Stefan–Boltzmann formula is in error by more than 5 %. In this region the total energy must be found by detailed numerical evaluation of the sum of the eigenfrequencies appropriate to the particular shape of cavity in question. In the intermediate domain, for which $TV^{\frac{1}{3}}$ is large compared with 1 cm K, but does not tend to infinity, the small deviations from the Stefan–Boltzmann formula have been calculated for the most common shapes of cavity. For the simple cylindrical cavity of radius r and length L, measured in centimetres, Baltes (1973) has given

$$U = \sigma T^4 \left[1 - \left(\frac{2r}{L} + 0.85\right)\left(\frac{0.1}{rT}\right)^2 + \left(\frac{2r}{L}\right)\left(\frac{0.1}{rT}\right)^3 \cdots\right]. \tag{8}$$

With the radiator and calorimeter dimensions used in the present work, the correction term for $T = 233$ K does not exceed the equivalent of 0.01 mK and is therefore quite negligible.

However, this relation is for a simple right circular cylinder and we have employed a more complex shape, as may be seen from figure 1. In particular, near the junction between the conical end of the radiator and the cylindrical wall, there is a region where the distance between surfaces becomes very much smaller than elsewhere in the cavity. Calculations have been made (Baltes 1972), however, for a small-angle prism, which indicate that even in this case departures from the Stefan–Boltzmann predictions would arise at the level of a few parts in 10^5 only over a few millimetres distance from the junction. The contribution of this region to the radiant flux from the whole radiator is sufficiently small for errors to be negligible.

Although the corrections to the Stefan–Boltzmann formula for the radiator and the calorimeter are negligible, this is not the case for the radiant power from the radiation trap, which is characterized by a much lower temperature (see figure 1). For 4.2 K radiation the Stefan–Boltzmann formula is in error by about 1 part in 10^5 for a cavity having the dimensions of the radiation trap. Further, the calorimeter, considered as a simple cylinder, would depart from a perfect absorber of 4.2 K radiation by nearly 1 part in 10^4. Fortunately, the level of thermal radiation from the radiation trap is sufficiently small for errors such as this to be negligible as well.

In addition to the effects of finite cavity size on the radiation density in a closed black-body cavity, the effect of the wavelength not being infinitesimal compared with the diameter of the aperture must now be considered. The straightforward case is that in which a plane electromagnetic wave is propagating normal to a plane conducting thin screen in which there is a circular aperture. This has been solved for electromagnetic radiation whose wavelength is large, or comparable with, the diameter of the aperture. The case in which the wavelength is small but not negligible, and in which the radiation approaches the aperture at an angle to the normal, is much more complex. This problem has received considerable attention since the 1950s with the growth of microwave technology and has been reviewed by King & Wu (1959) and more recently by James (1976).

For wavelengths much smaller than the radius, the effective cross-sectional area A of a circular aperture of radius R for electromagnetic radiation of wavenumber $k(=2\pi/\lambda)$ incident normally is given to a good approximation, for values of $kR \geqslant 1$, by Keller (1957) as

$$\frac{A}{\pi R^2} = 1 - \frac{1}{(kR)^{\frac{3}{2}}} \frac{2}{\sqrt{\pi}} \sin(2kR - \tfrac{1}{4}\pi). \tag{9}$$

This is an oscillatory function about unity, of amplitude of order $1/(kR)^{\frac{3}{2}}$, except for $1 \leqslant kR \leqslant 2$, for which A tends to zero. For the aperture diameters used here, the convolution of the correction term and the Planck function leads to net corrections in calculating T in the range 233–373 K of less than 1 part in 10^6 and is therefore negligible. For the 4.2 K radiation from the radiation trap, the effect is much larger. Nevertheless, because the overall correction due to radiation from this source is small, the net effect on the measured value of σ is insignificant.

To sum up this introductory discussion on the black-body radiator, we conclude that, at the level of 1 part in 10^5, the Stefan–Boltzmann formula should be adequate to describe the density of thermal radiation inside the radiator. The same conclusion is reached in respect of the absorptance of the calorimeter for this radiation. In addition, the diameters of the apertures are sufficiently large for their cross-sectional areas to be given simply by πR^2.

(*b*) *The black paint*

We come now to the more usual questions concerning black-bodies, namely the emittance of the walls and the effects of the presence of the aperture and of temperature gradients. The first of these to be discussed is the emittance of the walls, since this is the principal factor that influences the performance of the cavity. The inner walls of the radiator, radiation trap and calorimeter are coated with 3M Nextel black paint (proprietory product available in two grades (3M-C 401 and 3M-C 101) made by Minnesota Mining and Manufacturing Company, Minneapolis, U.S.A.). Many of the optical properties of this black are now well known, as are its thermal and outgassing behaviour. This paint was chosen because it has a high emittance over a wide wavelength range, it can be treated to have a low residual outgassing rate at temperatures up to and above 100 °C, it is straightforward to apply and is thermally stable up to a temperature of 230 °C.

The dried 3M paint is made from a mixture of silica spheres (80 % by mass) having a range of diameters from 5 to 100 μm, carbon black (about 20 % by mass) and a small amount of binder. The structure of the paint may be seen in figure 21, which shows the edges of the apertures viewed under a scanning electron microscope. The 3M-C 401 grade was used for the radiator and the 3M-C 101 grade for the calorimeter, radiation trap and apertures.

The optical properties of 3M black are summarized in figures 3–6. Figure 3 shows the total hemispherical emittance as a function of temperature (Hawks & Cottingham 1970; Westcott 1968). Figure 4 shows the normal spectral reflectance, both diffuse and specular, in the wavelength range from 2 to 400 μm (Stierwalt 1966, 1979; Compton *et al.* 1974; Pompea *et al.* 1983; Smith 1984); the peaks in the reflectance at about 9 and 20 μm are due to the well known reststrahlen bands in silica (Heaney *et al.* 1983; Shitzer & Kleinman 1961). Figure 5 shows the reflectance at high angles of incidence at wavelengths in the visible region, at 28, 118 and 337 μm (Hsia & Richmond 1976; Compton *et al.* 1974), and figure 6 shows the reflectance as a function of angle of incidence for angles greater than 60°. Data from figures 3, 4 and 6 will be used later in calculating the radiating and absorbing properties of the radiator

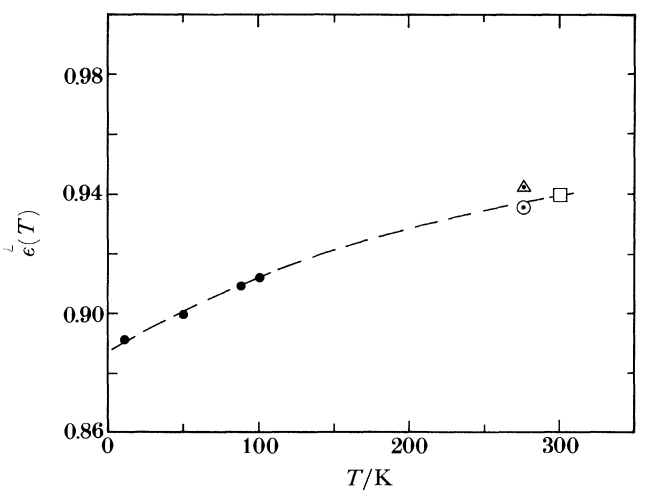

FIGURE 3. The total hemispherical emittance of 3M Nextel paint: ●, direct measurements by Hawks & Cottingham (1970); □, direct measurement by Westcott (1968); △, calculated by using the reflectance data of figure 4 for paint temperatures of 77 K and below; and ⊙, for paint temperature of 373 K.

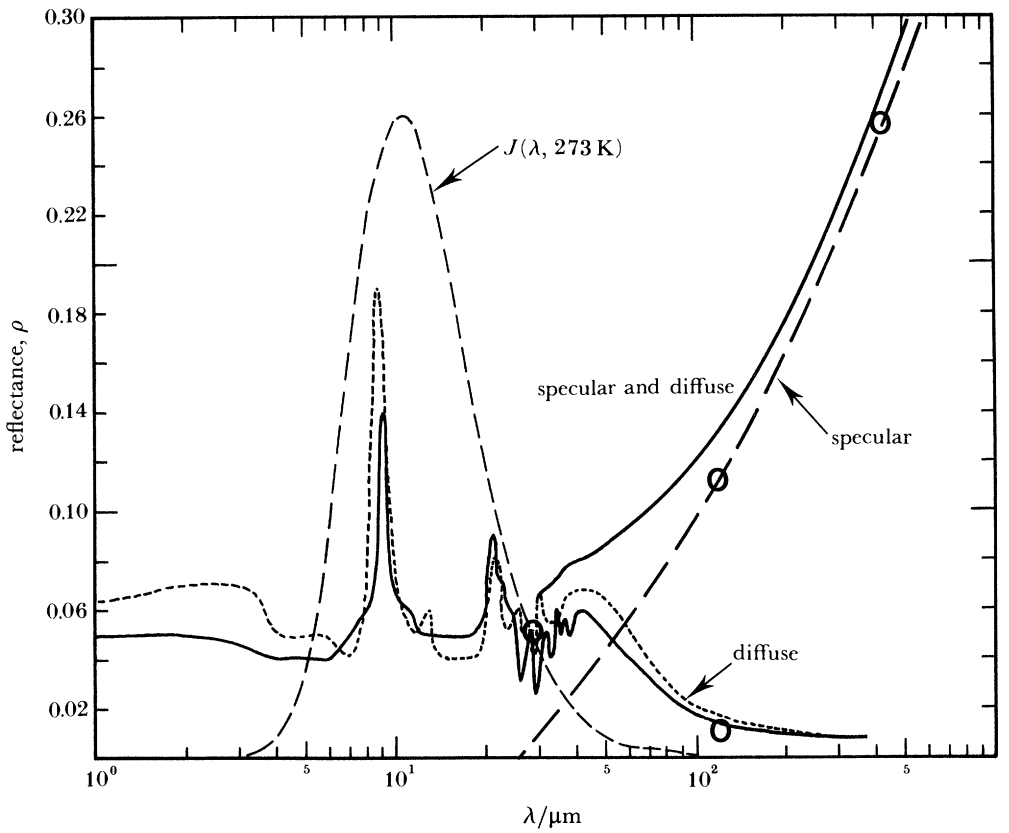

FIGURE 4. The normal spectral reflectance of 3M black: ——, for a paint temperature between 4 K and 77 K, and – – –, 373 K (Stierwalt 1966, 1979); O, diffuse and specular reflectance at room temperature (Compton *et al.* 1974); $J(\lambda, 273\ \mathrm{K})$ is the Planck function for 273 K radiation.

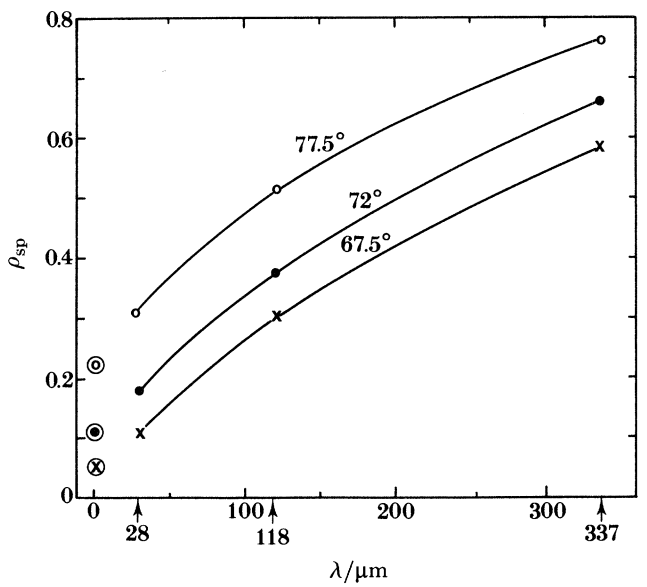

FIGURE 5. The specular reflectance, ρ_{sp}, of 3M black at three angles of incidence: ⊗, ⊙ and ◎ from Hsia & Richmond (1976); ×, ● and ○ from Compton *et al.* (1974).

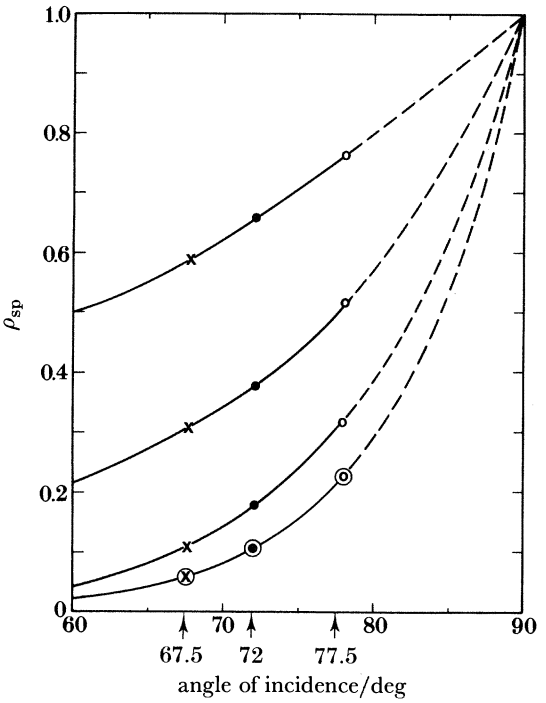

FIGURE 6. The specular reflectance, ρ_{sp}, of 3M black as a function of angle of incidence for four wavelengths, deduced from figure 5 and the data of Hsia & Richmond (1976).

and calorimeter. Figure 5, upon which figure 6 is based, shows that the measurements by Hsia & Richmond (1976) of reflectance as a function of angle of incidence at visible wavelengths are consistent with those of Compton *et al.* (1974) at 28, 118 and 337 μm. In figure 3, the total hemispherical emittance measurement by Westcott (1968) is in good agreement with the two values we have calculated from the data shown in figure 4.

Overall, these figures show that measurements made of the optical properties of 3M black give a consistent picture of its behaviour. The measurements by Compton *et al.* (1974) were made on two different types of the 3M black: type 401, which has an epoxy resin binder, and type 101, which has a hydrocarbon binder and which was available either in aerosol cans or undiluted for pressure-fed spray guns. Little difference was observed between the optical properties of the two versions, although there was some evidence that type 101 is a slightly better diffuse reflector than type 401.

An important optical property, which has so far not been mentioned, is the retroreflectance of 3M black. This is the fraction of the incident radiant flux that is reflected directly back along the direction of incidence, over and above the fraction predicted by lambertian reflection and irrespective of the orientation of the surface with respect to the incident flux. There have been many hypotheses, reviewed by Trowbridge (1978), proposed to explain retroreflection but it occurs on such a wide range of surfaces and surface shapes that no single mechanism provides a satisfactory explanation. For 3M black we would expect retroreflection to occur to some extent since this material is composed of spherical semitransparent particles embedded in a scattering matrix. The measurements of Hsia & Richmond (1976), however, showed no evidence of retroreflection at visible wavelengths. Measurements made by Zalewski (personal communication 1979) of the reflectance of a model of our calorimeter showed, however, a residual

reflectance in the deeper regions that was a little higher than calculations based upon diffuse reflectance predict. This we have interpreted as indicating a small amount of retroreflection, below the level detectable by the method used by Hsia & Richmond. That the retroreflection observed in 3M black is small at visible wavelengths is probably due to the presence of the relatively thick coating of carbon black on the surface of the spherical particles. On this hypothesis a somewhat larger retroreflection might be expected at very long wavelengths, since the absorption of amorphous carbon black falls off approximately as λ^{-1} in the infrared (Koike *et al.* 1980).

The calculation of the emittance of the radiator requires a value for the overall reflectance of the paint $\rho(T)$ for thermal radiation of a temperature T. This is given by the relation

$$\rho(T) = \int_{\lambda_1}^{\lambda_2} \rho(\lambda)\, J(\lambda, T)\, \mathrm{d}\lambda \Big/ \int_{\lambda_1}^{\lambda_2} J(\lambda, T)\, \mathrm{d}\lambda, \tag{10}$$

where $\rho(\lambda)$ is the spectral reflectance of the paint and $J(\lambda, T)$ is the Planck distribution for thermal radiation of temperature T.

By using the data presented in figure 4, $\rho(T)$ has been evaluated numerically from (10). The results are given in table 1. Our estimate of the uncertainty in $\rho(T)$, made on the basis of the overall consistency among the considerable number of independent measurements, is $\pm 10\,\%$ of its value. The reflectance does not appear to change significantly between 4.2 and 77 K (Stierwalt 1979).

TABLE 1. VALUES OF NET REFLECTANCE

paint temperature (kelvin)	radiation temperature (kelvin)	net reflectance, $\rho(T)$
373	273	0.064 ± 0.006
373	373	0.066 ± 0.006
$4.2 \rightarrow 77$	273	0.057 ± 0.006
$4.2 \rightarrow 77$	373	0.057 ± 0.006

The contribution of the long-wavelength specular reflectance is very small since it only becomes significant at wavelengths beyond about 80 μm, where less than 1 % of the total energy is to be found. It is easy to ensure that the designs of the radiator, calorimeter and radiation trap are such as to reduce to insignificant levels the effects of long-wavelength specular reflection. Specular reflection at short wavelengths, which becomes significant at higher angles of incidence, cannot be ignored, however, and plays an important role in the emission of radiation from the radiator.

(*c*) *Temperature control and temperature measurement*

The radiator, which is shown in detail in figure 7, was designed so that adequate uniformity of temperature could be obtained by controlling the temperature at just one location. Heat losses other than those through the aperture were reduced to very low levels by radiation screening, and the walls of the radiator were made of 5 mm thick copper to reduce gradients. The mass of the radiator is 40 kg. Such a design, of course, results in a radiator having a long thermal time constant. The radiator is suspended from the lower flange of the liquid nitrogen reservoir by six stainless-steel wires. These serve both as mechanical supports and heat links to the nitrogen reservoir. Temperature control is achieved by means of a ring heater located

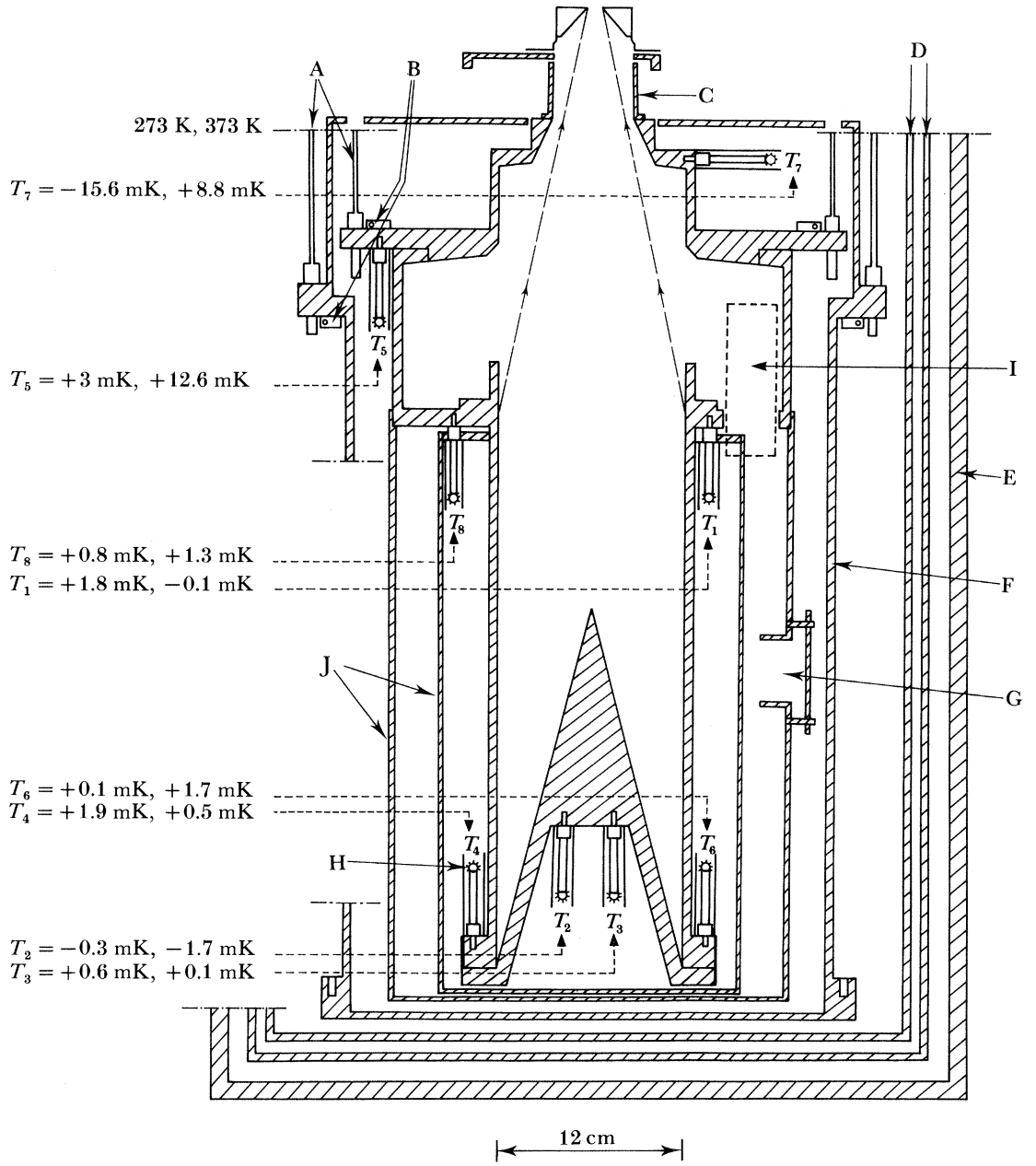

FIGURE 7. Details of the radiator, showing the positions of the eight platinum resistance thermometers measuring temperatures $T_1 \rightarrow T_8$. Examples of measured temperatures are shown for $T \approx 273$ and 373 K. A, stainless-steel supports attached to liquid-nitrogen reservoir; B, ring heaters; C, gold-plated cylindrical mirror (M_2 of figure 2*d*); D, floating radiation shields; E, outer stainless-steel case; F, temperature-controlled shield; G, pumping port; H, thermometer radiation screen; I, ion gauge; J, radiation shields.

just alongside the anchoring points of the stainless-steel wires. The radiator is shielded from room-temperature radiation and from the cold upper parts of the system by two floating shields, a temperature-controlled shield and two shields attached to the lower cylindrical part of the radiator. The temperature-controlled shield is independently suspended by stainless-steel wires from the 77 K reservoir and has its own ring heater for temperature control and two other

heaters to maintain temperature uniformity. In addition to these rigid shields, which have baffled pumping ports to improve the overall pumping rate of the system, the top of the radiator is wrapped with aluminized mylar film. The upper part of the radiator is enlarged to provide space, outside the direct beam, for the ion gauge.

The radiator was made in three principal parts: the cone, the cylindrical body, and the top, as shown in figure 7. The individual parts were painted internally before assembly with the 3M black and the whole was baked at 200 °C for 10 h in a vacuum furnace. The parts were bolted together with 5 mm copper bolts, which were tightened to a torque of 19 N m: to obtain as good a thermal contact as possible between the various parts of the radiator. The gold-plated cylindrical mirror bolted to the top of the radiator forms part of the mirror system designed to reduce diffraction losses (M_2 of figure 2*d*).

The effective temperature of the radiator is calculated by using measurements made with eight platinum resistance thermometers bolted to the radiator. Specially designed capsule-type thermometers were made for us by H. Tinsley & Co. Ltd. Each thermometer (see figure 8) has a threaded silver block brazed to the platinum sheath during manufacture. In this way the thermometer can be screwed directly into threaded holes in the radiator, which ensures good metal-to-metal contact while allowing them to be easily removed for calibration. It was necessary to enclose each thermometer in radiation screens, made from multilayers of aluminized mylar film, to ensure that the thermometer temperature was that of the radiator, and not affected by radiation of a slightly different temperature from an adjacent radiation screen. At room temperatures and above, the thermal anchoring of the leads of a capsule-type platinum resistance thermometer is very much less critical than at low temperatures. Nevertheless, the leads of each thermometer were anchored to the controlled shield. The thermometers were filled with dry air to a pressure of 50 kPa at room temperature.

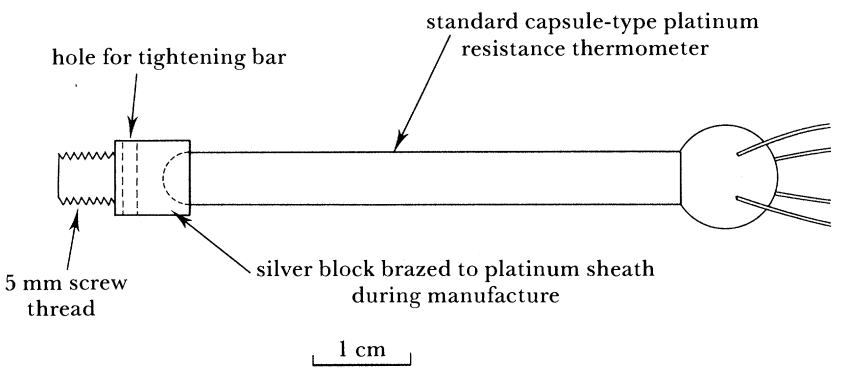

FIGURE 8. The capsule-type platinum resistance thermometer, eight of which were made for us by H. Tinsley & Co. for the measurement of the radiator temperature.

The thermometers were each calibrated on IPTS-68. A complete calibration, at the triple point of water and at the steam and tin points was made in 1975 and again at the end of the work in 1983 when a calibration at the boiling point of oxygen was also made. The values of α and δ deduced from these calibrations together with the consequent changes in T_{68} at 50 °C are shown in table 2. During use the thermometers were, from time to time, unscrewed from the radiator and measured in a triple-point-of-water cell brought to the cryostat. This was done so that the values of R_0, and their drift with time, could be determined by using the proper

leads of each thermometer running up through the cryostat to the resistance-measuring bridge. The values of R_0 measured *in situ* over the six year period from 1978 to 1984 are shown in figure 9. In the critical period during which measurements of thermodynamic temperature were being made from 1980 to 1983, the average change in R_0 was equivalent to 0.5 mK. The average standard deviation of the measured values of R_0 for each thermometer about a straight line was very much smaller, only 0.2 mK. The data of table 2, taken together with the almost linear changes observed in R_0 and in the values of the reference resistors during the period of measurement, have led us to conclude that the uncertainty in the T_{68} calibration of the thermometers, taken as a group, is ± 0.3 mK.

TABLE 2. CALIBRATIONS OF PLATINUM RESISTANCE THERMOMETERS

thermometer[a]	year	$10^3\,\alpha/°C^{-1}$	$\Delta T_{50}(\alpha)$[b]/mK	δ/°C	$\Delta T_{50}(\delta)$[b]/mK
223659 (T_8)	1975	3.9266629	+0.7	1.49749	−0.3
	1983	3.9266085		1.49624	
213868 (T_7)	1975	3.9268918	+0.4	1.49672	−0.3
	1983	3.9268603		1.495685	
221421 (T_1)	1975	3.9264626	−0.5	1.496526	+0.1
	1983	3.9265027		1.496779	
226234 (T_4)	1975	3.9264966	−0.1	1.496326	−0.1
	1983	3.9265068		1.495985	
226232 (T_5)	1975	3.9264142	−0.4	1.496349	+0.1
	1983	3.9264482		1.49668	
226237 (T_6)	1975	3.9266096	−0.1	1.496476	−0.1
	1983	3.9266161		1.49617	
226236 (T_3)	1975	3.9263736	+0.3	1.49703	−0.2
	1983	3.9263487		1.49633	
226233 (T_2)	1975	3.9264552	0.0	1.49683	−0.1
	1983	3.9264556		1.49659	

[a] The identifying number of each thermometer is followed in parentheses by its numbered position in the radiator (see figure 7).

[b] The change in temperature at 50 °C due to the change in α and δ between 1975 and 1983.

The disposition of the platinum resistance thermometers is shown in figure 7. The temperature differences indicated in the figure are typical of those observed for radiator temperatures near 273 and 373 K. The heating effect was measured periodically for each thermometer and the appropriate correction made to reduce the readings to zero current. The heating effect increased from an average, over all of the thermometers, of 4.8 mK at 0 °C to 5.4 mK at 100 °C. The resistance of the thermometer was measured with an a.c. bridge made at NPL and operating at 425 Hz with a Wilkins-type reference resistance calibrated by the NPL Electrical Science Division in November 1979 and 1980 and December 1982. The temperature coefficient of the standard resistance was small but not negligible (1 part in 10^6 per kelvin) and the necessary correction was applied.

A knowledge of the temperature distribution and drift rate in the radiator is important in three respects: first, we must be able to define an effective temperature for the radiation reaching the calorimeter; second, the temperature of the upper parts of the radiator, not directly visible from the calorimeter, must be sufficiently close to that of the lower parts not to affect the radiation reaching the calorimeter; and third, the overall drift rate must be small enough for accurate temperature measurements to be possible by using the platinum resistance thermometers. By careful control of the heaters on the radiator and temperature-controlled

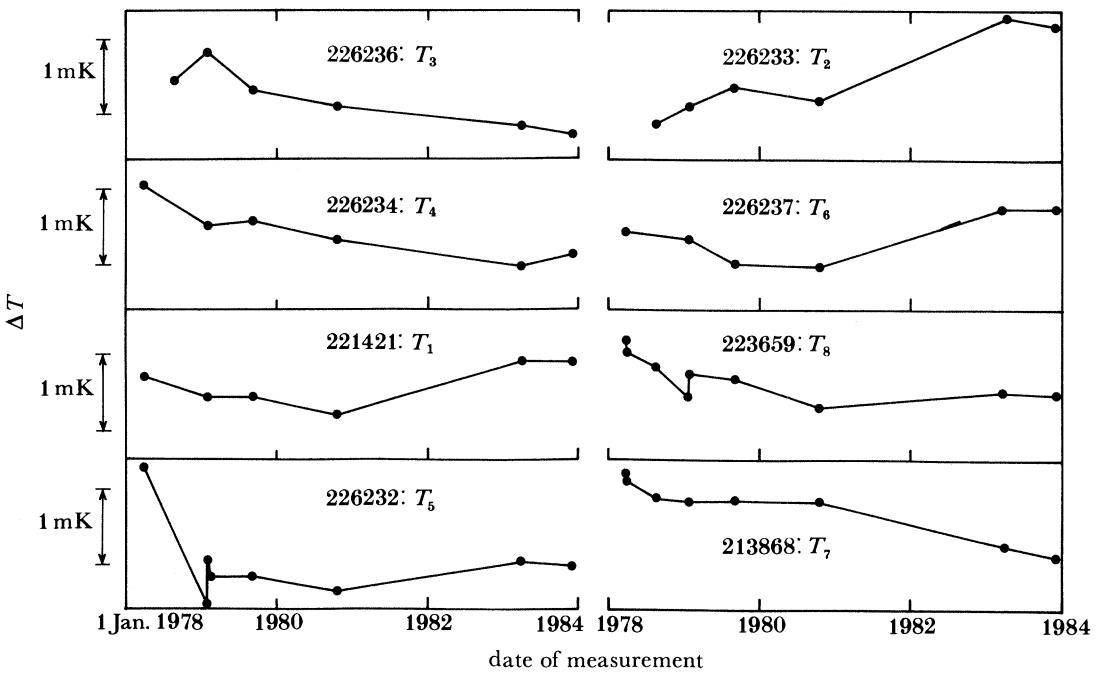

FIGURE 9. The changes in temperature, ΔT, at 273 K equivalent to the changes in R_0 observed during the course of the work for each of the eight platinum resistance thermometers attached to the radiator.

shield, it was possible to obtain drift rates during runs which were generally less than 0.3 mK min^{-1} but which occasionally rose to 0.6 mK min^{-1}. At these drift rates no correction needs to be applied for the response time of the thermometers.

The principal heat loss from the lower parts of the radiator takes place through the aperture into the cold radiation trap. The large thermal mass of the cone and its relatively poor thermal contact with the rest of the radiator result in the temperature of the cone always lagging behind that of the lower flange of the cylinder.

To calculate the effective temperature of the radiator it is necessary to know the temperature distribution over all of those parts of the radiator visible from the calorimeter, namely the lower cylindrical part and the cone. With such low drift rates, the temperature differences along the cylinder, from one end to the other, and in the cone were small. Those along the cylinder were in the range zero to about 28 mK, depending upon the temperature and sign and magnitude of the drift rate. Those in the cone were very much smaller due to the much larger cross section of the cone. The temperature of the cone was measured about halfway along its length and calculations indicate that the effect of ignoring temperature gradients in the cone would lead to errors not exceeding 0.3 mK in the worst case. It is not possible, however, to ignore the temperature gradients in the cylinder. Although the simple assumption of a linear gradient between the top and bottom of the cylinder is unlikely to lead to significant error, a better estimate has been obtained by taking into account the probable heat flow in the cylinder. It was observed that over the period of measurement, some two hours, both the temperature distribution over the cylinder and cone and the drift rate of the whole assembly remained practically constant. Under these conditions the heat flow down the cylinder is constant and is equal to the sum of the heat loss by the radiator and that required to raise the temperature

of the radiator assembly. In Appendix A we derive the following equation, which describes this situation:

$$T(x,t) = T_1(t) - \tfrac{1}{2}N(M^{-1}-x^{-1}) - \tfrac{1}{2}J(M^2-x^2) - J(c+L)\,(x-M), \tag{11}$$

where $c = 36$ cm, $L = 60$ cm and $M = 23$ cm, $T_1(t)$ is the slowly drifting temperature of the top of the cylindrical part of the radiator and $T(x,t)$ is the slowly drifting temperature of an element of the cylinder a distance x from the aperture. Also, from Appendix A,

$$J = \rho s \kappa^{-1}\,\partial T/\partial t \tag{12}$$

and

$$N = \epsilon H R_0^2\,\sigma T^4/\kappa\,\Delta H, \tag{13}$$

in which ρ, s and κ are respectively the density, heat capacity and thermal conductivity of copper, H is the radius of the cylinder (6 cm), R_0 the effective radius of the lower aperture derived in Appendix A, ΔH the wall thickness of the cylinder (0.5 cm) and ϵ the emittance of the surface.

A good test of the validity of (11) can be made by calculating $T(x,t)$ for $x = 60$, since this is also a measured temperature T_6 (see figure 7) and we assume that if (11) predicts the correct value for $x = 60$ it will do so for other values of x along the cylindrical part of the radiator. In addition, if the model upon which (11) is based is a good one, the differences between the measured and calculated values of T_6 should be small over the whole range of conditions observed. Figure 10 shows that this is indeed the case. For temperature differences between one end of the cylinder and the other from $+8$ to -28 mK and drift rates from $+0.5$ to -0.4 mK min^{-1} and at temperatures over the whole range of those encountered, the standard deviation of the difference between measured and calculated values of T_6 is, for the large aperture pair, only 1.3 mK. We found that equally good agreement could be obtained for the small-aperture pair after the calculated value of N had been increased by 6%, an adjustment that we do not consider significant. The values of N and J adopted were as follows:

$$J = 0.82\,\partial T/\partial t \text{ s cm}^{-2},$$

$$N = 9.5\times10^{-11}\ T^4 \text{ cm K}^{-3} \text{ for the large-aperture pair,}$$

$$N = 5.3\times10^{-11}\ T^4 \text{ cm K}^{-3} \text{ for the small-aperture pair.}$$

The final values of $T(x)$ for each value of x were obtained by first calculating $T(x = 60)$ and hence deducing the difference between T_6 (measured) and T_6 (calculated) and then adding this small difference proportionally to the calculated values of $T(x)$.

It now remains only to examine the possibility of a significant gradient existing through the paint before the discussion of the thermal behaviour of the radiator is brought to a close. The room-temperature thermal conductivity of the dried paint given by the manufacturer is 0.29 W m^{-1} K^{-1}. This figure is consistent with that estimated from the work of Garrett & Rosenberg (1974), who measured the thermal conductivity, from 2 to 300 K, of a wide range of composite materials made up of an epoxy-resin binder with various volume concentrations of spheres and powders of glass and quartz. At room temperature the conductivity depends mostly upon the volume concentration of the spheres, whereas at liquid-helium temperature Garrett & Rosenberg found a significant size effect. The smaller the diameter of the spheres, particularly below 6 μm, the lower was the overall conductivity. From our electron microscope photographs of the 3M paint we estimate a mean sphere diameter of between 10 and 20 μm.

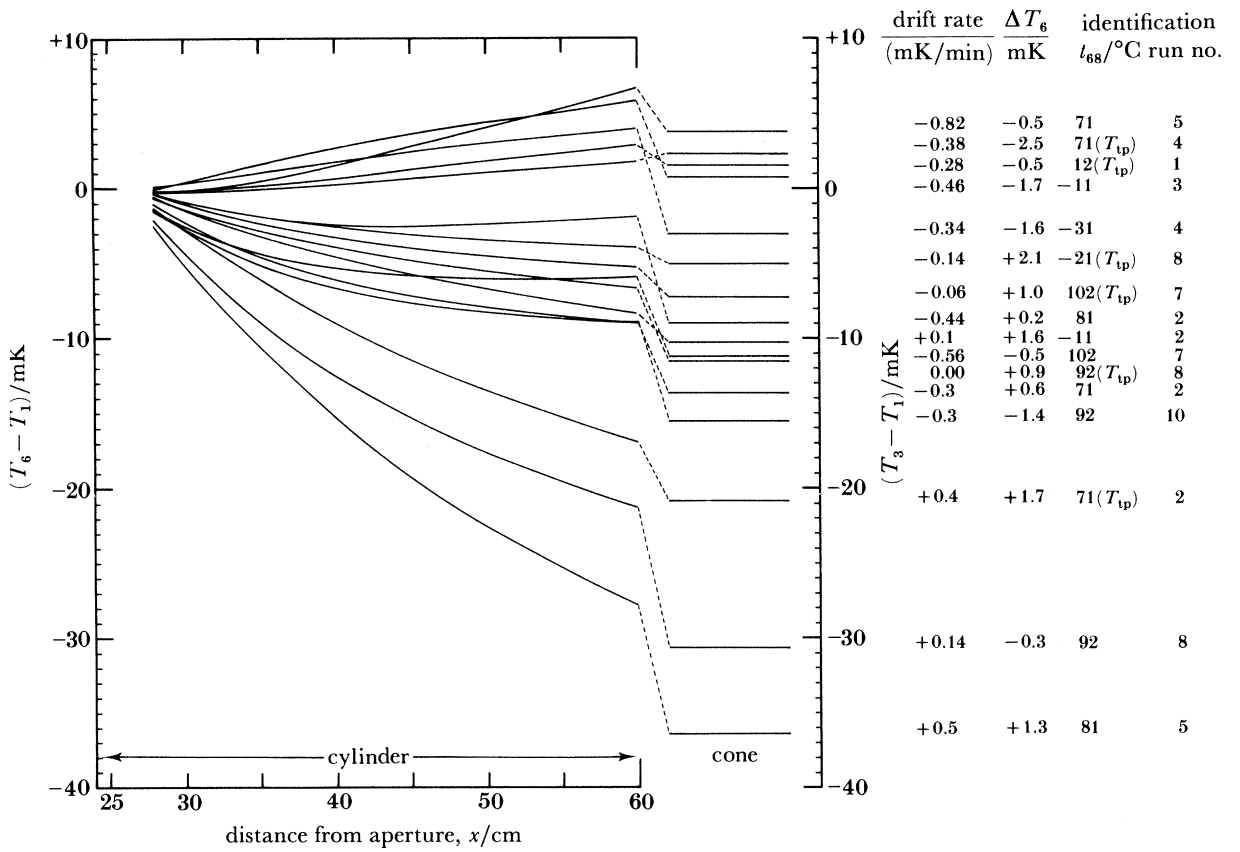

FIGURE 10. Temperature distributions along the cylindrical part of the radiator calculated by using (11). The measured temperatures of the cone, the measured drift rate, the difference ΔT_6 between the measured and calculated values of T_6 and the identification of the run are given for each curve. Values $t_{68} = 71$, run no. 5, for example, indicate the fifth run in the series at 71 °C and $t_{68} = 71$ (T_{tp}), run no. 4, the fourth run in the corresponding series at T_{tp} (see table 19).

This suggests that the size effect is insignificant and we conclude, on the basis of Garrett & Rosenberg's results, that the conductivity at 4.2 K is about 0.05 W m^{-1} K^{-1}. The heat flux $\delta\dot{Q}(x)$ through the paint from an element of the cylindrical wall a distance x from the aperture is greatest at the top of the cylinder near the aperture and is given by (A 4) of Appendix A. At temperatures near 373 K we find that $\delta\dot{Q}(x)$ for such an element is equal to 1.2 W m^{-2}. For a paint thickness of 100 μm and a thermal conductivity of 0.29 W m^{-1} K^{-1} this leads to a maximum temperature drop across the paint of only about 0.4 mK. This can be ignored since this is a maximum value (for $x = 23$) and it varies as x^{-3} along the length of the cylinder from $x = 23$ cm to $x = 60$ cm.

In conclusion, we estimate the overall uncertainty in the measured values of T_{68} in the radiator to be ±0.6 mK near 273 K rising to 1 mK at temperatures near 373 K. These values result from combining in quadrature the uncertainties in the T_{68} calibrations of the thermometers (±0.3 and ±0.5 mK at the extremes of the temperature range) and the uncertainties stemming from the longitudinal and transverse temperature gradients in the radiator (±0.5 and ±0.9 mK).

3. The calorimeter and 2 K reservoir

(*a*) *Thermal behaviour of the whole assembly*

Although the radiator and calorimeter must each approximate an ideal black body very closely, their functions otherwise are quite different. As we have seen, the radiator must provide thermal radiation over a solid angle of 2π sr at the lower aperture and the effective temperature of this radiation must be known to within 1 mK. The calorimeter, on the other hand, acts as a detector of this radiation. To do so it must subtend a solid angle of 2π sr at the upper aperture. The calorimeter must absorb practically all of the radiation passing through the aperture and it must have a means of measuring the thermal radiative power thus absorbed. The measurement is made by the substitution of electrical power for the thermal radiative power and by using the heat-flow calorimeter as a null detector. It must be demonstrated, therefore, that the calorimeter responds in the same way to electrical and radiative heating. It is in doing this that one sees the overwhelming advantages of a low-temperature detector.

Figure 11 shows a schematic outline of the calorimeter and 2 K reservoir assembly. The individual components of which can be readily identified in the detailed drawing of figure 12. The central requirement is that the temperature rise measured by the germanium resistance thermometer at D must depend only upon the amount of power absorbed over the black-body calorimeter between G and E and not upon whether this power is of electrical or radiative origin.

Radiant flux entering the copper calorimeter is absorbed in the black paint over the whole of the internal surface. The radiant power is not, and need not be, absorbed uniformly over the surface, but once absorbed it can follow only one path out of the calorimeter and towards the heat link to the 2 K reservoir. This path is through the supporting ring A and along the copper link AB, which also acts as a radiation screen for the heater windings. The thermometer is placed at D in good thermal contact with B. Similarly, when electrical energy is supplied the heat is developed only in the heater varnished to the outside of the calorimeter. The heater leads are superconducting and so no electrical power is developed in them. The question of thermal conduction in the leads and their thermal anchoring is an important one, which is dealt with later. As is the case for radiant heating, electrical energy developed in the heater can only flow through the walls of the calorimeter to A and hence via B to the stainless-steel heat link. The thermal diffusivity of copper at 4 K is about 10^3 times its room temperature value, due mainly to its very much smaller heat capacity at low temperatures. This allows one to use a relatively large mass of copper for the calorimeter, about 300 g, while maintaining a relatively short response time. The time constant of the whole calorimeter and heat link assembly increases linearly from just over 3 min at a calorimeter temperature of 4 K to 6 min at a calorimeter temperature of 8 K.

The presence of temperature gradients in the calorimeter can be ignored because the temperature of the calorimeter ($\leqslant 8$ K) and its surroundings (2 K) are much too low for radiative losses from the calorimeter to its surroundings to lead to significant errors. For such errors to reach 1 part in 10^6 of the measured power, a difference of more than 1 K along the length of the calorimeter would be required. The maximum such temperature difference that could exist, if all the heat were to be applied at one end, is about 40 mK for a total power input of 1 mW. The question of energy transfer by gas conduction is dealt with later, in § 8. Except for particular effects observed with the small pair of apertures, which result from

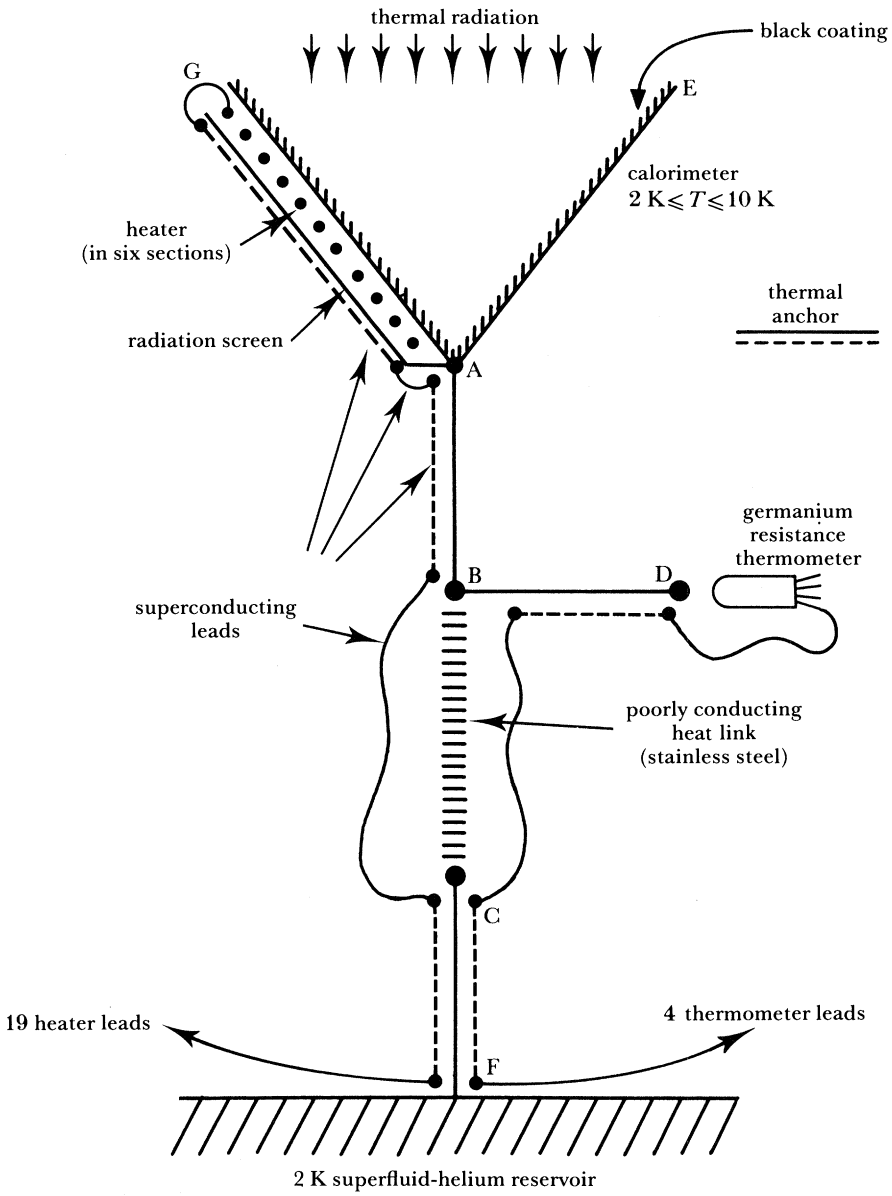

FIGURE 11. A schematic representation of the calorimeter, stainless-steel heat link and 2 K reservoir.

condensation of hydrogen, the corrections that must be applied for gas conduction are small because the pressures rarely exceed 10^{-5} Pa (7×10^{-8} Torr).

The absorptivity of the calorimeter is not calculated separately, but is part of the overall thermal radiation transfer function, which is calculated in §4. The only question that needs to be considered here is the effect of a finite thermal conductivity of the black paint. We have already deduced that the thermal conductivity of 3M black at liquid-helium temperatures is about 0.05 W m^{-1} K^{-1}. The maximum radiant power is absorbed about halfway down the calorimeter (see §4), but this does not exceed 0.1 W m^{-2}. For a layer of paint 100 μm thick this leads to a temperature drop across the paint of 0.2 mK, which is negligible.

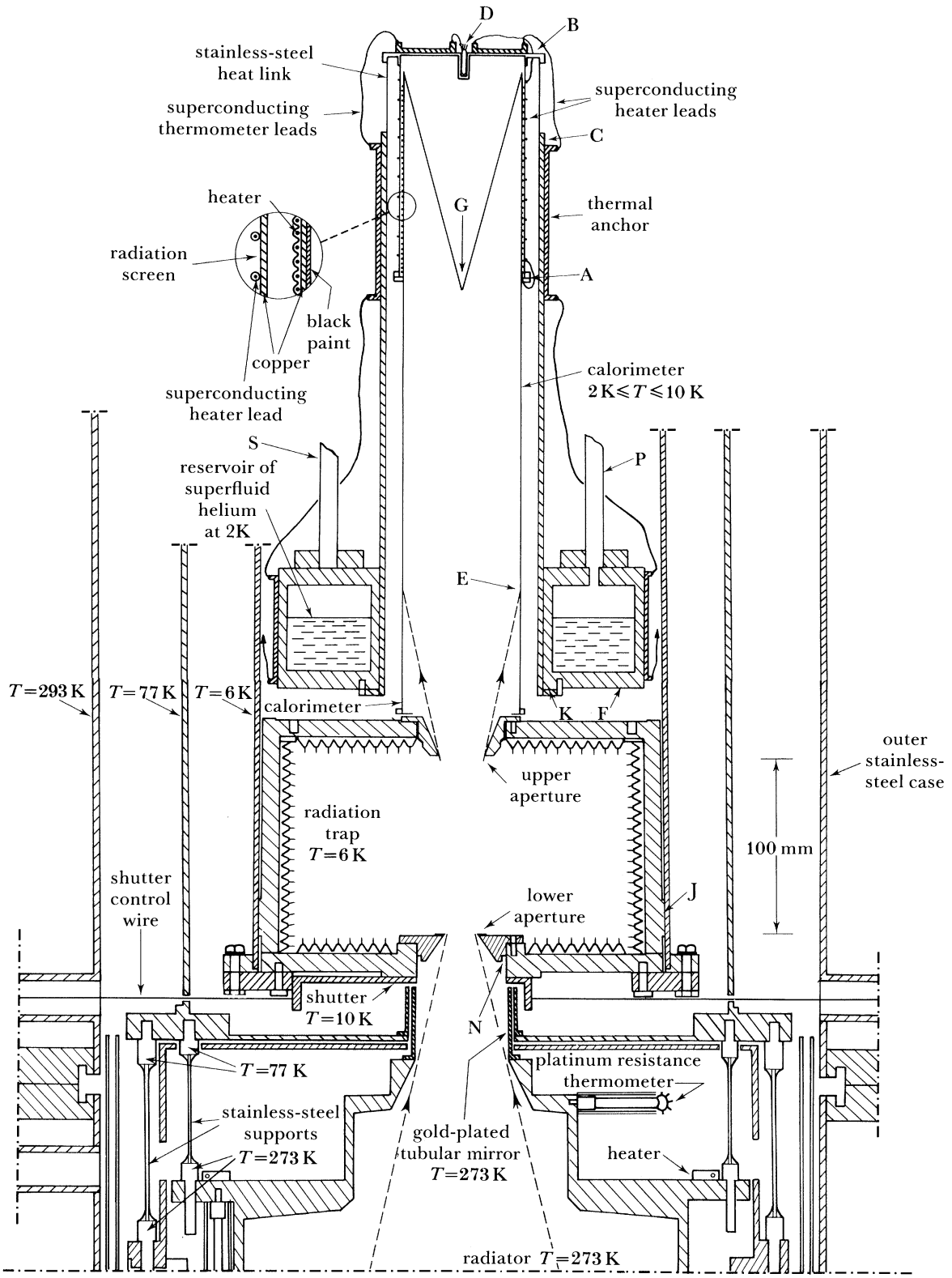

FIGURE 12. Details of 2 K reservoir, calorimeter, radiation trap and apertures illustrating the optical system. The letters A to F refer to locations shown schematically in figure 11, J and K are reference surfaces referred to in §10 and N is an annular absorbing area referred to in Appendix A. S and P are also referred to in §10.

(*b*) *The construction of the calorimeter and* 2 K *reservoir*

The detailed designs of the calorimeter and the 2 K reservoir are shown in figure 12. The calorimeter itself is made from electro-formed copper 0.25 mm thick and is coated on the inside with a 100 μm thick layer of 3M-C 101 paint; it is 7 cm in diameter and 38 cm long and has a re-entrant cone soldered at the closed end. The supporting ring A is soldered in place and bolted to the lower flange of the radiation screen. The upper flange of the radiation screen, which also supports the calorimeter, is bolted to the top plate, which is made from 1 mm thick copper. The well in which the germanium thermometer is placed is soldered in the top plate, which is bolted to the cylindrical stainless-steel heat link. The latter is 9 cm in diameter, 4 cm long and 0.25 mm thick and is soldered to the top of a copper cylinder bolted to the 2 K superfluid-helium reservoir. The 2 K reservoir is made from oxygen-free high-conductivity (o.f.h.c.) copper and the top and bottom plates were joined to the side walls by electron-beam welding to reduce the likelihood of leaks to superfluid helium.

(*c*) *Temperature measurement and control of the calorimeter and* 2 K *reservoir*

The purpose of the 2 K reservoir is to provide a constant-temperature heat sink into which the heat absorbed or developed in the calorimeter can be passed via the stainless-steel heat link.

The accuracy with which it is necessary to control the temperature of the 2 K reservoir and to measure the temperature of the calorimeter depends upon two factors: first, upon the accuracy sought in the comparison of radiant and electrical powers, in this case 1 part in 10^5, and second, upon the variation of the thermal conductivity of stainless steel with temperature. For a thermal conductivity that is independent of temperature, it is only necessary to ensure that the temperature difference between calorimeter and reservoir is the same to 1 part in 10^5 for radiant and electrical heating. This is not the case here, however, since the thermal conductivity $\kappa(T)$ of an 18%Cr–8%Ni stainless steel between 2 and 10 K is given by the relation (Touloukian *et al.* 1970)

$$\kappa(T) = 3.5 \times 10^{-4}\ T^{1.35}\ \mathrm{W\ cm^{-1}\ K^{-1}}.$$

So for a stainless-steel heat link of cross-sectional area A and length L, the steady-state heat flow $\dot{Q}$ across an element of length $\mathrm{d}l$ is

$$\dot{Q} = 3.5 \times 10^{-4}\ T^{1.35}\ A\ \mathrm{d}T/\mathrm{d}l, \tag{14}$$

which we write as

$$\dot{Q} = CA T^{1.35}\ \mathrm{d}T/\mathrm{d}l \tag{15}$$

so that

$$\dot{Q} \int_{l=0}^{L} \mathrm{d}l = CA \int_{T_{\mathrm{rs}}}^{T_{\mathrm{c}}} T^{1.35}\ \mathrm{d}T, \tag{16}$$

where T_{rs} is the temperature of the 2 K reservoir and T_{c} the temperature of the calorimeter. Hence

$$\dot{Q} = CA(T_{\mathrm{c}}^{2.35} - T_{\mathrm{rs}}^{2.35})/2.35\,L. \tag{17}$$

The change in heat flow, $\delta\dot{Q}$, for incremental changes in temperature δT_{rs} and δT_{c} of the ends of the heat link is

$$\delta\dot{Q} = CAL^{-1}\ T_{\mathrm{c}}^{1.35}\,\delta T_{\mathrm{c}} - CAL^{-1}\ T_{\mathrm{rs}}^{1.35}\,\delta T_{\mathrm{rs}}, \tag{18}$$

so that

$$\frac{\delta\dot{Q}}{\dot{Q}} = 2.35\left(\frac{T_{\mathrm{c}}^{1.35}\,\delta T_{\mathrm{c}} - T_{\mathrm{rs}}^{1.35}\,\delta T_{\mathrm{rs}}}{T_{\mathrm{c}}^{2.35} - T_{\mathrm{rs}}^{2.35}}\right). \tag{19}$$

For $\delta\dot{Q}/\dot{Q}$ equal to 1×10^{-5}, we show in figure 13 the magnitudes of δT_{rs} and δT_c that can be permitted. This is reflected in the sensitivity of the calorimeter, i.e. the change in resistance of the germanium resistance thermometer for a given increment of radiant power absorbed by the calorimeter expressed in ohms per milliwatt, and shown in figure 14 as a function of T_c. It is necessary to measure T_c to rather better than 4 parts in 10^6 to achieve an equality of radiant and electrical heat input with an accuracy of 1 part in 10^5. Figure 14 also shows the sensitivity of the germanium resistance thermometer. It is clear that the overall sensitivity of the calorimeter as a detector of thermal radiation is greatest at the lowest temperatures.

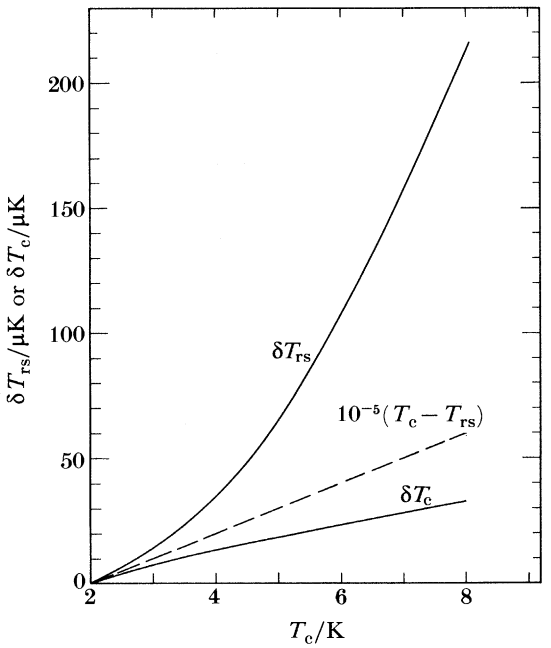

FIGURE 13. The permitted changes in temperature of the 2 K reservoir, δT_{rs} and the calorimeter δT_c, which still allow an accuracy of 1 part in 10^5 in the comparison between radiant and electrical power.

The helium in the 2 K reservoir is continuously pumped through a precision needle valve and an a.c. bridge system is arranged to provide the final temperature control. For radiant powers in the range 175 μW to 5 mW we require (see figures 13 and 14) a temperature stability at the smallest powers of better than 5 μK. Figure 15 shows an outline of the control system. The a.c. bridge is arranged to provide, at balance, an offset current of about 25 mA, which flows through the heater H, directly immersed in the superfluid helium, to generate up to 20 mW of power. The sensor for the controller is a germanium resistance thermometer having a perforated case directly immersed in the superfluid helium. Over a period of 2 h the total drift and short-term fluctuations in the temperature of the 2 K reservoir do not exceed 4 μK.

The temperature of the calorimeter is measured by means of a germanium resistance thermometer (Cryocal CR 1000) attached as shown (D in figure 12). The resistance of this thermometer is measured by using a Cryobridge Model 103 (ASL Ltd). This is an a.c. potentiometric system, operating at a frequency of 25 Hz, which in our measuring range of 200 Ω to 1000 Ω has a resolution of 2 parts in 10^6. Using the data shown in figure 14, we can calculate the sensitivity of the whole system, i.e. the minimum detectable change in radiator

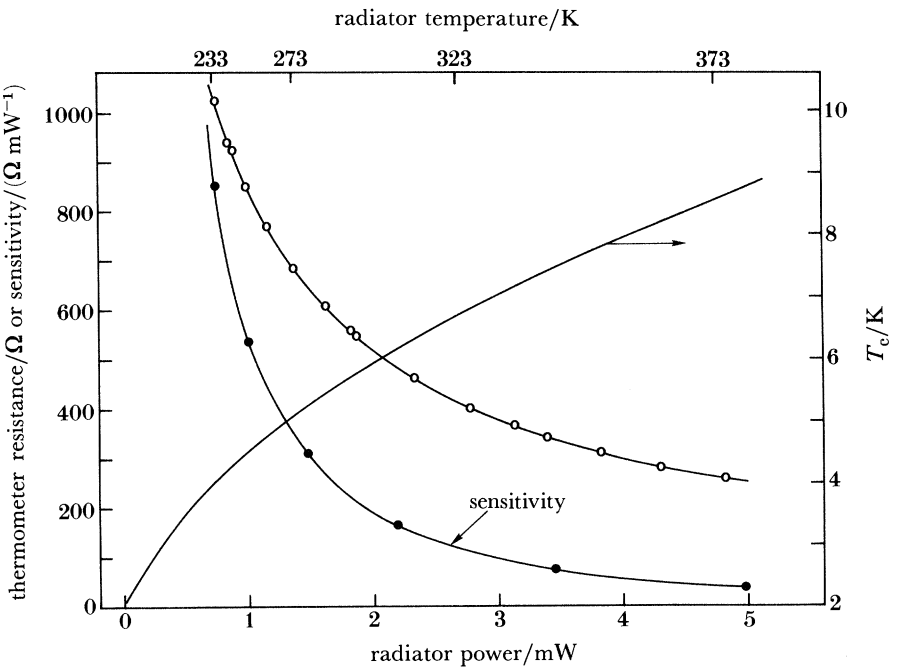

FIGURE 14. The resistance of the calorimeter thermometer, ○; its temperature, ——; and sensitivity in ohms per milliwatt of measured power, ●.

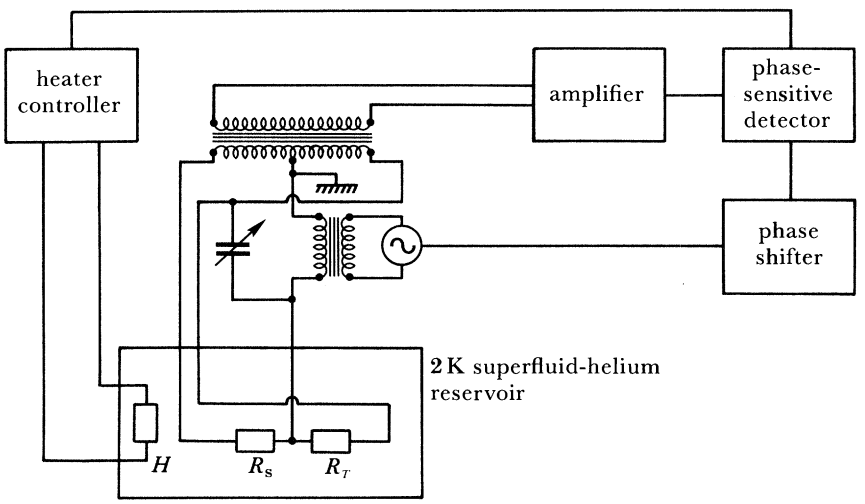

FIGURE 15. Outline of the control system for the 2 K reservoir. R_S is a 3.9 kΩ wire-wound resistor, R_T is Cryocal germanium resistance thermometer element (a thermometer having a perforated case) and H is a 30 Ω wire-wound heater.

temperature ΔT that can be measured by the calorimeter. This is shown in table 3 for various radiator temperatures between -40 and $+100$ °C. At each temperature the table also shows the resistance R_c and the sensitivity S, in ohms per milliwatt, of the calorimeter thermometer.

(*d*) *The calorimeter heaters*

Electrical energy is developed in a wire-wound heater on the outside of the calorimeter. In designing the heaters it was decided to provide a sufficient range of resistance to cover the power

TABLE 3. THE SENSITIVITY OF THE SYSTEM

(In this range of resistances the self-heating in the thermometer due to the measuring current causes an increase in thermometer temperature of about 8 mK for a power input of 0.9 μW. This power must remain stable to within 0.3%.)

R_c/Ω	$S/(\Omega\ \mathrm{mW}^{-1})$	T/K	ΔT/mK
1017	830	233	0.1
700	330	273	0.15
400	110	326	0.3
340	80	344	0.3
256	50	375	0.4

range from about 175 μW up to 17.2 mW, while at the same time allowing a measure of redundancy among the windings to allow the same power to be developed using different heaters. The maximum power is equivalent to a radiator temperature, for the large pair of apertures, of just over 230 °C, the freezing point of tin. A very convenient way of measuring the heater power is by means of voltage and current measurements made with a digital voltmeter displaying, in turn, the voltage across the heater and across a similar standard resistor in series. It was decided to use an S.E. Laboratories six-decade voltmeter with a resolution of 1 μV on the 1.1 V range. Tests showed a linearity within ±2 μV over the whole of this range. This range was chosen to enable direct comparisons to be made with a standard cell.

To cover the whole of the range of expected power and at the same time maintain adequate voltage resolution, we chose the resistances of the individual sections of the heater in the following way. We require a heater having n sections of resistance $R, aR, a^2R \ldots a^{n-1}R$ and specify a minimum of $V_{\min}$ and a maximum $V_{\max}$, where $V_{\max} = 1$ V, across each section. Since $V_{\min}^2/a^{n-1}R = 175\ \mu\mathrm{W}$ and $V_{\max}^2/R = 17.2$ mW, we deduce that $R \approx 58\ \Omega$. For there to be continuity from one section to another we must have $V_{\min}^2/R = V_{\max}^2/aR$, i.e. $a = V_{\max}^2/V_{\min}^2$. To choose $V_{\min}$ a criterion must be selected in terms of the required resolution in the temperature of the absorbed radiation. Since the absorbed power $\dot{Q} \propto T^4$ for radiant heating and $\dot{Q} \propto V^2$ for electrical heating, $\mathrm{d}V/V_{\min} = 2\,\mathrm{d}T/T$, where $\mathrm{d}V$ is the voltage resolution for a temperature resolution $\mathrm{d}T$. So for a voltmeter resolution of 1 μV and a temperature resolution of 0.2 mK at $T = 273$ K, we require $V_{\min} \approx 0.68$ V and hence $a \approx 2.15$. Substituting for $V_{\min}$, R and a leads to $n \approx 6$. The values of the resistances required in the six sections of the heater and the six standard resistances are given in table 4, after slight rounding to get an integral number of turns.

TABLE 4. RESISTANCE OF THE SIX HEATER SECTIONS

resistance/Ω	number of turns
2645	194
1230	90
572	42
266	20
124	9
57.5	4

The heater wire is varnished 0.1 mm diameter 'Eureka' having a resistance per unit length at 4.2 K of about 62 $\Omega\ \mathrm{m}^{-1}$ and is held in place by GE 7031 low-temperature varnish. For each heater section the equivalent standard resistance was made for us by the Croydon Precision Instrument Co. Ltd. The measured power is given by $V_s\,V_c/R_s$, where V_s and V_c are the voltage

drops across the standard and heater resistances respectively, and R_s is the value of the standard resistance. Each measurement is the mean of the measured values before and after current reversal.

The heater circuit is shown in figure 16. The power supply was designed to supply a constant current in the range 0.1–15 mA with a stability of 1 part in 10^6. The value of the current is set manually by means of a potentiometer. The current source and the standard resistances are all maintained in a constant-temperature enclosure at (24.0 ± 0.1) °C. The current through the heater circuit is set and reversed manually, but the readings of V_s and V_c are taken from the digital voltmeter by the HP 85 microcomputer. The heater standard resistances are calibrated against Tinsley class S 100 or 1000 Ω standards calibrated in turn against the standard of the ohm, maintained by the NPL, at the end of 1979, 1980 and 1982. The digital voltmeter was calibrated against a Tinsley standard voltage enclosure calibrated against the standard of the volt maintained by the NPL. The enclosure was continuously monitored in the NPL Electrical Science Division over a period of three years up to 1978 and re-checked in 1981.

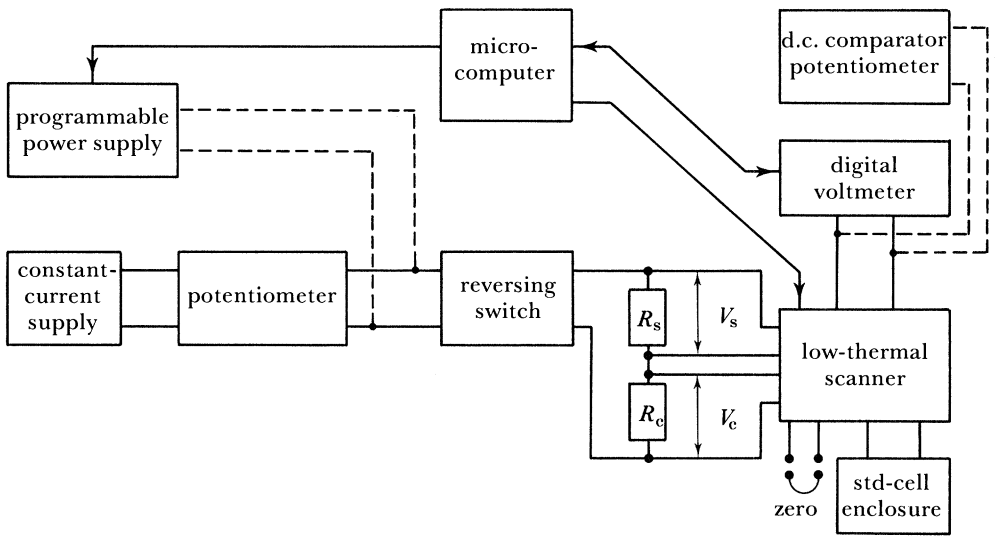

FIGURE 16. Outline of the power supply for the calorimeter heater. The broken lines indicate connections made during tests of the system with alternative instruments.

The internal consistency of the electrical power measurement was checked by supplying the same power to the calorimeter in two different ways: first by using a low-resistance heater and high current and, second, a high-resistance heater and low current. No significant difference in the response of the calorimeter could be observed within the limits of resolution of the digital voltmeter. Current reversal, which was made during every run, resulted in changes in observed power that rarely exceeded 2 parts in 10^5. Two further independent checks were also made: the digital voltmeter was replaced by a Guildline Direct Current Comparator Potentiometer Model 9930, and the power supply was replaced by a programmable power supply, an Adret d.c. Voltage and Current Standard Model 103 A. Neither of these changes resulted in detectable differences in measured power.

Uncertainties stemming from electrical power measurements are estimated to be 2 parts in

10^5 for the absolute measurements and 0.5 parts in 10^5 for the ratio measurements. They do not therefore contribute significantly to the overall uncertainty of either the Stefan–Boltzmann or thermodynamic-temperature measurements.

(*e*) *Thermal anchoring of heater and thermometer leads*

From the six sections of the heater a total of nineteen leads pass through the supporting ring at A (figure 12) and require thermal anchoring on the copper shield between A and B. Four leads from the germanium resistance thermometer must be anchored between D and B. If, as is necessarily the case during electrical heating, the heater wires are at a slightly higher temperature than the calorimeter upon which they are wound, the heater leads must be thermally anchored between A and B (figure 12) before they cross the stainless-steel heat link to C. If this is not the case, the essential condition that the germanium resistance thermometer responds equally to radiant and electrical heating of the calorimeter will not be met. The temperature difference between the heater wire and the calorimeter is difficult to calculate with precision since it depends upon the thermal contact between them and this is difficult to evaluate. However, a conservative calculation leads to the conclusion that the largest temperature difference likely to be encountered in the present work is about 10 mK. This occurs when the largest power is being supplied, namely about 4.5 mW (equivalent to a radiator temperature of 100 °C for the large apertures), which is developed in the 124 Ω heater section.

The heater leads are made from Nb–50 % Ti superconducting wire, 0.25 mm in diameter, from which a 0.04 mm thick coating of copper is removed, except at the ends where it is kept for soldering purposes. Each of the 19 leads is threaded through a polyethylene tube of internal diameter 0.5 mm and wall thickness 0.25 mm. The insulated leads, each 1 m long, are wound on the outside of the radiation screen AB (figure 12) and then pass across the stainless-steel heat link to the thermal anchor at C.

If the temperature difference between the heater and the calorimeter is ΔT_0, the temperature difference ΔT_x between an element of the lead, which is a distance x from the heater, and the radiation screen at the same temperature as the calorimeter is given, to a sufficiently good approximation, by

$$\Delta T_x = \Delta T_0 \, \mathrm{e}^{-mx}, \tag{20}$$

where $m^2 = h(\kappa A)^{-1}$, in which h is the rate of heat transfer to the substrate per unit length per unit temperature difference, κ the thermal conductivity of the wire and A its cross-sectional area. We estimate h to be 8×10^{-7} W cm^{-1} K^{-1} and we know that for the superconducting wire κ is given quite closely by $\kappa = 0.77 \times 10^{-4} \, T^{1.8}$ W cm^{-1} K^{-1} in the temperature range 3 K to the superconducting transition temperature, *ca.* 10 K (Schmidt 1979). These data lead to a value of m equal to 0.83, so that any temperature difference is reduced by a factor of 1/e of its value over a length of about 2 cm. Thus a total length of 100 cm is sufficient to reduce a temperature difference of 10 mK to negligible proportions.

The four germanium thermometer leads are thermally anchored to the top plate of the calorimeter, DB in figure 11, by varnishing about 30 cm of lead to the surface. This is adequate for the thermometer leads because all that is required for them is good stability in the thermal anchoring.

There remains the question of the total amount of heat that passes through the leads from B across the stainless-steel heat link to C. There are 23 Nb–Ti superconducting leads between

B and C, each one having had its thin copper layer dissolved away to reduce the overall thermal conductivity. Using the relation given above for the thermal conductivity of Nb–Ti, we can write down an expression for the heat conducted from B to C by analogy with that for the stainless-steel heat link itself, equation (17) above:

$$\dot{Q}(\text{leads})/\text{W} = 23CA(T_{\text{c}}^{2.8} - T_{\text{rs}}^{2.8})/2.8L, \tag{21}$$

where $C = 0.77 \times 10^{-4}\,\text{W cm}^{-1}$, $A = 2.3 \times 10^{-4}\,\text{cm}^2$ and $L \approx 8\,\text{cm}$. $\dot{Q}$(leads) increases from about 1.5 μW, i.e. about 0.1 % of the total measured power, for $T_{\text{c}} = 5\,\text{K}$, to 1.2 mW, or 26 % of the total measured power, at $T_{\text{c}} = 8.6\,\text{K}$. Although these are not large fractions, it is crucial to the success of the measurements that they be reproducible to a small percentage. For this we rely upon the stability of the thermal anchoring at B and at C, which is provided by an 8 cm length of 'Biccastrip' firmly bound with copper wire to the copper cylinder. Biccastrip is a proprietary flat multi-way cable made from thin strips of copper, 0.1 mm × 2 mm, embedded in a polyester plastic having a total thickness of 0.3 mm. For the dimensions we have used, m (equation (20)) is estimated to be 1 cm^{-1}, i.e. temperature differences are reduced by a factor 1/e of their value for each centimetre of anchoring. With 8 cm length it is clear that the thermal anchoring is adequate.

4. Thermal-radiation transfer function

Having described separately the radiator and the calorimeter, we come now to the question of the transfer of thermal radiation from the one to the other. To do this we calculate an overall thermal-radiation transfer function $F(\epsilon, a)$, considering as a whole the system formed by the radiator, the apertures and the calorimeter. Each element of the internal walls of radiator and calorimeter has its own value of (effective) emissivity, ϵ, or absorptance, a. These depend upon the distance of each element from the respective aperture and its orientation with respect to the aperture. In addition, we must take into account the vignetting effect of the upper aperture with respect to the lower. The effect of temperature gradients over the radiator must also be included. This is done by developing an expression for an 'effective temperature' of the thermal radiation absorbed by the calorimeter in terms of the temperature gradients in the radiator and the other factors mentioned above.

(*a*) *The effective temperature of the radiator*

The radiant power $\text{d}P(T_x)$ absorbed by the calorimeter from an element of width $\text{d}x$ at temperature T_x situated on the cylindrical wall of the radiator a distance x from the aperture (see figure 17) is given by

$$\text{d}P(T_x) = V(x)\, a_x(y_1 y_2)\, \text{d}E(T_x), \tag{22}$$

where $V(x)$ is what we call the 'view factor' and represents the vignetting effect of the upper aperture on the lower aperture when viewed from $\text{d}x$; $a_x(y_1 y_2)$ is the mean absorptivity of the calorimeter between y_1 and y_2 for radiation incident from the direction of $\text{d}x$, and $\text{d}E(T_x)$ is the radiant power emitted by the element $\text{d}x$ that passes through the lower aperture. The subscript x indicates a quantity or an element on the cylindrical wall of the radiator or calorimeter. The addition of a subscript c indicates a quantity or an element on the conical wall of the radiator or calorimeter. Thus we can write down an expression for the radiant power

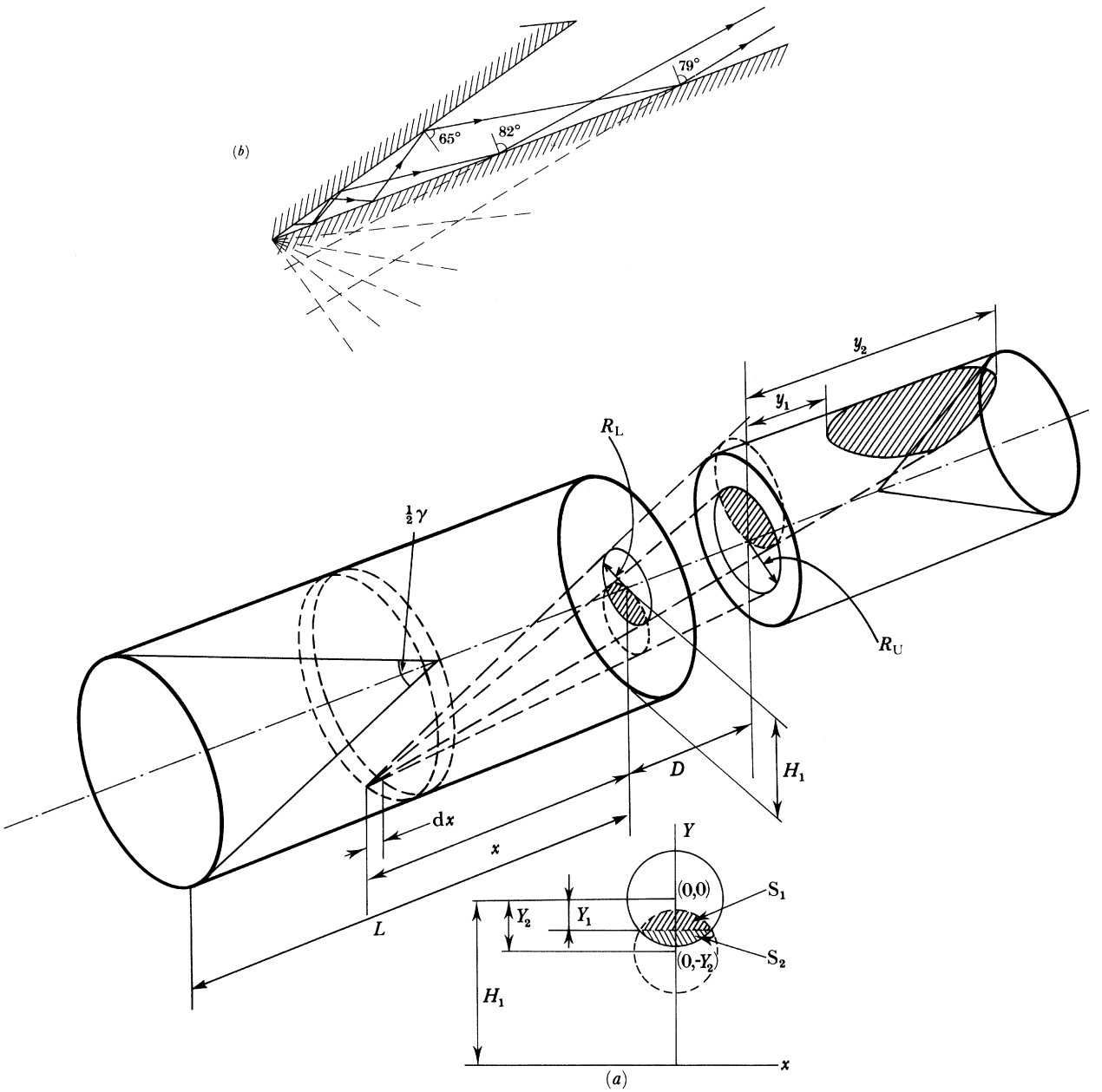

FIGURE 17. The geometry used in the derivation of the thermal-radiation transfer function. The inset (*a*) shows the geometry used in the calculation of the view factor $V(x)$, and (*b*) shows rays undergoing specular reflection at high angles of incidence in the radiator (cf. figure 6).

$\mathrm{d}P(T_{cx})$ absorbed by the calorimeter from an element $\mathrm{d}x$ on the conical base of the radiator having a temperature T_{cx}:

$$\mathrm{d}P(T_{cx}) = V_c(x)\, a_{cx}(y_1 y_2)\, \mathrm{d}E(T_{cx}), \tag{23}$$

where $\mathrm{d}E(T_{cx})$ is the radiant power emitted by the element $\mathrm{d}x$ situated on the cone that passes through the lower aperture. The paired subscripts x, c indicate a quantity that includes terms from both the cylindrical and conical walls. Thus the total radiant power $P(T_{x,c})$ absorbed

by the calorimeter from elements on the cylindrical wall of the radiator and from its conical base can be written

$$P(T_{x,c}) = \int_{\text{cylinder}} V(x)\, a_x(y_1 y_2)\, \mathrm{d}E(T_x)\, \mathrm{d}x + \int_{\text{cone}} V_c(x)\, a_{cx}(y_1 y_2)\, \mathrm{d}E(T_{cx})\, \mathrm{d}x. \quad (24)$$

Taking the expressions for $\mathrm{d}E(T_x)$ and $\mathrm{d}E(T_{cx})$ derived in Appendix C, we have:

$$P(T_{x,c}) = \int_{\text{cylinder}} \frac{2\pi\epsilon(x)\, a_x(y_1 y_2)\, H^2 R_L^2\, V(x)\, E(T_x)\, x\, \mathrm{d}x}{(x^2+H^2)^2} + \int_{\text{cone}} 2\pi R_L^2\, Q \tan^2 \tfrac{1}{2}\gamma (x^{-2} - Qx^{-3})\, V_c(x)\, \epsilon_c(x)\, a_{cx}(y_1 y_2)\, E(T_{cx})\, \mathrm{d}x, \quad (25)$$

where $E(T_x)$ is the total radiant exitance of the element $\mathrm{d}x$ at a temperature T_x, $\epsilon(x)$ and $\epsilon_c(x)$ are the emittances of elements on the cylindrical walls and cone respectively, γ is the angle of the cone (30°) and Q the distance of the tip of the cone from R_L (36.5 cm); the radius of the cylinder is H (6 cm).

Let $P(T)$ be the radiant power absorbed by the calorimeter for a uniform radiator, temperature T, such that

$$E(T_x) = E(T) + \Delta E(T_x) \quad \text{and} \quad E(T_c) = E(T) + \Delta E(T_{cx}), \quad (26)$$

where $\Delta E(T_x)$ and $\Delta E(T_{cx}) \ll E(T)$. We can thus write

$$\frac{P(T_{x,c})}{P(T)} = \left\{ \int_{\text{cylinder}} \frac{\epsilon(x)\, a_x(y_1 y_2)\, H^2 V(x)\, [E(T) + \Delta E(T_x)]\, x\, \mathrm{d}x}{(x^2+H^2)^2} + \int_{\text{cone}} Q \tan^2 \tfrac{1}{2}\gamma (x^{-2} - Qx^{-3})\, V_c(x)\, \epsilon_c(x)\, a_{cx}(y_1 y_2)\, [E(T) + \Delta E(T_{cx})]\, \mathrm{d}x \right\} \times \left\{ \int_{\text{cylinder}} \frac{\epsilon(x)\, a_x(y_1 y_2)\, H^2 V(x)\, E(T)\, x\, \mathrm{d}x}{(x^2+H^2)^2} + \int_{\text{cone}} Q \tan^2 \tfrac{1}{2}\gamma (x^{-2} - Qx^{-3})\, V_c(x)\, \epsilon_c(x)\, a_{cx}(y_1 y_2)\, E(T)\, \mathrm{d}x \right\}^{-1}. \quad (27)$$

Writing the first term of the denominator of (27) as $E(T)\, B_1(\epsilon, a)$ and the second term as $E(T)\, B_2(\epsilon, a)$ and rearranging we find

$$\frac{P(T_{x,c})}{P(T)} = \left\{ E(T)\, [B_1(\epsilon, a) + B_2(\epsilon, a)] + \int_{\text{cylinder}} \frac{\epsilon(x)\, a_x(y_1 y_2)\, H^2 V(x)\, \Delta E(T_x)\, x\, \mathrm{d}x}{(x^2+H^2)^2} + \int_{\text{cone}} Q \tan^2 \tfrac{1}{2}\gamma (x^{-2} - Qx^{-3})\, V_c(x)\, \epsilon_c(x)\, a_{cx}(y_1 y_2)\, \Delta E(T_{cx})\, \mathrm{d}x \right\} \times \{E(T)\, [B_1(\epsilon, a) + B_2(\epsilon, a)]\}^{-1} \quad (28)$$

$$= 1 + \left\{ \int_{\text{cylinder}} \frac{\epsilon(x)\, a_x(y_1 y_2)\, H^2 V(x)\, \Delta E(T_x)\, x\, \mathrm{d}x}{(x^2+H^2)^2} + \int_{\text{cone}} Q \tan^2 \tfrac{1}{2}\gamma (x^{-2} - Qx^{-3})\, V_c(x)\, \epsilon_c(x)\, a_{cx}(y_1 y_2)\, \Delta E(T_{cx})\, \mathrm{d}x \right\} \times \{E(T)\, [B_1(\epsilon, a) + B_2(\epsilon, a)]\}^{-1}. \quad (29)$$

But since $\epsilon(x)$, $\epsilon_c(x)$, $a_x(y_1 y_2)$ and $a_{cx}(y_1 y_2)$ are very close to unity and $\Delta E(T_x)$ and $\Delta E(T_{cx}) \ll E(T)$, we shall for the time being set $\epsilon(x) = \epsilon_c(x) = a_x(y_1 y_2) = a_{cx}(y_1 y_2) = 1$ and write $B_1(\epsilon, a) = B_1$ and $B_2(\epsilon, a) = B_2$. Later on we shall return to $B_1(\epsilon, a)$ and $B_2(\epsilon, a)$ for calculating the overall radiant energy transfer function. First, however, we derive expressions that allow us to calculate an effective temperature T for the radiator on the basis of known temperature distributions T_x and T_{cx}.

From (29) we can write

$$\frac{P(T_{x,c}) - P(T)}{P(T)} = \frac{1}{B_1 + B_2} \int_{\text{cylinder}} \frac{H^2 V(x)\, \Delta E(T_x)\, x\, dx}{E(T)\, (x^2 + H^2)^2} + \frac{1}{B_1 + B_2} \int_{\text{cone}} Q \tan^2 \tfrac{1}{2}\gamma \left(\frac{1}{x^2} - \frac{Q}{x^3}\right) V_c(x)\, \frac{\Delta E(T_{cx})}{E(T)}\, dx. \quad (30)$$

However, the dimensions of the cone, its thermal diffusivity and measured temperature-drift rates allow us to say that T_{cx} is uniform over the whole of the cone, and noting that $\epsilon_c(x) = a_{cx}(y_1 y_2) \approx 1$ and writing $E(T_{cx}) - E(T) = \Delta E(T_c)$ we can write

$$P(T_{x,c}) - P(T) = \Delta P(T_x\, T_c),$$

and remembering that the integral in the last term of (30) is the same as B_2, from (29) we can write

$$\frac{\Delta P(T_x\, T_c)}{P(T)} = \frac{1}{B_1 + B_2} \int_{\text{cylinder}} \frac{H^2 V(x)\, \Delta E(T_x)\, x\, dx}{E(T)\, (x^2 + H^2)^2} + \frac{B_2}{B_1 + B_2} \frac{\Delta E(T_c)}{E(T)}. \quad (31)$$

But because of the fourth-power dependence of P upon T we can write

$$\frac{\Delta P(T_x\, T_c)}{P(T)} = \frac{4\, \Delta T(T_x\, T_c)}{T}; \quad \frac{\Delta E(T_x)}{E(T)} = \frac{4\, \Delta T_x}{T} \quad \text{and} \quad \frac{\Delta E(T_c)}{E(T)} = \frac{4\, \Delta T_c}{T}, \quad (32)$$

where $\Delta T_x = T - T_x$ and $\Delta T_c = T - T_c$ in which T is an arbitrary temperature close to T_x and T_c. We can therefore write

$$\Delta T(x, c) = \frac{1}{B_1 + B_2} \int_{\text{cylinder}} \frac{H^2 V(x)\, \Delta T_x\, x\, dx}{(x^2 + H^2)^2} + \frac{B_2}{B_1 + B_2} \Delta T_c. \quad (33)$$

We shall take $T = T_1$, i.e. the temperature of the thermometer on the radiator (see figure 7) so that in terms of the temperature given by the thermometer the effective temperature $T(x, c)$ or strictly $T_{68}(x, c)$ becomes

$$T(x, c) = T_1 + \frac{1}{B_1 + B_2} \int_{\text{cylinder}} \frac{H^2 V(x)\, \Delta T_x\, x\, dx}{(x^2 + H^2)^2} + \frac{B_2}{B_1 + B_2} \Delta T_c. \quad (34)$$

In this expression $\Delta T_c = T_3 - T_1$, where T_3 is the temperature of the cone given by the mean of thermometers 3 and 2, and $\Delta T_x = T'_x - T_1$ where T'_x is the effective temperature of the radiation from the element x. Were $\epsilon(x)$ equal to or close to unity (approximately equal to 0.95, for example) we could write $T'_x = T_x$, but owing to the large specular reflectance of 3M paint at high angles of incidence such an assumption is not good enough, despite the fact that ΔT_x is small. Over most of the cylindrical wall the angle of incidence of the radiation passing to R_L is greater than 78°. This is illustrated in figure 17*b*. By calculating the angle of incidence as a function of x and using the specular reflectance shown in figure 6 as a function of angle of incidence, we find that, to a good approximation, the specular reflectance $\rho_{sp}(x)$ for a ray

striking the cylindrical wall for $27 \leqslant x \leqslant 60$ is given by $\rho_{sp}(x) = 0.012x$, and for the same ray striking the cone by $\rho_{sp}(cx) = 0.002x$. The radiation from an element dx thus comprises the fraction $(1-0.012x)$ of radiation of temperature T_x with the rest coming from the cone and regions further down the cylinder. Since the specular component of reflectance is very low at angles of incidence less than 70°, we can deduce that most of this remaining radiation originates from the cone with only a small further proportion coming from the cylindrical wall near the second reflection, which occurs at values of $x \approx 57$ cm. Since both ΔT_x and ΔT_c are small, we take the effective temperature T'_x of element dx to be given by

$$T'_x = (1-0.012x)\, T_x + 0.012x[(1-0.002x)\, T_c + 0.002x T(x = 57)]. \tag{35}$$

So that, finally, we can write

$$T(x, c) = T_1 + \frac{1}{B_1+B_2} \int_{\text{cylinder}} \frac{H^2 V(x)\,(T'_x - T_1)\, x\, dx}{(x^2+H^2)^2} + \frac{B_2}{B_1+B_2}\,(T_3 - T_1). \tag{36}$$

The view factor $V(x)$ is evaluated in Appendix B for the two pairs of apertures. The temperature distribution in the radiator T_x is calculated on the basis of measured values of T_x, as described in §2 (*c*).

(*b*) *Thermal-radiation transfer function, $F(\epsilon, a)$*

Having shown how to assign an effective temperature to the radiation leaving the radiator and absorbed by the calorimeter, we now return to the evaluation of the integrals B_1, B_2 and also $B_1(\epsilon, a)$ and $B_2(\epsilon, a)$ of (27).

The thermal-radiation transfer function, $F(\epsilon, a)$, or net emissivity–absorptivity of the system, is given by

$$F(\epsilon, a) = [B_1(\epsilon, a) + B_2(\epsilon, a)]/(B_1 + B_2). \tag{37}$$

To evaluate $B_1(\epsilon, a)$ and $B_2(\epsilon, a)$ it is necessary to find expressions for the emittance of elements over the cylindrical wall and cone of the radiator and of the calorimeter.

The calculation of these quantities is relatively straightforward because the emittance of 3M black is very high, about 0.94, and for the radiator the solid angle subtended by the aperture at all wall elements of both the cylinder and cone is very small. The effective emittance and reflectance of 3M black for thermal radiation is discussed in §2 (*b*). Here we take only the result that it behaves as a diffuse emitter and reflector of thermal radiation and has a reflectance, which we have already estimated, of about 0.06 at angles to the normal of less than about 70°, and at higher angles it becomes an increasingly specular reflector.

Taking first the radiator, for an element dx on the cylindrical wall a distance x from the aperture, we can write down its apparent emissivity $\epsilon(x)$ in the direction of the aperture by using the series reflection method (Quinn 1980, 1983) as

$$\epsilon(x) = 1 - R(x), \tag{38}$$

where $R(x)$ is the fraction of the radiant flux incident on dx from the direction of the aperture that is eventually reflected out of the aperture after one or more reflections inside the radiator. This fraction can be written down as a series of terms in increasing order of $\rho(x)$, the reflectance of the wall. For simple cavity configurations such as ours (a cylinder having a conical or inclined base) it has been shown that, provided the emittance of the walls is high and the aperture relatively small, the emissivity calculated by the series reflection method using only the first

few terms is very close to the exact value (Quinn 1980). For a simple cylindrical cavity we can write,

$$\epsilon(x) = 1-\rho(x)\,\pi^{-1}\,\mathrm{d}\Omega(x)\,\cos\theta - I_2(x)\,\rho(x)^2 - \sum_{n=3}^{\infty}[\rho(x)]^n\,I_n(x), \tag{39}$$

where $\mathrm{d}\Omega(x)$ is the solid angle subtended by the aperture at the element $\mathrm{d}x$, θ is the angle of incidence of a ray coming through the aperture striking the wall at x, and the I_n are geometrical factors (see below).

For the cylindrical part of the radiator for which $23 \leqslant x \leqslant 60$ cm, this can be written

$$\epsilon(x) = 1-\rho(x)\,\frac{R_0^2\,xH}{(x^2+H^2)^2} - \frac{R_0^2}{H^2}\,I_2(x)\,\rho(x)^2 - \sum_{n=3}^{\infty}[\rho(x)]^n\,I_n(x), \tag{40}$$

where R_0 is the effective radius of the aperture as defined in Appendix A, H is the radius of the cylindrical part of the radiator and the last term represents a series of geometrical factors giving the fractions of radiation reflected out through the aperture after n successive reflections in the cavity. For $x = 25$ cm, we find that $I_2' \approx 0.05$ and falls rapidly for increasing values of x (Quinn 1980), so the term in $[\rho(x)]^2$, although equal to 3×10^{-5} at $x = 25$, rapidly falls below 1×10^{-5} for larger values of x and can therefore be ignored. Similarly, the remaining terms fall very rapidly since $[\rho(x)]^n$ is so small. We can thus write, to a sufficiently good approximation,

$$\epsilon(x) = 1-\rho(x)\,R_0^2\,xH/(x^2+H^2)^2. \tag{41}$$

This expression, however, must be modified to take into account specular reflection at high angles of incidence and we must write

$$\epsilon(x) = 1-\rho(x)\,R_0^2\,xH(x^2+H^2)^{-2}\,[1-\rho_{\mathrm{sp}}(x)] - R'(x)\,\rho_{\mathrm{sp}}(x), \tag{42}$$

where $\rho_{\mathrm{sp}}(x)$ is the fraction of the radiant flux specularly reflected at x and is given by $\rho_{\mathrm{sp}}(x) = 0.012x$, as we have already seen, and $R'(x)$ is the fraction of this specularly reflected flux that is subsequently reflected out through the aperture. When calculating the effective temperature of the radiator, we remarked that the multiple reflections between the cone and the cylinder are such that the angle of incidence very rapidly falls below 70° and the reflections become, once again, diffuse and small. $R'(x)$ is thus practically constant and represents the fraction of radiation reflected out of the aperture after reflection from elements of the radiator in the region of $x = 57$ cm. Thus, finally,

$$\epsilon(x) = 1-\rho(x)\,R_0^2\,xH(x^2+H^2)^{-2}\,(1-0.0125x) - 0.012x\,R'(x=57), \tag{43}$$

but

$$R'(x=57) = \rho(x)\,R_0^2\,xH(x^2+H^2)^{-2}\cos\theta, \tag{44}$$

but also since $R'(x = 57)$ is less than about 10^{-5} it is negligible so that

$$\epsilon(x) = 1-\rho(x)\,R_0^2\,xH(x^2+H^2)^{-2}\,(1-0.0125x). \tag{45}$$

For the conical part of the radiator we need take account only of the term in $\rho(x)$ in (39). The specular component of reflectance for elements on the surface of the cone a distance x from the aperture is given by

$$\rho_{\mathrm{sp}}(x,c) = 0.0067x, \tag{46}$$

obtained in the same way as the expression for $\rho_{\mathrm{sp}}(x)$. The emittance of an element on the surface of the cone can be written

$$\epsilon_c(x) = 1-\rho(x)\,\mathrm{d}\Omega(x)\,\cos\theta\,[1-\rho_{\mathrm{sp}}(x,\mathrm{c})], \tag{47}$$

which for the particular case of the conical part of the radiator becomes

$$\epsilon_c(x) = 1 - \frac{\rho(x)\, Q \sin \tfrac{1}{2}\gamma\, R_0^2 (1 - 0.0067x)}{[x^2 + (x-Q)^2 \tan^2 \tfrac{1}{2}\gamma]^{\frac{3}{2}}}. \tag{48}$$

We come now to the calculation of the absorptance of elements on the cylindrical and conical walls of the calorimeter, for which the distances from the aperture are represented by y. We find that we must take into account the equivalent term in $I_2(x)$ of (39), since not only is the smallest value of y equal to 6 cm, rather than 23 cm as for the radiator, but the aperture is larger as well. For the calorimeter we write the absorptivity $a(y)$ as

$$a(y) = 1 - [\rho(y)\, \pi^{-1}\, d\Omega(y) \cos\theta + \rho(y)^2 \pi^{-2} I_2(y)]\, [1 - \rho_{sp}(y)] - \rho_{sp}(y)\, R'(y). \tag{49}$$

The specular component of the reflectance of elements on the cylindrical wall, deduced as before, is given by $\rho_{sp}(y) = 0.022y$.

In this case we find that $R'(y)$, for $y = 35$, is equal to 2×10^{-5} (not negligible), so that we write

$$a(y) = 1 - \left[\rho(y)\, \frac{R_{U_1}^2\, y H_c}{(y^2 + H_c^2)^2} + \left(\frac{\rho(y)}{\pi}\right)^2 \frac{R_{U_1}^2}{H_c^2}\, I_2(y/H_c)\right] [1 - \rho_{sp}(y)] - 2.10^{-5} \rho_{sp}(y), \tag{50}$$

where H_c is the radius of the cylindrical calorimeter, equal to 3.5 cm, and R_{U_1} is the radius of the virtual image of R_U in the aperture cone and is equal to 2.2 and 1.9 cm for the large and small aperture pairs respectively. Using the tabulated values for I_2 (Quinn 1983) for a cylindrical cavity, we find that the term in $I_2(y)$ falls very rapidly with increasing values of y and falls below 10^{-5} for those parts of the calorimeter more than about 25 cm from the aperture.

Similarly, for the cone of the calorimeter,

$$a_c(y) = 1 - \rho(y)\, \pi^{-1} \cos\theta\, d\Omega_c(y)\, [1 - \rho_{sp}(y)] - \rho_{sp}(y)\, R'(y), \tag{51}$$

where in this case $\rho_{sp}(y, c) = 0.002y$, so that

$$a_c(y) = 1 - \frac{\rho(y)\, Q \sin \tfrac{1}{2}\gamma\, R_{U_1}^2 (1 - 0.002y)}{[x^2 + (x-Q)^2 \tan^2 \tfrac{1}{2}\gamma]^{\frac{3}{2}}} - 2 \times 10^{-5}\, \rho_{sp}(y, c). \tag{52}$$

We now have expressions for the emissivity of elements along the cylindrical wall, $\epsilon(x)$, and of elements on the cone of the radiator, $\epsilon_c(x)$, and the absorptivity of elements along the cylindrical wall, $a(y)$, and of elements on the cone of the calorimeter, $a_c(y)$. Hence, we can proceed to a numerical evaluation of the integrals of (29). Before doing so, however, we come to the experimental measurement of the absorptivity of the calorimeter.

Measurements of reflectance were made for us by E. Zalewski of the NBS on a replica of the calorimeter having the same dimensions and painted on the inside with 3M-C 101 in the same way. The reflectance of the cavity was measured by using a laser reflectometer at a wavelength of 633 nm. The overall uncertainty of the experimental measurements was estimated as 6%. The results are shown in figure 18, together with curves for the values calculated from (50) and (52). The agreement between the measured values and those calculated here is generally very good, but at large values of y the measured values of reflectance are consistently higher than the calculated ones.

Calculations (Bedford, personal communication 1983) made by using the more exact integral equation method, but assuming a diffusely reflecting surface with no specular reflection also led to calorimeter reflectances lower than those measured by Zalewski for large values of y.

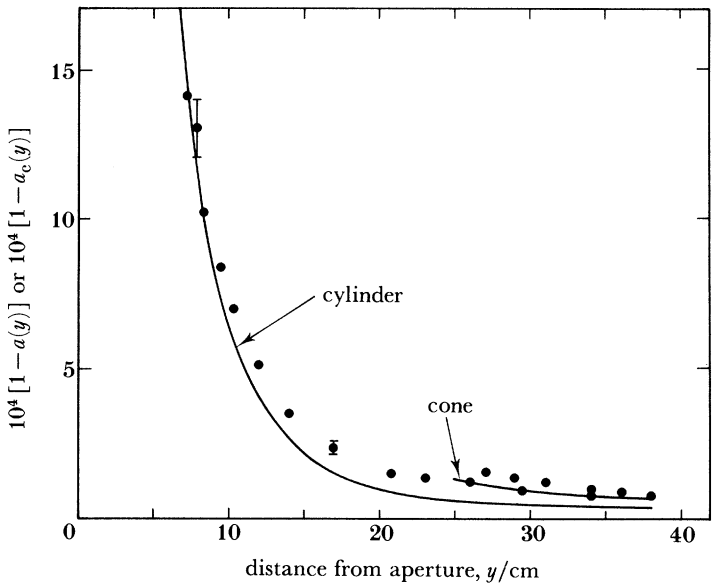

FIGURE 18. The reflectance of the calorimeter for the large pair of apertures, $[1-a(y)]$ and $[1-a_c(y)]$, calculated from (50) and (52): ●, measured values of (Zalewski, personal communication (1979)).

The most likely explanation for this difference between measured and calculated reflectances, as has been suggested already in §2(*b*), is that 3M paint exhibits a small amount of retro-reflection, about 0.5×10^{-4} at 633 nm. It is probable that slightly more retro-reflection occurs at longer wavelengths due to the structure of the paint and the increasing transparency of carbon black and silica. We have, therefore, adopted an overall correction for retro-reflection of $(1\pm0.5)\times10^{-4}$. This correction applies equally to the absorptivity of the calorimeter and to the emissivity of the radiator and thus contributes a correction of $(2\pm1)\times10^{-4}$ to the thermal-radiation transfer function. This correction is made after the evaluation of the integrals contained in (29).

Returning to the evaluation of these integrals, we must first use (50) and (52) to find values of $a_x(y_1y_2)$ and $a_{xc}(y_1y_2)$. These are the weighted mean values of $a(y)$ and $a_c(y)$ between y_1 and y_2 when viewed through the apertures from the element dx in the radiator (see figure 17). The values of y_1 and y_2 are calculated while taking into account the vignetting effect of the apertures. For each value of x a weighted mean is deduced from the geometry of figure 17 and the values of $a_x(y_1)$, $a_x(y_2)$, $a_{xc}(y_1)$ and $a_{xc}(y_2)$ are calculated from (50) and (52).

Since all the calculations of emissivity and absorptivity are made in terms of reflectance, it is convenient to define the functions $G(x)$ and $G_c(x)$ given by

$$G(x) = 1-\epsilon(x)\,a_x(y_1y_2), \tag{53}$$

$$G_c(x) = 1-\epsilon_c(x)\,a_{cx}(y_1y_2). \tag{54}$$

We thus write $B_1(\epsilon,a)$ from (29) in the form

$$B_1(\epsilon,a) = \int_{x=x_1}^{x_2} \frac{[1-G(x)]\,H^2V(x)\,x\,dx}{(x^2+H^2)^2}, \tag{55}$$

and similarly we rewrite for $B_2(\epsilon, a)$,

$$B_2(\epsilon, a) = \int_{x=x_2}^{x_1} [1-G_c(x)]\, Q \tan^2 \tfrac{1}{2}\gamma(x^{-2}-Qx^{-3})\, V_c(x)\, dx. \tag{56}$$

$G(x)$ and $G_c(x)$ represent the departures from the ideal thermal-radiation transfer between an element at x on the radiator and the calorimeter. Figure 19 shows $G(x)$ and $G_c(x)$ for both the large and small pairs of apertures.

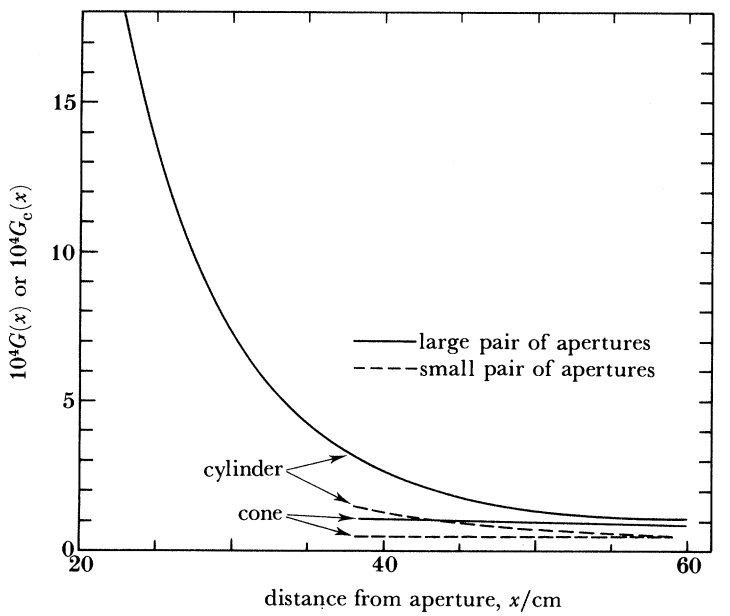

FIGURE 19. $G(x)$ and $G_c(x)$, defined in (53) and (54), as a function of distance from the lower aperture along the cylindrical part of the radiator. Values for both large and small pairs of apertures are shown. The ordinate is a measure of the departure from ideal black-body conditions of the radiator–calorimeter system.

Now returning to (37), we find that numerical integration leads to the following results.

(1) For the cylindrical part of the radiator:

$B_1(\epsilon, a) = 4.75252 \times 10^{-3}$ (large apertures), $B_1(\epsilon, a) = 7.67027 \times 10^{-4}$ (small apertures),

where $x_1 = 23$ and 40 for large apertures and small apertures respectively, and $x_2 = 60$;

$B_1 = 4.75412 \times 10^{-3}$ (large apertures), $B_1 = 7.67128 \times 10^{-4}$ (small apertures),

where x_1 and x_2 are the same as for $B_1(\epsilon, a)$.

(2) For the conical part of the radiator:

$B_2(\epsilon, a) = 3.73444 \times 10^{-3}$ (large apertures), $B_2(\epsilon, a) = 3.17221 \times 10^{-3}$ (small apertures),

where $x_1 = 60$ and $x_2 = 38.5$;

$B_2 = 3.73628 \times 10^{-3}$ (large apertures), $B_2 = 3.1724 \times 10^{-3}$ (small apertures),

where x_1 and x_2 are the same as for $B_2(\epsilon, a)$.

Substituting the values into (37) for the thermal-radiation transfer function:

$$F(\epsilon, a) = 8.48696/8.4904 = 0.99959 \text{ (large apertures)},$$

$$F(\epsilon, a) = 3.93924/3.93953 = 0.99993 \text{ (small apertures)}.$$

The values of B_1 and B_2 evaluated above are used in (36) to calculate the effective temperature of the radiator. If we assume that the temperature of the cylinder (as well as that of the cone) is uniform, (36) shows that fractions $B_1/(B_1+B_2)$ and $B_2/(B_1+B_2)$ of the measured radiation come from the cylinder and cone respectively. For the large pair of apertures these fractions are 0.56 and 0.44, and for the small pair 0.195 and 0.805, respectively. The numerical integration and evaluation of the various terms in (32) have been made to six significant figures and only the final results have been rounded to 1 part in 10^5.

To obtain the final values of $F(\epsilon, a)$ we must take into account the retro-reflection estimated at $(1 \pm 0.5) \times 10^{-4}$ for both $\epsilon(x)$ and $a(y)$. This leads to a reduction in $F(\epsilon, a)$ of $(2 \pm 1) \times 10^{-4}$ so that, corrected for retro-reflection,

$$F(\epsilon, a) = 0.99939 \text{ (large apertures)}, \quad F(\epsilon, a) = 0.99973 \text{ (small apertures)}.$$

The uncertainty in these values of $F(\epsilon, a)$ comes from the following sources.

(*a*) *The geometrical calculation of* $V(x)$ *and* $V_c(x)$. This is considered to be insignificant.

(*b*) *The values of* $G(x)$ *and* $G_c(x)$. This source of uncertainty is an important one because it enters directly into the calculation of $B_1(\epsilon, a)$ and $B_2(\epsilon, a)$. Since the surface reflectance ρ enters into the expression for $G(x)$ twice, once in $\epsilon(x)$ and once in $a_x(y_1 y_2)$, and these two are correlated, the uncertainty in $G(x)$ is 20 % of its value. This leads to an uncertainty of 20 % in $(1 - F(\epsilon, a))$, namely 8.2×10^{-5} and 1.4×10^{-5} for the large and small pairs of apertures respectively.

(*c*) *The retro-reflection correction.* This is estimated to be 50 % of its value, namely 1×10^{-4}. This has been estimated on the basis that the observed difference of 5×10^{-5} between the calculated and measured values of $a(y)$ at large values of y is due to retro-reflection and, further, that at long wavelengths the increasing transparency of carbon black and silica suggest that the retro-reflection is likely to be somewhat larger.

(*d*) *The specular reflection factor* $\rho_{sp}(x)$. This is considered to lead to uncertainties in $G(x)$ and hence $F(\epsilon, a)$ of less than 2×10^{-5}. In evaluating the effective temperature of the radiator, the specular reflection plays a significant role when temperature gradients are unusually large. That it correctly represents the optical behaviour of the paint is indicated by the fact that no systematic difference in measured values of $T - T_{68}$ has been observed that can in any way be related to the presence of temperature gradients. Any such effects were less than the standard deviation in $(T - T_{68})$ values, equivalent to 2×10^{-5} in $F(\epsilon, a)$.

(*e*) *The absence of higher-order terms in* (42), (48), (50) *and* (52). This is estimated to be 3 parts in 10^5 for the large pair of apertures and 1 part in 10^5 for the small pair of apertures.

(*f*) *The uncertainty in the geometrical disposition of the calorimeter and upper aperture.* Since $a(y)$ increases very rapidly as the element dy approaches the aperture, any displacement of the calorimeter along its axis towards or away from the aperture could make a significant difference to the value of $G(x)$. The mechanical design is such that the distance from the bottom of the calorimeter to the aperture should be 2 mm. If instead this distance were 4 mm, the value of $G(x)$ would increase by 3×10^{-5} for the large pair of apertures. The tolerances are such that the uncertainty in the separation of the upper aperture is estimated to be 2 mm and hence we

take this uncertainty to be 3×10^{-5} for the large pair of apertures. It is negligible for the small pair.

Taking all these uncertainties (a)–(f) together and considering them to be independent we find, from the square root of the sum of the squares, that for the large apertures we have an uncertainty of 1.4×10^{-4}, and for the small apertures an uncertainty of 1×10^{-4}, so that

$$F(\epsilon, a) = 0.999\,39 \pm 0.000\,14 \text{ (large apertures)},$$

$$F(\epsilon, a) = 0.999\,73 \pm 0.0001 \text{ (small apertures)}.$$

The most significant contributing factors to these uncertainties are the uncertainty in (c), the long-wavelength retro-reflection, and in (b), the weighted diffuse reflectance of the paint. The possibility of a significant reduction in these two sources of uncertainty is discussed in §11.

5. The apertures

(a) *Manufacture and measurement*

Two pairs of apertures were employed to enable systematic errors varying with aperture size to be detected. The principal pair had diameters of 18 and 26 mm for the lower and upper apertures respectively. These dimensions were chosen to give the best compromise between conflicting requirements. A large diameter reduces diffraction and measurement errors and facilitates construction, while a small diameter is needed to reduce black-body errors. The second pair of apertures had diameters of 10 and 18 mm. In both pairs the lower aperture was made smaller in diameter than the upper one to reduce the amount of radiation that could scatter through the upper aperture after direct specular reflection between them.

The shape of the apertures is shown in figure 20. The system comprising the apertures and the radiation trap (shown in figure 28) was designed to meet the following requirements:

(a) diffraction and scattering effects should be minimized;

(b) the thermal contraction on cooling from room temperature to liquid-helium temperatures should be known and should not lead to significant distortion;

(c) the design and choice of material should allow repeated assembly of the system, and allow measurement of the aperture diameters and their separation to within a few parts in 10^5 at room temperature.

This last requirement was one of the most difficult to meet, since it requires that the edges of the apertures be sufficiently well defined to allow meaningful measurements to be made of diameter to within about 0.5 μm and of the distance between them to within about 2 μm.

To reduce diffraction effects it is necessary (see §1 (d)) to arrange for hemispherical illumination of the lower aperture by the radiator, and hemispherical collection of transmitted radiation at the upper aperture. This is helped by making the conical entry to the lower aperture and the similar conical exit from the upper one as highly reflecting as possible. The apertures should have as sharp an edge as is consistent with the requirements that the edges have a well defined geometry and are not damaged by the measurement process.

It was originally decided to make the apertures and radiation trap of copper, because it was the only material whose thermal contraction down to liquid-helium temperatures was sufficiently well known. In addition, being a pure metal having a high thermal conductivity,

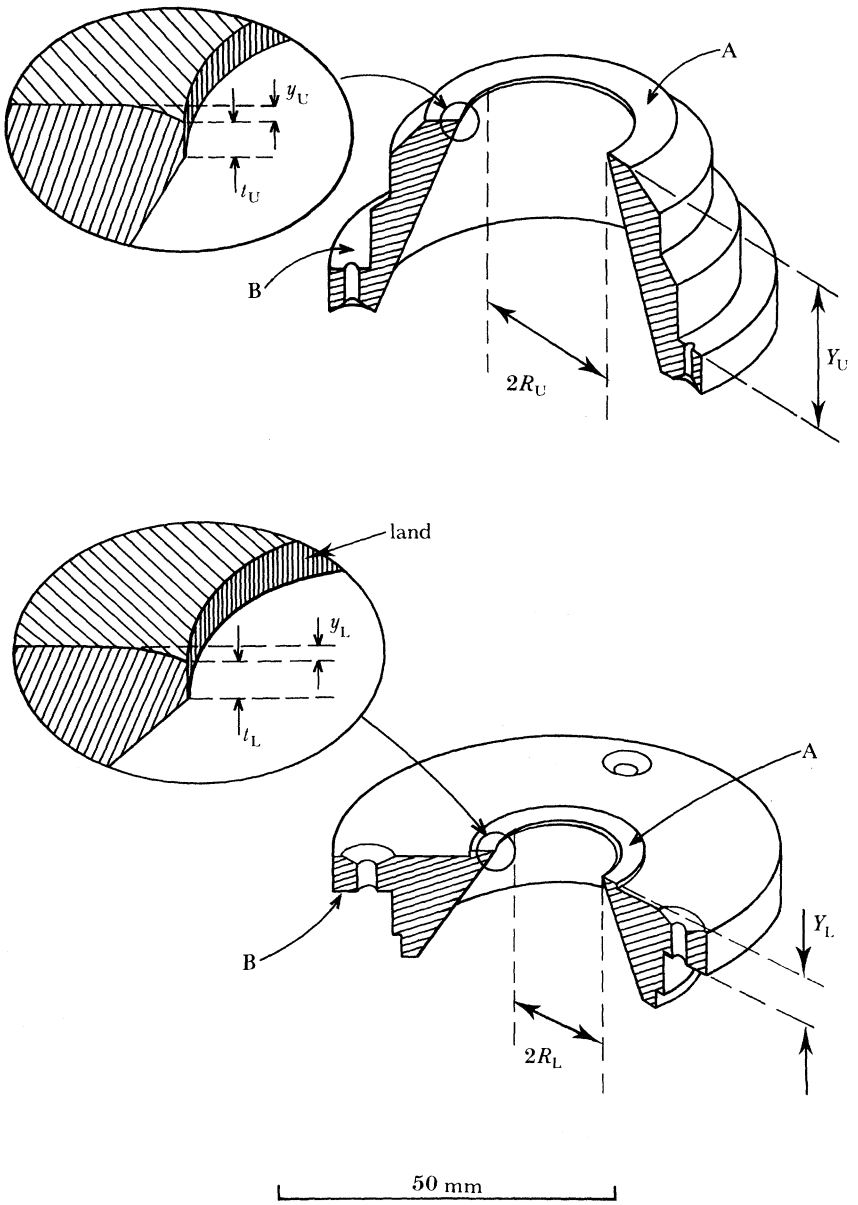

FIGURE 20. Cut-away sketches of the upper and lower apertures (large pair). A and B reference surfaces (see figure 28 and text for explanation of these and other symbols).

distortion on cooling was likely to be small. However, although the radiation trap was successfully made in pure copper, it was found impossible to make satisfactory apertures from the same material. The aperture edges could not be made sufficiently sharp: a rounded profile having a radius of curvature of between ten and twenty micrometres being obtained. It was eventually decided to make them instead from Cu–1.8 %Be (Be–Cu 250, Telcon Metals Ltd). This can be precipitation hardened by heat treatment to a Vickers hardness number between 350 and 400, and has good machining and lapping properties.

The apertures were first machined in the soft state and then, after heat treatment, the conical entry and the flat reference surfaces were lapped. The completed aperture was held in a specially

constructed and hardened 'Pitho-Steel' jig having a precisely aligned central hole through which a 'Tufnol' lap impregnated with diamond paste could be pushed. In this way it was ensured that the edges of the apertures, although less than 100 μm wide, were precisely cylindrical, having an axis normal to the front face. Photographs of the Cu–Be apertures taken with a scanning electron microscope are shown in figure 21. After the final lapping of the lands, the conical surfaces were coated with an evaporated layer of gold to enhance the reflectance.

The roundness of the apertures was measured with a 'Talycenta' (Rank Taylor-Hobson Ltd), and from the traces produced by this instrument (figure 22), the positions of the minimum and maximum diameters were identified. This information allowed the apertures to be positioned on the NPL 'Internal-Diameter Measuring Machine' (manufactured by Quantum Science Ltd) for these diameters to be measured.

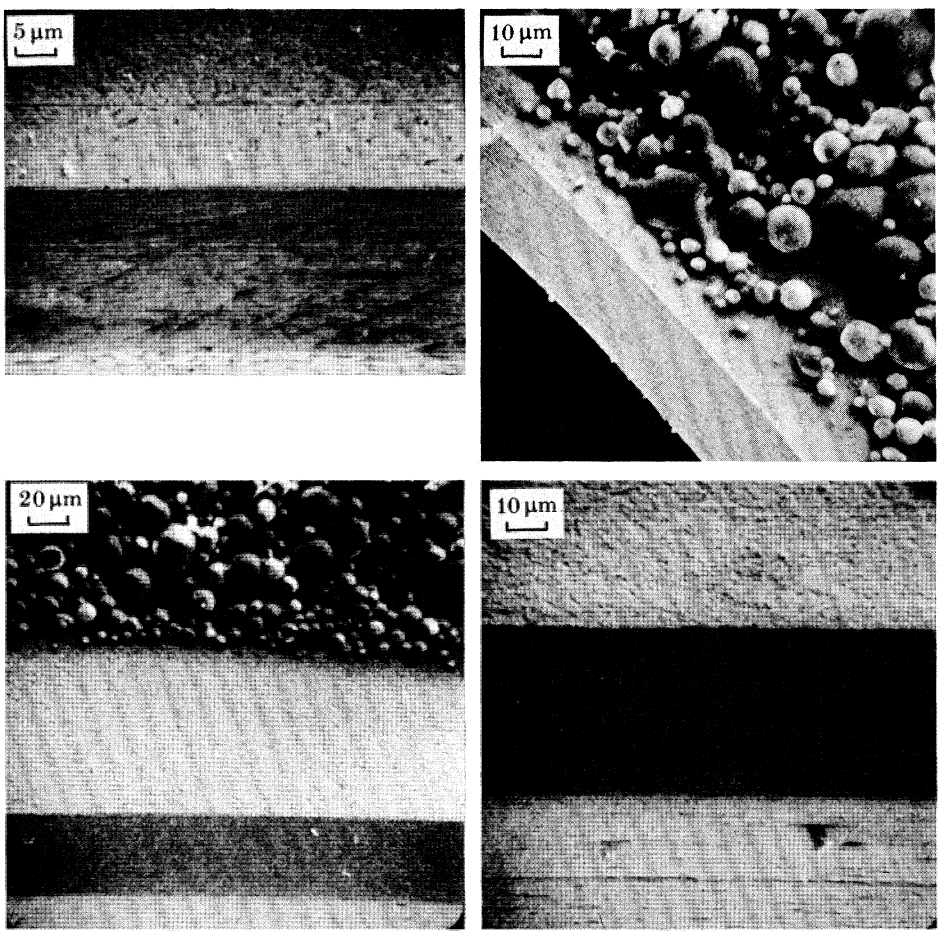

FIGURE 21. Representative views of the edges of the four apertures obtained by a scanning electron microscope. In some views the silica spheres of the 3M black paint are visible.

The results of measurements of the diameter of the apertures together with associated uncertainties are shown in table 5. Preliminary measurements showed that, as expected, the dimensions of the apertures were unaffected by repeated cycling to liquid-helium temperatures. It was also necessary to measure the distances Y_U and Y_L on the upper and lower apertures, respectively: these are the distances between the plane surfaces that define the front of the

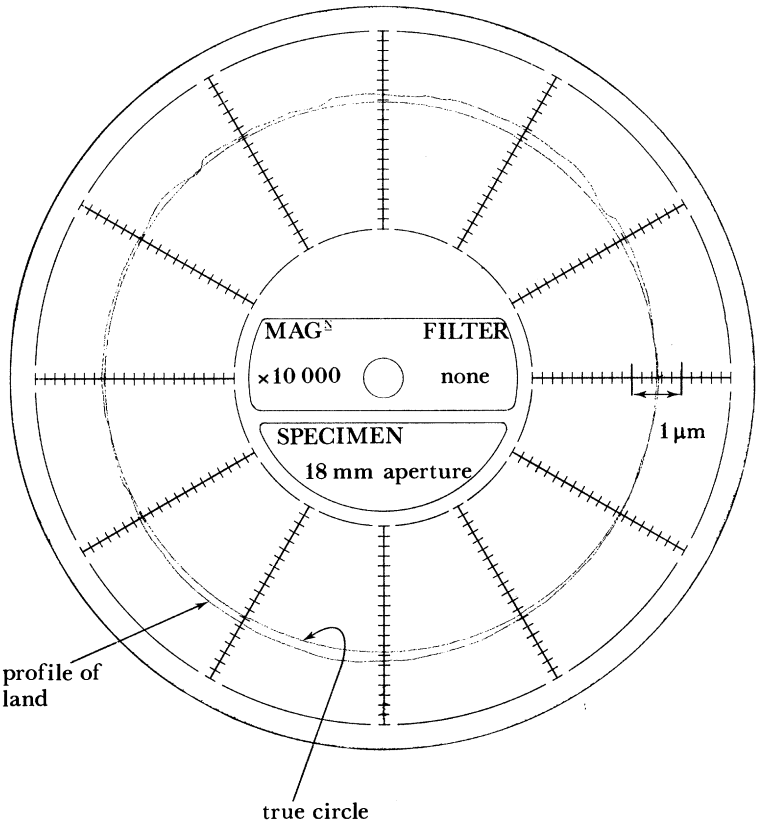

FIGURE 22. The circularity of the apertures: 'Talycenta' trace for the 18 mm diameter lower apperture.

TABLE 5. THE DIMENSIONS OF THE APERTURES (IN MILLIMETRES) AT 293 K

(See figures 20 and 28.)

large pair of apertures

upper aperture	lower aperture
December 1980	
$2R_U(\max) = 26.1014$, $2R_U(\min) = 26.1008$ } $2R_U(\text{ave}) = 26.1011$	$2R_L(\max) = 18.1538$, $2R_L(\min) = 18.1533$ } $2R_L(\text{ave}) = 18.1536$
$Y_U = 21.4727$, $y_U = 0.0012$,	$Y_L = 4.9629$, $y_L = 0.0003$,
$t_U = 0.100$	$t_L = 0.055$
January 1983	
$2R_U(\max) = 26.104$, $2R_U(\min) = 26.1006$ } $2R_U(\text{ave}) = 26.1010$	$2R_L(\max) = 18.1537$, $2R_L(\min) = 18.1535$ } $2R_L(\text{ave}) = 18.1536$
$a = 0.0028$	$b = 0.0070$

small pair of apertures

upper aperture	lower aperture
February 1983	
$2R_U(\max) = 18.2469$, $2R_U(\min) = 18.2467$ } $2R_U(\text{ave}) = 18.2468$	$2R_L(\max) = 10.2014$, $2R_L(\min) = 10.2013$ } $2R_L(\text{ave}) = 10.2014$
$Y_U = 21.3390$, $y_U = 0.0000$,	$Y_L = 4.9080$, $y_L = 0.0003$,
$t_U = 0.046$, $a = 0.0026$	$t_L = 0.028$, $b = 0.0042$
December 1983	
$2R_U$(one measurement) = 18.2467	$2R_L$(one measurement) = 10.2010

Estimated uncertainties in the measurements are: for $2R_U$ and $2R_L$, ± 0.0003 mm; for Y_U and Y_L, ± 0.0002 mm; for y_U and y_L, ± 0.0003 mm; for t_U and t_L, ± 0.002 mm and for a and b, ± 0.0005 mm.

apertures (A in figure 20) and the rear annular reference surfaces B, which are the locating surfaces of the apertures with respect to the radiation trap. These were measured by using either a 'Tesa' electronic indicator (Tesa S.A.) or a Trimos Vertical 500 (Trimos S.A.). These distances are needed for the calculation of the overall distance between the apertures, which we shall come to in §6.

Although the mean plane A of the front surface of the aperture is well defined, the final lapping of the land resulted in a small distortion of the front face close to the edge. This is shown in the insets of figure 20. These distortions were measured with a Hilger & Watts interference microscope and hence the values of the small corrections y_U and y_L were deduced. A more significant correction is due to small departures from flatness of the reference surfaces B of the apertures. These departures from flatness were in the range 2–7 μm; they are referred to in table 5 and figure 28 as a and b for the upper and lower apertures, respectively, and were measured by a Talycenta.

Finally, each of the apertures was examined in a scanning electron microscope to ensure that the edges were sharp and that there were no burrs. Photographs taken with the electron microscope (shown in figure 21) allowed the widths of the lands (t_U and t_L in figure 20) to be deduced from a knowledge of the angle of view and magnification of the microscope.

After the final measurements of the distances Y and y had been made, the front faces A were hand painted with 3M-C 101 black. Ideally, the surface A should be non-reflecting right up to the aperture edge to reduce the contribution from specular reflections to the measured radiant power. This was not possible, however, as the presence of paint at the aperture edge renders its geometrical position somewhat indeterminate. The layer of paint, therefore, extended to about 80 μm from the edge. The paint was applied by hand under an optical microscope. The paint is visible in some of the electron microscope photographs of figure 21. We show later that the remaining annular ring of reflecting Cu–Be makes a small but significant contribution to the scattered radiation entering the calorimeter.

(*b*) *Thermal expansion of* Cu–Be

The thermal expansion of Cu–Be between liquid-helium temperature and room temperature was not well known at the outset of this work. The eventual choice of Cu–Be in place of pure copper was only made possible by an offer, by C. A. Swenson of Iowa State University, to measure it for us. The results of this work by Holtz & Swenson (1983) showed that there is a significant difference between the expansion coefficients of pure copper and Cu–Be and that, further, the precipitation-hardened alloy differs significantly from the solution-heat-treated alloy at temperatures below about 100 K. Similar results, although of somewhat lower accuracy, but obtained by a novel technique, were subsequently obtained by Radcliffe *et al.* (1983).

The fractional change in linear dimension of precipitation-hardened Cu–Be, $[L(T)-L(293.15\text{ K})]/L(293.15\text{ K})$ for $T \leqslant 20$ K, was found by Holtz & Swenson to be -3.071×10^{-3}, which is to be compared with the equivalent value of -3.257×10^{-3} for pure copper (Kroeger & Swenson 1977). These figures have been used in the calculation of g in §6. Their uncertainty is estimated to be $\pm0.1\,\%$, which implies an additional uncertainty in our diameters at low temperatures of ±3 parts in 10^6. This does not contribute significantly to the overall uncertainty in g.

(*c*) *Reflections at the aperture lands*

The fraction of the radiant flux reaching the calorimeter that comes by reflection from the edges (or lands) of the apertures is not negligible. Were the lands perfectly reflecting, the size of this fraction would be of no consequence, but unfortunately this is not the case. Indeed, as we shall see, at the high angles of incidence that occur for such reflections ($\geqslant 77°$) the reflectance falls substantially below that at normal incidence and only recovers and then exceeds its normal-incidence value at angles greater than 89.8°.

First of all, however, we ignore this variation of reflectance with angle of incidence and make an approximate estimate of the magnitude of the fraction by using very simple angle-factor algebra. Although providing only an approximate expression, it is nevertheless useful because the expression is correct in the limit of small values of R_L/D and R_U/D (where D is the distance between the apertures) and is thus a useful check on the more complex calculation that is made later.

From angle-factor algebra we know that the fraction f_{L-U} of the radiation leaving a uniform, lambertian circular disc of radius R_L, which reaches a second disc of radius R_U a distance D from the first disc and coaxial with it, is given by

$$f_{L-U} = \frac{R_U^2}{D^2 + R_U^2 + R_L^2}. \tag{57}$$

This expression is a sufficiently good approximation when R_L and $R_U \ll D$. The exact expression is given in (81) in §6 (*c*), which deals with the optical properties of the radiation trap. If the second disc is displaced along the common axis by an amount δD_U, we can write

$$\frac{\delta f_{L-U}}{\delta D_U} = -\frac{2DR_U^2}{(D^2 + R_U^2 + R_L^2)^2} \tag{58}$$

and hence

$$\frac{\delta f_{L-U}}{f_{L-U}} = -\frac{2D\,\delta D_U}{D^2 + R_U^2 + R_L^2} \approx -\frac{2\,\delta D_U}{D}. \tag{59}$$

This expression gives approximately the fraction of the radiation passing through the upper aperture after reflection from the land of the upper aperture. Similarly, the fraction of the radiation passing through the upper after reflection from the land of the lower aperture is given by $2\,\delta D_L/D$. For the large pair of apertures we find that $\delta D_L (= t_L) = 55$ μm, $\delta D_U (= t_U) = 100$ μm and $D = 100$ mm; so that the sum of the two estimated fractions calculated in this way is 0.3 %. For the correction due to absorption at the lands to be less than 0.01 % we thus require that the absorptance at the lands be less than about 0.03. Since this is about the absorptance of many metals in the infrared, it is clear that a much more careful evaluation of this correction is required. To do this we first estimate the absorptance (equal to one minus the reflectance) of Cu–Be over a range of wavelengths and at high angles of incidence at temperatures near 4 K, and we then make a more exact calculation of the fractions given approximately by $2\,\delta D/D$.

(*d*) *Low-temperature reflectance of* Cu–Be

We do not know of any measurements of the reflectance of Cu–Be at low temperatures and at high angles of incidence ($\geqslant 77°$). The sole experimental measurements (see table 6) of the reflectance of Cu–Be in the infrared, of which we are aware, were made at room temperature

TABLE 6. THE NORMAL SPECTRAL REFLECTANCE AND RESISTIVITY OF Cu–Be

(The normal spectral reflectance of Cu–Be: (*a*) measured values of Holmes *et al.* (1973); (*b*) corrected values taken to apply to our Cu–Be following measurement by Freeman (1983).)

reflectance

λ/μm	(*a*)	(*b*)
1	0.943	0.940
5	0.974	0.970
10	0.979	0.976
15	0.982	0.979
20	0.983	0.980

resistivity

	resistivity/$\mu\Omega$ cm	
T/K	hard[1]	soft[2]
293	6.462	9.337
77	4.34	6.705
4.2	4.016	6.705

(1) Annealed for 2 h at 330 °C (precipitation hardened).
(2) Annealed for 1 h at 800 °C (beryllium in solid solution).

and cover the wavelength range from 1 to 20 μm (Holmes *et al.* 1973). Nevertheless, it is possible to make an estimate of the low-temperature reflectance of Cu–Be on the basis of these measurements and the following information: our measurements of the d.c. resistivity of Cu–Be at 293, 77 and 4.2 K (also given in table 6); the theory of the optical properties of metals and alloys (see, for example, Sievers 1978); the experimental values of the low-temperature reflectance and d.c. resistivity of certain aluminium alloys (Tsujimoto *et al.* 1982*a*) and measurements made for us of the room-temperature reflectance at normal and high angles of incidence of Cu–Be and pure copper (Freeman, personal communication 1983).

At wavelengths of concern to us, namely those between about 2 and 400 μm, the frequency ω of the radiation is very much less than the plasma frequency and so we can consider the interaction of the electromagnetic radiation with the metal in terms of its surface impedance Z, which is a complex quantity and a function of frequency, and which we can write as $Z = R + \mathrm{i}X$. If Z_0 is the impedance of free space, the normal reflectance of the metal is given by (Sievers 1978)

$$\rho(0) = \left(\frac{1 - Z/Z_0}{1 + Z/Z_0}\right)^2 \tag{60}$$

and the normal absorptance by

$$\alpha(0) = 1 - \rho(0) = \frac{4(R/Z_0)}{(1 + R/Z_0)^2 + (X/Z_0)^2}. \tag{61}$$

Since we know that R/Z_0 and $X/Z_0 \ll 1$, the normal absorptance becomes simply

$$\alpha(0) \approx 4R/Z_0. \tag{62}$$

Now, the calculation of R/Z_0 is difficult because R depends upon the details of the interaction of the electromagnetic radiation with the metal. However, we have enough other information available for us to be able to make a reasonable estimate of the value of $\alpha(0)$, and hence of $4R/Z_0$, at low temperatures. We make this estimate in the following way.

The room-temperature normal reflectance data of Cu–Be given by Holmes *et al.* (1973),

shown in table 6, are for a highly polished mirror surface. The surface of our Cu–Be at the aperture lands is certainly less well polished than this and would have a higher surface impedance and hence a higher absorptivity. Evidence for this is given by measurements made for us by Freeman (personal communication 1983). He measured at room temperature the ratio of the reflectance of a sample of highly polished copper to that of a sample of our Cu–Be, at normal and 76° incidence, at a wavelength of about 25 μm. At normal incidence the ratio was found to be 1.0077 ± 0.0010 compared with the value of 1.005 ± 0.001 based upon the results of Holmes *et al.* (1973). We have, therefore, made the appropriate correction to their results and taken the corrected values to apply to our Cu–Be. They are given in table 6 and figure 23. This figure also shows the normal spectral reflectance of an aluminium alloy, from Tsujimoto *et al.* (1982*a*), which has electrical resistivities at room-temperature and liquid-helium temperatures very close to those of Cu–Be (see table 6).

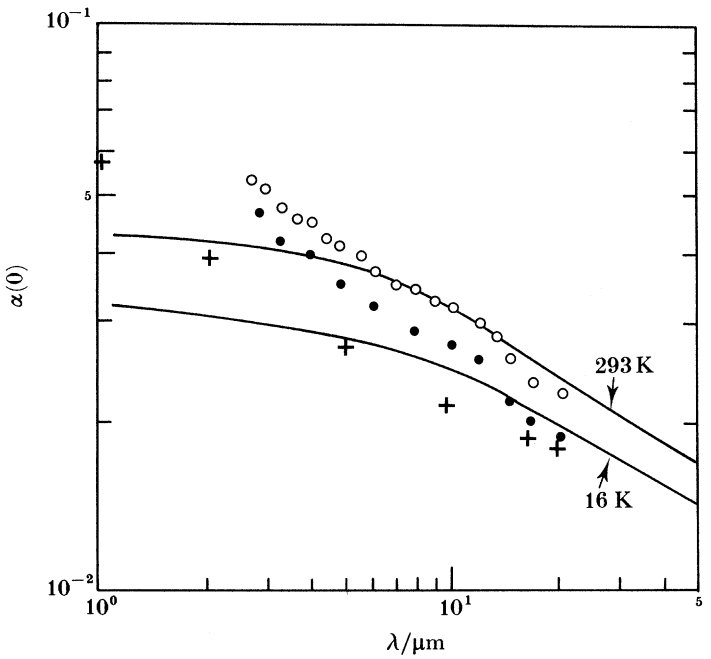

FIGURE 23. The spectral normal absorptance, $\alpha(0)$, of Cu–Be, at 293 K: +, Holmes *et al.* (1973); ○, an aluminium alloy at 306 K; ●, 16 K; ——, calculations of Tsujimoto *et al.* (1982*a*, *b*).

The room-temperature normal spectral reflectance and the temperature dependence of the electrical resistivity of both the aluminium alloy studied by Tsujimoto *et al.* (1982*a*) and our samples of Cu–Be are very similar. We have therefore assumed that the temperature dependence of the normal spectral reflectance of Cu–Be is similar to that of their aluminium alloy. Figure 24 shows the low-temperature normal spectral reflectance of our Cu–Be alloy deduced on this basis together with our estimate of the uncertainty.

Remembering that the normal absorptance is given by $4R/Z_0$, we can obtain the absorptance at high angles of incidence by making use of the Fresnel relations, which lead to

$$\epsilon_{\parallel}(\theta) = \alpha_{\parallel}(\theta) = \frac{(4R/Z_0)\cos\theta}{\cos^2\theta + (2R/Z_0)\cos\theta + (R^2+X^2)/Z_0^2} \tag{63}$$

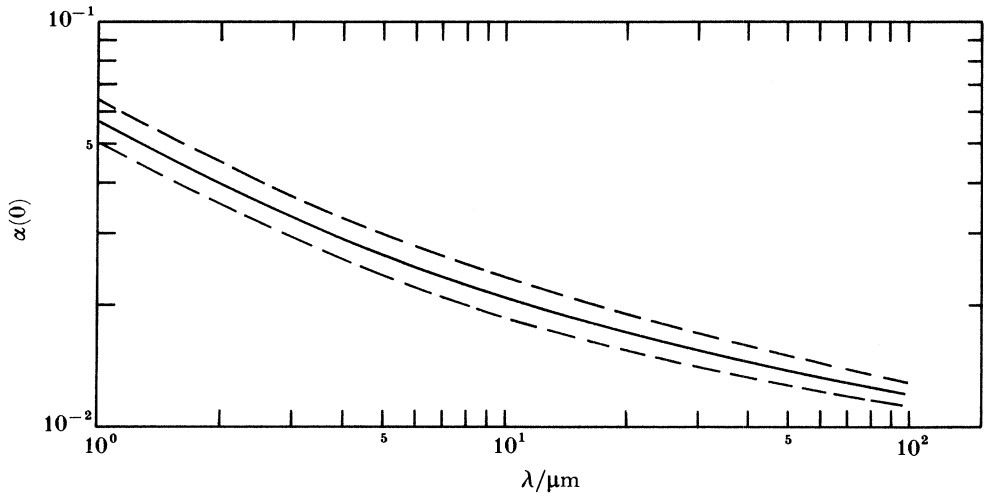

FIGURE 24. Estimated spectral normal absorptance of our Cu–Be at liquid-helium temperatures. The broken lines indicate the estimated uncertainty.

and
$$\epsilon_\perp(\theta) = \alpha_\perp(\theta) = \frac{(4R/Z_0)\cos\theta}{1+(2R/Z_0)\cos\theta}, \tag{64}$$

where $\epsilon_\parallel(\theta)$ and $\alpha_\parallel(\theta)$ are the emissivity and absorptivity, respectively, for linearly polarized radiation having the plane of vibration of the electric vector parallel to the plane of incidence, and $\epsilon_\perp(\theta)$ and $\alpha_\perp(\theta)$ are the same, but for the plane of vibration normal to the plane of incidence, all at an angle of θ to the normal.

Also,
$$\epsilon(\theta) = \tfrac{1}{2}[\epsilon_\parallel(\theta)+\epsilon_\perp(\theta)] \quad \text{(unpolarized)} \tag{65}$$

and the maximum absorptance occurs at an angle of incidence θ_m given by $\theta_m = \arccos(2R/Z_0)$.

Using values of R/Z_0 deduced from the values of $\alpha(0)$ given in figure 24, we can now calculate the absorptance and reflectance for high angles of incidence. Figure 25 shows the calculated reflectance of Cu–Be at low temperatures and for angles of incidence greater than 77°, for a wavelength of about 20 μm. For the aperture geometries in question, the angle of incidence for land reflections lies within the range shown in the figure.

By using (63) and (64), the ratio of the spectral reflectances of Cu–Be and pure copper have been calculated for an angle of incidence of 76°. For Cu–Be, the normal spectral absorptance was taken from table 6 column (*b*), for a wavelength of 20 μm. For pure copper the value was deduced from the measurements of Holmes *et al.* (1973). The calculated ratio of reflectances was 0.968. This is in good agreement with the value of 0.967 ± 0.001 measured by Freeman (personal communication 1983) at the same angle of incidence. Although not a fully independent result, it nevertheless gives further support to the small adjustment we have made to the measured values of Holmes *et al.*

(*e*) *Land reflections; a more detailed treatment*

Having made an estimate of the likely reflectance of the lands as a function of angle and wavelength, we now come to the more detailed analysis of the reflection losses at the lands.

We take first the thermal radiation from the black body that reaches the upper aperture after

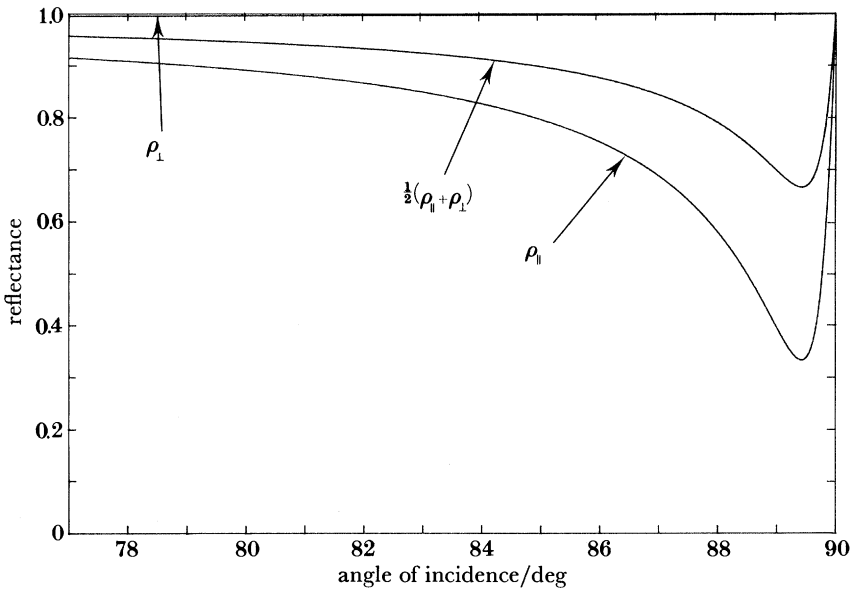

FIGURE 25. The reflectance of Cu–Be, for the components polarized normal, $\rho_\perp$, and parallel, $\rho_\parallel$, to the surface, as a function of angle of incidence at a wavelength of 20 μm, calculated by using (63) and (64) with $R/Z_0 = 0.005$.

a specular reflection at the land of the lower aperture. The geometry of the calculation is shown in figure 26*a*. The width of the land is t_L, the distance between the apertures D, and their radii R_L and R_U; for the purposes of the calculation we take $t \ll R_L$, and $R_L \approx R_U \approx 0.1D$. From the figure, we can write down an expression for the radiant flux dJ_L reaching an element dS in the upper aperture and reflected from an element dL on the land, having a projected area dA in the direction of dS, which is irradiated by radiation of radiance $J(T)$ from the radiator:

$$dJ_L = J(T)\, dA \frac{dS}{\pi(D^2+c^2)} \cos\beta\, \alpha(\theta) \tag{66}$$

$$= J(T)\, R_L\, d\Psi t_L \frac{c}{(D^2+c^2)^{\frac{1}{2}}} \cos\psi \frac{c\, d\psi\, dc}{\pi(D^2+c^2)} \frac{D}{(D^2+c^2)^{\frac{1}{2}}} \alpha(\theta) \tag{67}$$

$$= J(T) \frac{t_L D R_L}{\pi} \frac{c^2}{(D^2+c^2)^2} \alpha(\theta)\, d\Psi \cos\psi\, d\psi\, dc, \tag{68}$$

where $\alpha(\theta)$ is the absorptance of the land given by the sum of equations (63) and (64). By writing $(2R/Z_0) = B$ so that $B = \frac{1}{2}\alpha(0)$ and assuming that $(R/Z_0)^2$ and $(X/Z_0)^2 \ll 1$, the absorptance

$$\alpha(\theta) = 2B \cos\theta\, [(\cos^2\theta + 2B\cos\theta + B^2)^{-1} + (1+2B\cos\theta)^{-1}] \tag{69}$$

in which

$$\cos\theta = c(D^2+c^2)^{-\frac{1}{2}} \cos\psi. \tag{70}$$

The variation of $\alpha(0)$ with wavelength is shown in figure 24.

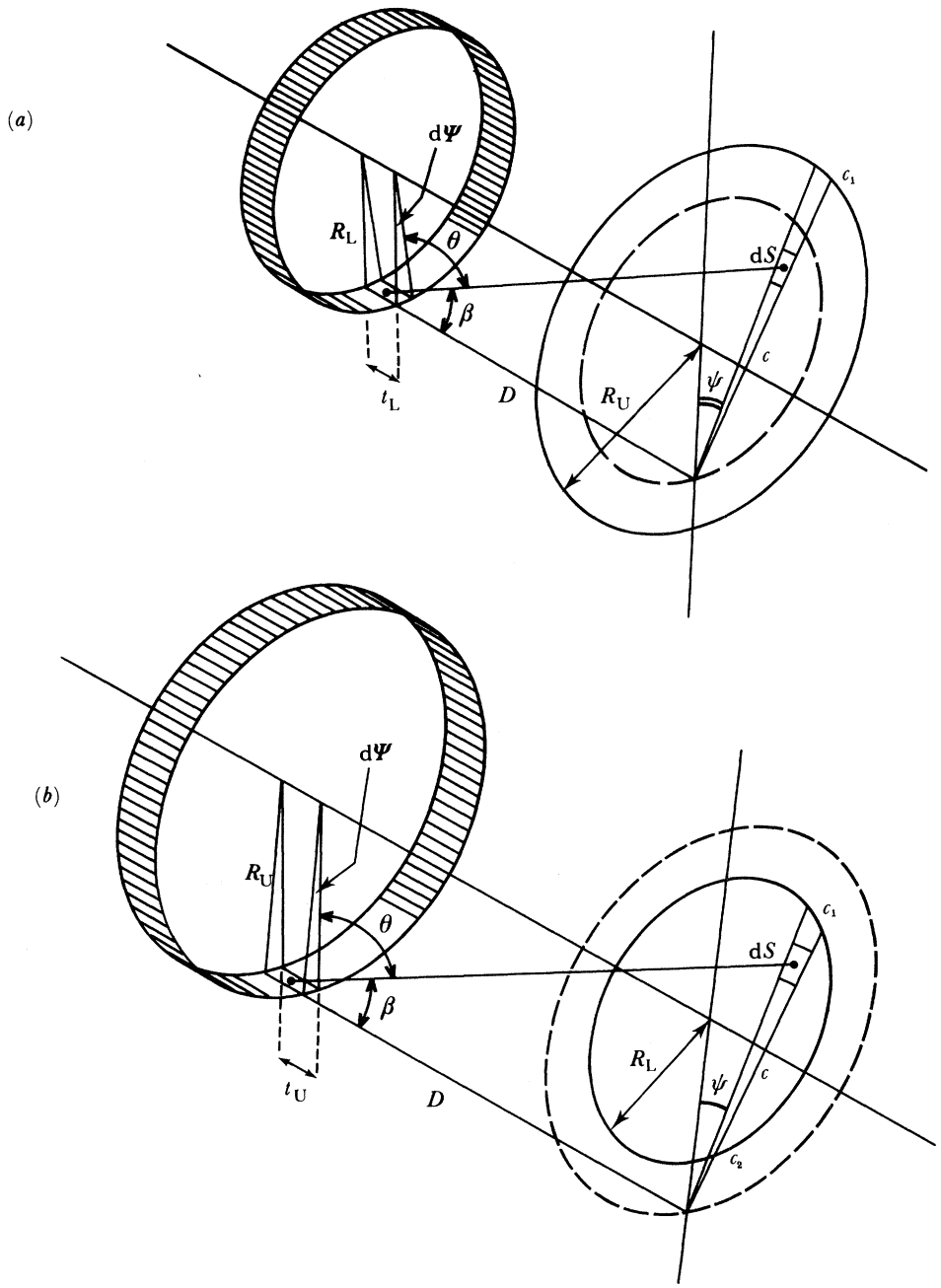

FIGURE 26. The geometry used in the derivation of the expressions for absorption at the aperture lands (equation (66) etc.).

The radiant flux incident over the whole of the upper aperture coming from the whole of the land on the lower aperture is thus

$$J_L = J(T) \int_{\Psi=0}^{2\pi} 2R_L \frac{t_L D}{\pi} \, d\Psi \int_{\psi=0}^{\frac{1}{2}\pi} \cos\psi \, d\psi \int_{c=0}^{c_1} \frac{c^2}{(D^2+c^2)^2} \alpha(\theta) \, dc, \tag{71}$$

where

$$c_1 = R_L \cos\psi + (R_L^2 \cos^2\psi - R_L^2 + R_U^2)^{\frac{1}{2}} \tag{72}$$

By integrating with respect to Ψ this leads to

$$J_L = 4J(T)\, R_L\, t_L\, D \int_{\psi=0}^{\frac{1}{2}\pi} \cos\psi \, d\psi \int_{c=0}^{c_1} \frac{c^2}{(D^2+c^2)^2}\, \alpha(\theta)\, dc. \tag{73}$$

The fraction F_L of the total radiant flux passing from the lower aperture through the upper that comes after reflection from the lower land is thus given by

$$F_L = J_L/[J(T)\, g], \tag{74}$$

where g is the geometrical throughput given by (81) and the ratio $J_L/J(T)$ may be found from (73).

We come now to the radiant flux that comes from the lower aperture and strikes the land of the upper aperture. This is of course identical to the radiant flux that would come from the annulus of the upper aperture through the lower aperture if the direction of the radiation were reversed, and it is in this way that we calculate it. The geometry for the calculation is shown in figure 26*b*. The calculation is similar to that for F_L, except that the limits of integration are different.

As before, we write down an expression for the flux dJ_U reaching an element dS in the lower aperture from an element dU on the land of the upper aperture:

$$dJ_U = J(T)\, R_U\, d\Psi \frac{t_U\, D}{\pi} \frac{c^2}{(D^2+c^2)^2} \cos\psi \, d\psi \, dc\, \alpha(\theta), \tag{75}$$

but now

$$J_U = 2J(T) \frac{R_U\, t_U\, D}{\pi} \int_{\Psi=0}^{2\pi} d\Psi \left[\int_{\psi=0}^{P} \cos\psi \, d\psi \int_{c=0}^{c_1} \frac{c^2}{(D^2+c^2)^2}\, \alpha(\theta)\, dc \right.$$
$$\left. - \int_{\psi=0}^{P} \cos\psi \, d\psi \int_{c=0}^{c_2} \frac{c^2}{(D^2+c^2)^2}\, \alpha(\theta)\, dc \right], \tag{76}$$

where $P = \arcsin(R_L/R_U)$ and

$$c_1 = R_U \cos\psi + (R_U^2 \cos^2\psi - R_U^2 + R_L^2)^{\frac{1}{2}} \quad \text{and} \quad c_2 = R_U \cos\psi - (R_U^2 \cos^2\psi - R_U^2 + R_L^2)^{\frac{1}{2}}. \tag{77}$$

The fraction F_U of the total radiant flux passing from the upper aperture through the lower that comes after reflection from the upper land is

$$F_U = J_U/[J(T)\, g], \tag{78}$$

where the ratio $J_U/J(T)$ may be evaluated by using (76). This is identical to the fraction we require, namely the fraction of radiation from the lower aperture passing through the upper aperture that strikes the upper land.

Equations (74) for F_L and (78) for F_U are more exact expressions than the one derived at the beginning of this section (equation (59)); but setting $\alpha(\theta) = 1$ we find that numerical evaluation leads to values of F_U and F_L, which, in the limit of large D/R_U or D/R_L, are asymptotically approached by the value given by (59). These expressions for the fractions F_L and F_U do not take into account the variation of $\alpha(\theta)$ with wavelength shown in figure 24 for normal incidence. To do this it is necessary to convolute these expressions with the Planck distribution $J(\lambda, T)$. We wish to obtain the fraction of the radiation from the black body at

temperature T that is lost due to absorption at the lands. This fraction, $\{F_L(\lambda, T) + F_U(\lambda, T)\}$, which we subsequently refer to as $L(T)$, is given by

$$L(T) = \left[\int_{\lambda=0}^{\infty} F_L J(\lambda, T)\, d\lambda + \int_{\lambda=0}^{\infty} F_U J(\lambda, T)\, d\lambda\right] \Big/ \int_{\lambda=0}^{\infty} J(\lambda, T)\, d\lambda \qquad (79)$$

in which F_L and F_U are given by (74) and (78). Numerical integration of these expressions leads to results shown in table 7.

TABLE 7. FRACTIONAL LOSSES DUE TO ABSORPTION AT THE APERTURE LANDS

T/K	$10^4 F_L(\lambda T)$	$10^4 F_U(\lambda T)$	$10^4 L(T)$
	large-aperture pair (t_L = 55 μm, t_U = 100 μm)		
233	0.98±0.08	1.33±0.11	2.31±0.19
273	1.02±0.09	1.39±0.12	2.41±0.21
373	1.11±0.11	1.53±0.14	2.64±0.25
	small-aperture pair (t_L = 28 μm, t_U = 46 μm)		
233	0.82±0.06	0.87±0.07	1.69±0.07
273	0.86±0.07	0.92±0.08	1.78±0.15
373	0.93±0.10	1.01±0.10	1.94±0.20

The values of $L(T)$ given in table 7 are shown in figure 27 as a function of temperature. The uncertainties shown in the table, and by the broken lines in figure 27, are obtained by re-evaluating (74) and (78) for the upper and lower estimates of $\alpha(0)$, shown by the broken lines in figure 24. Since the uncertainties in F_L and F_U are strongly correlated, the uncertainty in $L(T)$ is the arithmetic sum of the uncertainties in F_L and F_U.

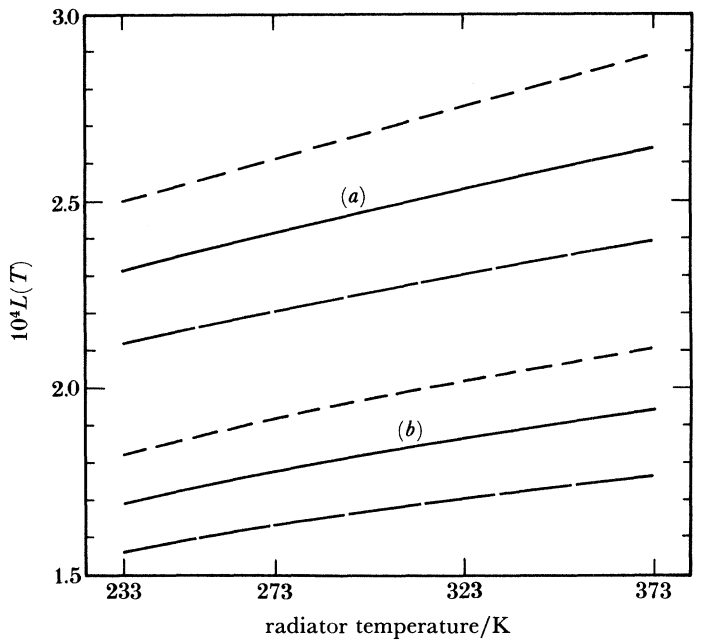

FIGURE 27. The fractional corrections, to be added to the measured radiant energies, due to absorption at the aperture lands, (a) for the large pair of apertures and (b) for the small pair. The broken lines show uncertainties stemming from the uncertainties in $\alpha(0)$ (cf. figure 24).

6. The radiation trap and shutter

(*a*) *The construction of the radiation trap*

The radiation trap and shutter assembly are shown in figure 12. The function of the radiation trap is twofold: first it must absorb the radiation passing through the lower aperture that is not in the direct beam to the upper aperture, and second it must act as the support for the apertures and define the distance between them. Both of these functions are crucial to the success of the measurements.

The radiation trap (see figure 28) is made from o.f.h.c. copper and constructed in the form of an open drum to which is bolted a lower circular copper plate. Various surfaces are lapped, indicated by heavy lines in the figure, and are designed to act as reference surfaces during the assembly and measurement procedure. The inside of the radiation trap is lined with baffle plates having multiple V-grooves on the inside faces. These baffle plates are also made from o.f.h.c. copper and have copper strips soldered between the V-grooves, as shown in figure 12, and also figure D 1 in Appendix D. The edges of these copper strips were honed to a fine edge before the V-grooves and strips were painted with 3M-C 101 black. After baking and before assembly in the radiation trap, the painted edges of the copper strips were filed to a sharp edge to reduce scattering of radiation to a minimum. This was an important operation because scattering from the edges of strips is, as we shall see, one of the sources of scattered radiation entering the calorimeter. It was also a very time-consuming operation since there are some 230 individual strips, giving a total length of more than 16 m of edge to be sharpened!

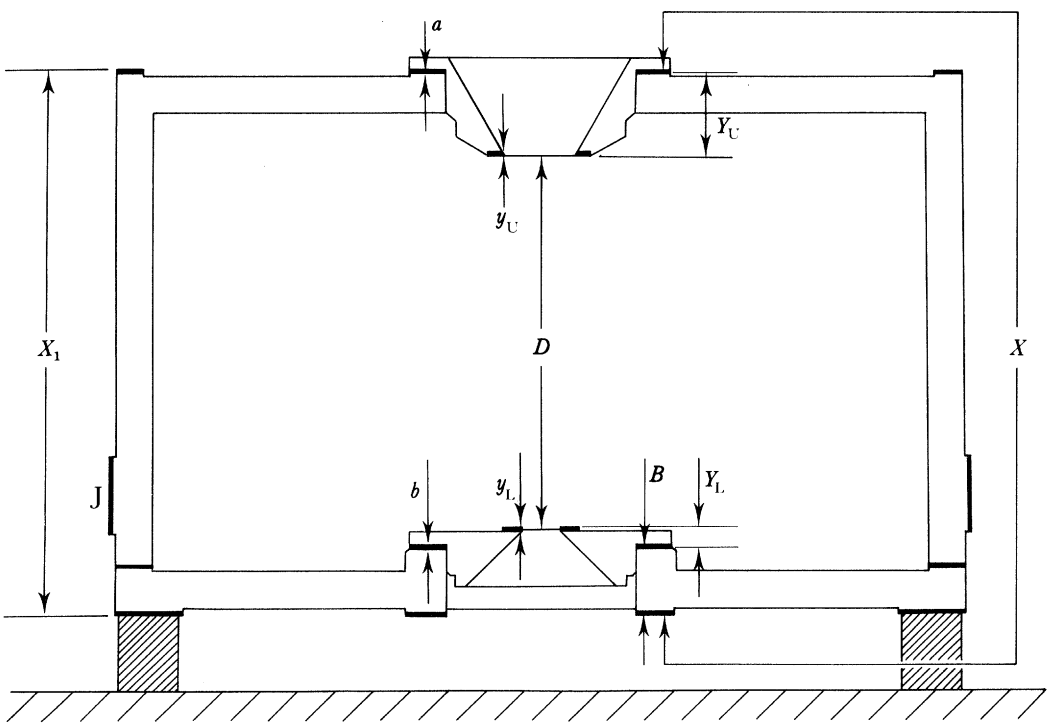

FIGURE 28. The body of the radiation trap showing the reference surfaces (in heavy lines), which allow precise mechanical measurements to be made. During measurements of its dimensions the radiation trap is supported as shown on a flat measuring table. The positions of the baffle plates that cover all the inside surfaces of the radiation trap are shown in figure 12. The lettering is explained in the text.

About 98 % of the radiation entering the radiation trap from the radiator through the lower aperture is absorbed by the baffle plates. It is necessary to keep the consequent temperature rise as small as possible. The change in direct radiation emitted by the radiation trap and passing into the calorimeter on opening and closing the shutter is proportional to the difference between the fourth powers of the radiation-trap temperatures with shutter open and closed. The baffle plates and lower plate are firmly bolted together with brass bolts and 'schorr' washers.

(*b*) *The measurement of the radiation trap*

The radiation trap not only supports the apertures, but must also allow the distance between them to be measured to within a few parts in 10^5. Figure 28 shows schematically how the radiation trap was designed to allow this to be done. The lapped reference surfaces are flat and parallel to within a few micrometres. If the required distance between the apertures is D, we find that

$$D = X-[(Y_{\mathrm{U}}-y_{\mathrm{U}})-\tfrac{1}{2}a]-[B+\tfrac{1}{2}b+(Y_{\mathrm{L}}-y_{\mathrm{L}})]. \tag{80}$$

Tables 8 and 9 show the results of all the measurements of these quantities made in 1980 and 1983, that is just before and just after the principal series of measurements of σ and T. The values are given at 293 K and also, after correction for thermal contraction, at liquid-helium temperatures.

TABLE 8. DIMENSIONS OF THE RADIATION TRAP AND APERTURES (MILLIMETRES)

large pair of apertures

		December 1980[a]		January 1983[b]	
		$T = 293$ K[c]	$T \approx 4$ K[d]	$T = 293$ K[c]	$T \approx 4$ K[d]
X[e]	*	142.8186	142.3534	142.8225	142.3573
$Y_{\mathrm{U}}-y_{\mathrm{U}}$	**	21.4715	21.4056	—	—
$\frac{1}{2}a$	—	0.0014	0.0014	—	—
B	*	16.4003	16.3469	16.4000	16.3466
$Y_{\mathrm{L}}-y_{\mathrm{L}}$	**	4.9626	4.9474	—	—
$\frac{1}{2}b$	—	0.0035	0.0035	—	—
R_{U}	**	13.0506	13.0104	13.0505	13.0104
R_{L}	**	9.0768	9.0489	9.0768	9.0489
D	—	—	99.6515	—	99.6557

small pair of apertures

		February 1983[a]		December 1983[b]	
X[e]	*	142.8225	142.3573	142.8220	142.3568
$Y_{\mathrm{U}}-y_{\mathrm{U}}$	**	21.339	21.2735	—	—
$\frac{1}{2}a$	—	0.0013	0.0013	—	—
B	*	16.4000	16.3466	—	—
$Y_{\mathrm{L}}-y_{\mathrm{L}}$	**	4.9077	4.8926	—	—
$\frac{1}{2}b$	—	0.0021	0.0021	—	—
R_{U}	**	9.1234	9.0953	9.1234	9.0953
R_{L}	**	5.1007	5.0850	5.1005	5.0848
D	—	—	99.8439	—	99.8434

[a] Just before measurements began.
[b] Just after measurements ended.
[c] In this column are given the measured values at $T = 293$ K.
[d] In this column are given the values after correction for thermal contraction from 293 to 4 K.
* Correction for o.f.h.c. copper $= -3257 \times 10^{-6}$.
** Correction for Cu–Be $= -3071 \times 10^{-6}$.
[e] Measurements of the dimension X were also made in 1976 and 1977 (see table 9).

TABLE 9. THE DIMENSIONS X AND B OF THE RADIATION TRAP (MILLIMETRES)

(Uncertainties in the measurements for X and B are ± 0.0002.)

	X	B
February 1976	142.8173	—
October 1977	142.8192	—
December 1980	142.8186	16.4003
January 1983	142.8225	16.4000
December 1983	142.8220	—

Dimensions Y_U, y_U, a, b, Y_L and y_L come from the aperture measurements already given in table 5. Dimensions X and B are derived from measurements of the radiation trap and the lower plate. Various measuring instruments and techniques were used, but chiefly the Tesa Electronic Indicator and the Trimos Vertical 500. Distance B is measured before the apertures are bolted in place and distances X and X_1 after the lower plate has been bolted to the drum. Distance X_1 is used only as a check to show that the lower plate has been bolted in place without trapping dust between the reference surfaces. Distance X is measured with the radiation trap supported, as shown in the figure, with the weight being taken at the outer edge by end gauges resting on a steel measuring table. The deflections in the radiation trap are then similar to those present when the radiation trap is mounted in the cryostat, where the weight is also taken around the outer lower reference surface. The reproducibility of dimension X over the short term, after bolting and unbolting the lower plate from the drum, was found to be about 2 μm. However, a long-term change was detected between measurements in 1980 and 1983. The change in X amounted to 4 μm, equivalent to a change in g of 6 parts in 10^5. In the absence of any firm indication as to when this change took place, we have taken the average of the measurements made in 1980 and 1983 and have associated with it an uncertainty of ± 3 parts in 10^5.

(*c*) *The throughput 'g'*

According to geometrical optics, the fraction f of radiation diffusely emitted by an aperture of radius R_L that is intercepted by a second, coaxial, parallel aperture of radius R_U a distance D from the first, is given by

$$f = 2R_U^2\{R_U^2 + R_L^2 + D^2 + [(R_U^2 + R_L^2 + D^2)^2 - 4R_U^2 R_L^2]^{\frac{1}{2}}\}^{-1}. \tag{81}$$

This formula is exact and is one of the classical formulas of photometry. In the present case, radiant power passing through the upper aperture when the lower aperture is irradiated by a black body at a temperature T is therefore

$$M'(T) = \pi R_L^2 f \sigma T^4 \tag{82}$$

$$= g\sigma T^4. \tag{83}$$

From the measured values of R_U, R_L and D corrected for thermal contraction, given in table 8, we deduce the following values for g:

$$g = 0.0427714 \pm 0.0000038 \quad \text{(large pair of apertures)},$$

$$g = 0.00666838 \pm 0.00000107 \quad \text{(small pair of apertures)}.$$

(d) Scattering of thermal radiation in the radiation trap

The second function of the radiation trap is to absorb all the radiation emerging from the lower aperture except the small fraction f that is in the direct beam passing through the upper aperture, namely 1.7% for the large pair and 0.85% for the small pair of apertures. For our measurement of the Stefan–Boltzmann constant, we require that less than 1 part in 10^4 of the measured radiation has been scattered in the radiation trap.

There are six ways in which significant fractions of radiant flux might be reflected inside the radiation trap and hence reach the upper aperture. These are illustrated in figure 29 and are denoted by fractions F_1–F_6. To evaluate these fractions it is necessary to calculate the geometrical angle factors for reflection between the various components of the radiation trap and also the diffuse reflectances of each of the surfaces in question. The contribution due to specular reflection is considered at the end of this section.

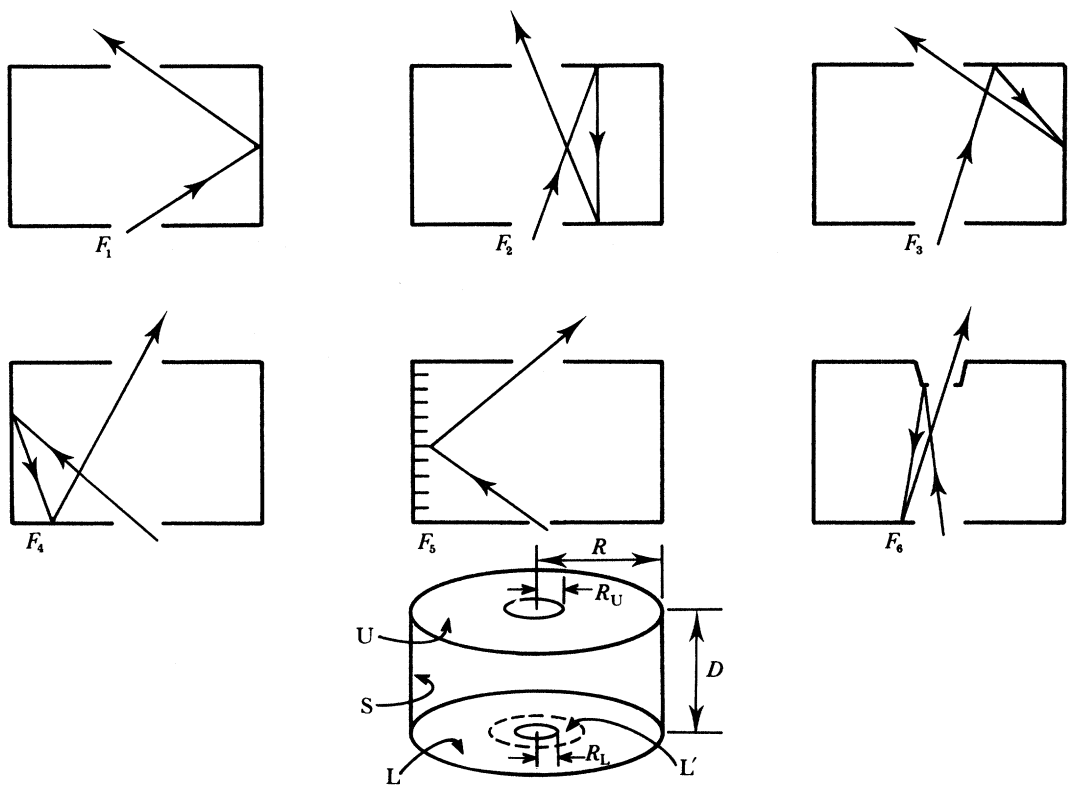

FIGURE 29. The principal ways in which radiation may be scattered in the radiation trap. The fractions F_1–F_6 are specified in (84)–(89) and the lettering is explained in the text.

Taking the fractions F_1–F_6 in turn we can write down expressions for each of them in terms of the fractions of radiation leaving the lower aperture that are intercepted by the top plate U, the side walls S and the lower plate L. Denoting the lower aperture by A1 and the upper by A2,

$$F_1 = F_{\mathrm{A1\text{–}S}} F_{\mathrm{S\text{–}A2}} \rho(\mathrm{A1, S, A2}), \tag{84}$$

where $F_{\mathrm{A1\text{–}S}}$ is the fraction of radiation leaving A1 that is intercepted by the side walls S, $F_{\mathrm{S\text{–}A2}}$ is the fraction of the radiation leaving the side walls that passes directly through A2 and

$\rho(\mathrm{A1, S, A2})$ is the diffuse reflectance of S for radiation coming from A1 and leaving in the direction of A2. Similarly, expressions for the fractions F_2–F_4 can be written down:

$$F_2 = F_{\mathrm{A1-U}}\, F_{\mathrm{U-L}}\, F_{\mathrm{L-A2}}\, \rho(\mathrm{A1, U, L})\, \rho(\mathrm{U, L, A2}), \tag{85}$$

$$F_3 = F_{\mathrm{A1-U}}\, F_{\mathrm{U-S}}\, F_{\mathrm{S-A2}}\, \rho(\mathrm{A1, U, S})\, \rho(\mathrm{U, S, A2}), \tag{86}$$

$$F_4 = F_{\mathrm{A1-S}}\, F_{\mathrm{S-L}}\, F_{\mathrm{L-A2}}\, \rho(\mathrm{A1, S, L})\, \rho(\mathrm{S, L, A2}). \tag{87}$$

The remaining two fractions are evaluated a little differently from the first four because they concern the scattering from the edges of the internal baffles, S′, the specular reflection from the annular unpainted rings A2′, surrounding the apertures:

$$F_5 = F_{\mathrm{A1-S'}}\, F_{\mathrm{S'-A2}}\, \rho(\mathrm{A1, S', A2}), \tag{88}$$

$$F_6 = F_{\mathrm{A1-A2'}}\, F_{\mathrm{A2'-L'}}\, F_{\mathrm{L'-A2}}\, \rho(\mathrm{A1, A2', L'})\, \rho(\mathrm{A2', L', A2}), \tag{89}$$

where L′ represents the flat painted surround to the lower aperture (see figure 29).

We require that

$$\sum_{i=1}^{6} F_i/f \leqslant 10^{-4}. \tag{90}$$

The angle factors and reflectances of (84) to (89), which are individually evaluated in Appendix D, are shown in table 10.

TABLE 10. CALCULATED VALUES FOR ANGLE FACTORS AND REFLECTANCES WITH PERCENTAGE UNCERTAINTY WHERE APPROPRIATE

(The values in this table are calculated from the relations given in Appendix D.)

angle factors

	large apertures	small apertures
$F_{\mathrm{A1-U}}$	0.41	0.41
$F_{\mathrm{A1-S}}$	0.59	0.59
$F_{\mathrm{U-L}}$	0.32	0.32
$F_{\mathrm{U-S}}$	0.68	0.68
$F_{\mathrm{A1-S'}}$	6×10^{-3} (±30%)	6×10^{-3} (±30%)
$F_{\mathrm{S'-A2}}$	5×10^{-3}	2.4×10^{-3}
$F_{\mathrm{A1-A2'}}$	2.4×10^{-4} (±20%)	4.8×10^{-4} (±20%)
$F_{\mathrm{S-A2}}$	5×10^{-3}	2.5×10^{-3}
$F_{\mathrm{L-A2}}$	8×10^{-3}	4×10^{-3}
$F_{\mathrm{S-L}}$	0.28	0.28
$F_{\mathrm{L'-A2}}$	0.017	8.5×10^{-3}
$F_{\mathrm{A2'-L'}}$	1	1
f	0.017	8.5×10^{-3}

reflectances

ρ_{S}	= 0.057 (±10%)
$\rho(\mathrm{A1, S, A2})$	= 2.7×10^{-4} (±20%)
$\rho(\mathrm{A1, U, L})$	= 0.013 (±10%)
$\rho(\mathrm{S, L, A2})$	= 2.7×10^{-4} (±20%)
$\rho(\mathrm{L', A2})$	= 0.057 (±10%)
$\rho(\mathrm{A1, S', A2})$	= 6×10^{-4} (±10%)
$\rho(\mathrm{U, L, A2})$	= $\rho(\mathrm{L, U, L})$ = 0.013 (±10%)
$\rho(\mathrm{U, S, A2})$	= 0.006 (±10%)
$\rho(\mathrm{A1, U, S})$	= 8×10^{-3} (±20%)
$\rho(\mathrm{A1, S, L})$	= 0.014 (±10%)
$\rho(\mathrm{A1\text{–}A'L'})$	= 1
$\rho(\mathrm{A2', L', A2})$	= 0.057 (±10%)
ρ_{V}	= 0.026 (±10%)

Table 11 shows the values obtained for the fractions F_1–F_6 for the large pair of apertures together with their final sum from the data of table 10. The same value is obtained for the small pair of apertures. The overall correction that has to be made is thus -0.75×10^{-4} of the measured value of $M'(T)$ for both the large pair and the small pair of apertures.

TABLE 11. THE SCATTERING FRACTIONS FOR THE LARGE PAIR OF APERTURES

$$F_1 = (8 \pm 2) \times 10^{-7}$$

$$F_2 = (2 \pm 0.4) \times 10^{-7}$$

$$F_3 = (0.5 \pm 0.15) \times 10^{-7}$$

F_4 is negligible

$$F_5 = (0.2 \pm 0.06^* \text{ and } \pm 0.02) \times 10^{-7}$$

$$F_6 = (2 \pm 0.4^* \text{ and } \pm 0.2) \times 10^{-7}$$

$$\sum_{i=1}^{6} F_i = (12.7 \pm 2.8) \times 10^{-7}$$

and hence

$$\sum_{i=1}^{6} F_i/f = (0.75 \pm 0.20) \times 10^{-4}$$

* These uncertainties are uncorrelated with each other and with each of the other uncertainties.

The uncertainty in this correction for scattering comes from the uncertainty in the reflectance of the paint, ρ, which we have already estimated as 0.006 or 10% of its value, together with the uncertainties resulting from the approximations made in the calculation of the angle factors and reflectances of the walls. The uncertainties in the calculation of most of the angle factors are small and can be ignored because they stem from simple geometrical factors. This is not the case, however, for $F_{A1\text{–}S'}$, the fraction of radiant flux intercepted by the edges of the baffles, since it depends upon our evaluation of the width of the edges. We estimate the uncertainty in $F_{A1\text{–}S'}$ to be 30% of its value. The remaining uncertainties are those coming from our evaluation of the reflectances, and these are given in table 10.

In table 11 the two uncertainties marked with an asterisk are uncorrelated with each other and with each of the other uncertainties, whereas all of the others are strongly correlated because they are mainly due to the uncertainty in the value of ρ. These uncertainties are combined as follows: all of the correlated uncertainties are added linearly in proportion to the magnitude of the value of F concerned. This gives a total of $\pm 2.7 \times 10^{-7}$, which is then combined in quadrature with the two uncorrelated uncertainties of F_5 and F_6, $\pm 1.4 \times 10^{-7}$, to give a final uncertainty of $\pm 2.8 \times 10^{-7}$. We thus arrive at the final uncertainty in the scattering correction of $\pm 0.2 \times 10^{-4}$, which is given in the table.

The contribution from the specular reflections, which occur at long wavelengths, is insignificant. The average weighted specular reflectance for 273 K thermal radiation is, as we have seen, of the order of 5×10^{-4}. So, provided at least two reflections take place the fraction ultimately reflected is negligible, and this is the case.

In addition to the effect of scattered radiation entering the calorimeter, it is necessary to measure and correct for the change in temperature of the radiation trap. Although its temperature is very low, the thermal radiation emitted by the radiation trap and entering the calorimeter can be as much as three parts in 10^5 of the measured radiant energy from the

radiator. Since its temperature changes by about 0.5 K on opening or closing the shutter, the change in energy emitted by the radiation trap $\delta M'(T)$ is significant and must be corrected for. Three germanium resistance thermometers are mounted inside the radiation trap, in the top, side and bottom baffle plates. The readings of these three thermometers allow a mean change in temperature to be deduced from which the small correction $\delta M'(T)$ can be calculated.

(*e*) *The shutter*

The shutter is shown in figure 12. Thermal contact between the shutter and the radiation trap is provided by eight copper braids. These were made sufficiently flexible to allow the shutter to move a distance of 5 cm between the open and closed positions. The shutter slides on chromium-plated copper rods mounted on the underside of the copper flange supporting the radiation trap. The shutter is drawn back and forth by 0.5 mm diameter braided stainless-steel wires. These are attached to pulleys at room temperature, which are turned from the outside through ultra-high vacuum flexible bellows. It takes about one second to open or close the shutter. The underside of the shutter is gold plated to reduce heat absorption from the radiator when it is closed. Its temperature is monitored with a germanium resistance thermometer and varies from about 10 K, when the radiator is at 233 K, to 20 K when the radiator is at 373 K; despite these relatively high temperatures, the radiant power entering the calorimeter from the closed shutter is always less than 1 nW and is thus negligible.

It was occasionally observed that the temperature of the shutter, when closed, was higher than usual, which led to unusually high temperatures being observed in the radiation trap. It was finally concluded that this behaviour was due to the build-up of cryodeposits on the underside of the shutter giving it a much higher absorptance than when clean. One of the odd effects of this was that during measurements made under these conditions the temperature of the radiation trap was higher when the shutter was closed than when it was open, the opposite of what was expected and what was generally observed. However, provided that the appropriate corrections for the radiation-trap temperature were made ($\delta M'(T)$ of table 16), no difference could be detected in the results with or without a cryodeposit present on the shutter.

7. The evaluation of the diffraction losses

Having taken all possible steps to avoid diffraction losses, it remains necessary to make an estimate of the residual effects of diffraction that result from our failure to reproduce exactly the ideal conditions of figure 2. This we have done by using the expressions derived by Blevin (1970) for diffraction at a circular aperture. He showed that, to a good approximation, the fractional loss F in irradiance at a point A_1 on the axis of an optical system when irradiated through a circular aperture of radius R_L, a distance D from A_1, by a circular source of radius r_0 situated at a distance b from the aperture, where $r_0 = R_L(D+b)/D$, is given by

$$F = \left(\frac{\pi}{u}\right)^{\frac{1}{2}} H(t) + \frac{1}{\pi(u+v_0)}, \tag{91}$$

where

$$u = \frac{2\pi R_L^2}{\lambda}\frac{D+b}{Db}, \quad v_0 = \frac{2\pi R_L r_0}{\lambda b}, \quad t = \frac{v_0-u}{(\pi u)^{\frac{1}{2}}}$$

and

$$H(t) = 2\pi^{-1}[\tfrac{1}{2}-S(t_0)]\cos\tfrac{1}{2}\pi t_0^2 - 2\pi^{-1}[\tfrac{1}{2}-C(t_0)]\sin\tfrac{1}{2}\pi t_0^2 - t\{[\tfrac{1}{2}-C(t_0)]^2+[\tfrac{1}{2}-S(t_0)]^2\}, \tag{92}$$

where $C(t_0)$ and $S(t_0)$ are the Fresnel integrals defined by

$$C(t) = \int_0^{t_0} \cos \tfrac{1}{2}\pi\tau^2 \, \mathrm{d}\tau \quad \text{and} \quad S(t) = \int_0^{t_0} \sin \tfrac{1}{2}\pi\tau^2 \, \mathrm{d}\tau. \tag{93}$$

Diffraction effects are, of course, wavelength dependent but, for thermal radiation, Blevin (1970) showed that the effects can be evaluated using an effective wavelength λ_e given by

$$0.333 \leqslant \lambda_e \, T/c_2 \leqslant 0.37, \tag{94}$$

where $c_2 = 0.014388$ m K and we take 0.333 for $u \approx v_0$ and 0.37 for $u \ll v_0$. Since in our case we find that u covers a range of values from close to v_0 to very much less than v_0, we take the average and calculate an effective wavelength by using

$$\lambda_e = 0.35 \, c_2 / T. \tag{95}$$

Between 233 and 373 K, λ_e varies between 21.6 and 13.5 μm.

Although Blevin's (1970) expression for F is calculated for a point on the axis, it is unlikely that F is significantly different at other points over the surface of the top aperture since the angular displacements from the axis are small. We assume, therefore, that the diffraction losses calculated for the point at the centre of the aperture are representative of those over the whole of the aperture.

Figure 30 shows a scale drawing of sections of the aperture system, in which the upper half of the figure is drawn for the small pair of apertures and the lower half for the large pair. The irradiance at the point A_1 would be that calculated according to geometrical optics if all of the inner surfaces of the gold-plated mirror, the shutter, the base of the radiator and the lower aperture were perfect reflectors of the thermal radiation coming from the radiator. Since this is not the case, we must first calculate the fraction of the radiant flux reaching A_1 that would come from each of these surfaces in the perfectly reflecting case, and then make an estimate of their reflectance.

The fraction of the radiant flux reaching A_1 that comes from outside the geometrical beam is the fraction of flux coming from outside ray 1, which we call F_1. The fraction of radiant flux coming from outside ray 2 is F_2 and so on. Thus, the fraction of radiant flux coming from the gold-plated mirror is $F_2 - F_3$, and by grazing incidence from the conical inner surface of the aperture is F_3. For the small pair of apertures the fraction coming from the inner edges of the shutter is $F_3 - F_{3_A}$. Similarly, F_4 is the fraction of the radiant flux passing through the upper aperture that is diffracted so that it subsequently passes at grazing incidence into the calorimeter. Each of these fractions has been evaluated by using (91) and (92). The results are shown in table 12.

Having calculated the fractions of the diffracted radiation coming (in the ideal case) from each of the surfaces of the mirror system, we must now estimate the departure from perfect reflection for each fraction, and hence deduce the diffraction losses.

The largest fraction is that coming from the upper regions of the radiator from just outside the geometrical beam. These fractions amount to 2.2 % and 4.1 % for the large and small pairs of apertures, respectively. For there to be no error in the radiant flux entering the calorimeter greater than 1 part in 10^5, we require the mean temperature of these upper regions of the radiator, just outside the geometrical beam, not to differ from the effective radiator temperature by more than 31 mK (at 273 K) or 42 mK (at 373 K) for the large apertures and 17 mK (at 273 K) and 22 mK (at 373 K) for the small pair of apertures. As was demonstrated in §2, these requirements were met at all times during the measurements.

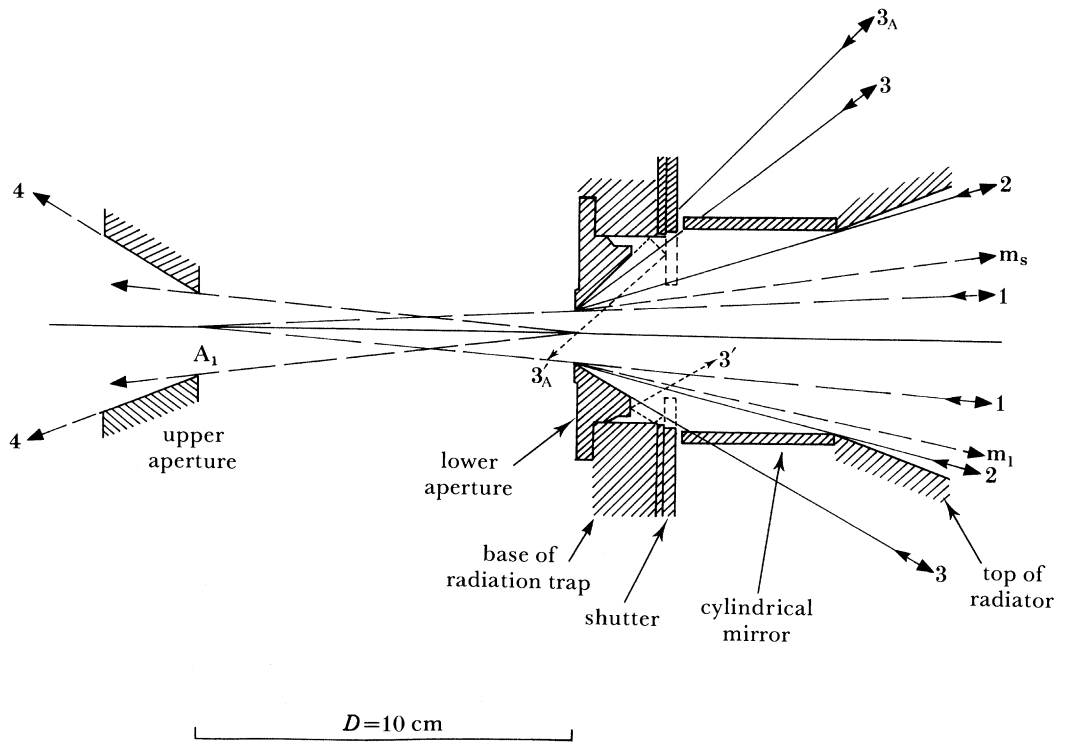

FIGURE 30. Sketch showing the principal components of diffracted radiation coming from outside the geometrical beam of radiation. The upper part of the sketch refers to the small pair of apertures and the lower part to the large pair, m_l and m_s represent the marginal rays for the large and small aperture pairs, respectively, and the numbers are explained in the text. Broken lines indicate positions of the shutter and rays reflected from the shutter during measurements of diffraction effects.

TABLE 12. FRACTIONS OF MEASURED RADIANT FLUX DUE TO DIFFRACTION

large pair of apertures ($\lambda = 18.4$ μm)

$$F_1 = 2.3 \times 10^{-2}$$
$$F_2 = 8.4 \times 10^{-4}$$
$$F_3 = 3.5 \times 10^{-4}$$
$$F_4 = 3.6 \times 10^{-4}$$

fraction from top of radiator, $F_1 - F_2 = 2.2 \times 10^{-2}$
fraction from cylindrical mirror, $F_2 - F_3 = 4.9 \times 10^{-4}$
fraction by grazing incidence at lower aperture, $F_3 = 3.5 \times 10^{-4}$
fraction by grazing incidence at upper aperture, $F_4 = 3.6 \times 10^{-4}$

small pair of apertures

$$F_1 = 4.2 \times 10^{-2}$$
$$F_2 = 10.5 \times 10^{-4}$$
$$F_3 = 4.7 \times 10^{-4}$$
$$F_{3A} = 3.6 \times 10^{-4}$$
$$F_4 = 3.3 \times 10^{-4}$$

fraction from top of radiator, $F_1 - F_2 = 4.1 \times 10^{-2}$
fraction from cylindrical mirror, $F_2 - F_3 = 5.8 \times 10^{-4}$
fraction from inner edge of shutter and base of radiation trap, $F_3 - F_{3A} = 1.1 \times 10^{-4}$
fraction by grazing incidence at lower aperture, $F_{3A} = 3.6 \times 10^{-4}$
fraction by grazing incidence at upper aperture, $F_4 = 3.3 \times 10^{-4}$

The fractions coming by reflection from the gold-plated tubular mirror, 4.9×10^{-4} and 5.8×10^{-4} for the large- and small-aperture pair respectively, are unlikely to be deficient. Not only is the mirror surface of polished gold, but being at the temperature of the radiator (within 1 K at least) any absorption will be compensated for by radiation of the correct temperature. We do not therefore consider any error from this source.

For the large pair of apertures there remains a fraction of 3.5×10^{-4}, which comes by grazing incidence at the conical surface of the aperture. This surface is gold-plated, but the quality of the polish of the Cu–Be substrate was not as high as we had hoped. In addition, since the apertures are at liquid-helium temperatures, layers of adsorbed gas may be expected on these conical surfaces. Tsujimoto *et al.* (1982*b*) have recently shown that the adsorptivity of adsorbed water films on cold surfaces rises very rapidly with film thickness. To investigate the reflectance of the cold surfaces close to the apertures and also to check the predictions of the diffraction calculations, the following measurements were made. We observed the radiant power entering the calorimeter while at the same time moving the shutter in incremental steps of about 1 mm from its fully open position to the positions shown by broken lines in figure 30. These final positions were chosen for each pair of apertures to bring the inner edge of the shutter close to the outer marginal rays of the geometric beam. The fraction of the diffracted radiation interrupted at the successive positions of the shutter was calculated by evaluating, by using (91), the diffracted radiation in each of the annular zones, and calculating the fraction of each annular zone obscured as the position of the shutter changed.

For the large pair of apertures, it is predicted that at the maximum movement of the shutter 24 % of diffracted radiation outside a radius of 1.8 cm should be obscured. If this fraction of the diffracted radiation were to be lost it should lead to a fractional decrease in the measured radiant power of 1.2×10^{-4}; in fact we observed a decrease of only $(0.7 \pm 0.3) \times 10^{-4}$. However, because of the geometry of the shutter and the large aperture (see the dotted path of ray 3′ in figure 30), we would not expect to observe any decrease in measured power had the surfaces of the shutter and base of the radiation trap been perfectly reflecting. The fact that we observed a fractional decrease in measured power of $(0.7 \pm 0.3) \times 10^{-4}$ allows us to deduce that the average reflectance of each of these three surfaces, for a ray such as 3′, was only 0.75 ± 0.12. Such a low reflectance for pure copper or gold-plated Cu–Be is not likely, but in view of the exposed position of these surfaces it is highly probable that they were covered with thin films of condensed water vapour or other condensed gases. An adsorbed water deposit having an absorptance of 0.25 for thermal radiation of 273 K requires, according to the measurements of Tsujimoto *et al.* (1982*b*), a thickness of the order of only a few micrometres.

Further evidence in support of this hypothesis was obtained from the results of similar measurements and calculations made for the small pair of apertures, for which a total movement of the shutter of 15 mm was calculated to lead to a fractional decrease in observed radiant power of 4×10^{-4} and, indeed, the observed decrease was $(4 \pm 0.3) \times 10^{-4}$. For the small pair of apertures, the included angle of the conical part of the lower aperture is 90°. Ray tracing shows that with this geometry much less of the radiation interrupted by the shutter is made up of radiation reflected from the conical surface of the aperture, and from the top of the partly closed shutter (see the dotted path of ray $3'_A$ in figure 30). We would, therefore, expect that practically all of the predicted decrease would be observed, as indeed was the case. This gives us confidence that the calculations we have made of diffraction effects represent sufficiently closely the actual

behaviour of the radiation and that our deduction of a reflection coefficient of 0.75 for the low-temperature surfaces, for angles of incidence near 45°, is reasonable.

We now return to the diffraction losses by the large pair of apertures. On the basis of a reflection coefficient of 0.75 at an angle of incidence of 45°, we must estimate the likely losses at grazing incidence. Under ideal conditions these would be zero, but taking into account the relatively poor polish obtained on the conical surfaces, we prefer to allow an absorptance of 0.15 ± 0.1. This loss takes place at both lower (F_3) and upper (F_4) apertures and leads to a total fractional diffraction correction $D(T)$ for the large pair of apertures, at a temperature $T = 273$ K, of

$$D(273\ \text{K}) = (1.1 \pm 0.7) \times 10^{-4}.$$

For the small pair of apertures the fractions in this case are F_{3_A} and F_4 for the lower and upper apertures, leading to a fractional loss of $(1 \pm 0.7) \times 10^{-4}$. In addition, for the small pair, a fraction (0.25 ± 0.15) of the sum of the fractions $(F_3 - F_{3_A})$ and $(1 - 0.15)F_{3_A}$ are lost on reflection at 45° from the inner surface of the bottom of the radiation trap. This amounts to $(1.1 \pm 0.7) \times 10^{-4}$. The total fractional loss for the small pair of apertures is thus

$$D(273\ \text{K}) = (2.1 \pm 1.2) \times 10^{-4}.$$

Note that the uncertainties in the two components of $D(T)$ are strongly correlated because they both depend to a large extent upon our estimate of the reflection loss at grazing incidence, hence the combined uncertainty of $\pm 1.2 \times 10^{-4}$.

The values of $D(T)$ given above correspond to an effective wavelength of 18.4 μm. Similar evaluations have been made for effective wavelengths of 13.5 μm ($T = 373$ K) and 21.6 μm ($T = 233$ K). The results of these calculations have shown that, within this range of wavelengths, the diffraction losses can be scaled simply in proportion to effective wavelength, i.e. inversely proportional to T. The diffraction losses are shown in figure 31 as a function of T for the large and small pairs of apertures.

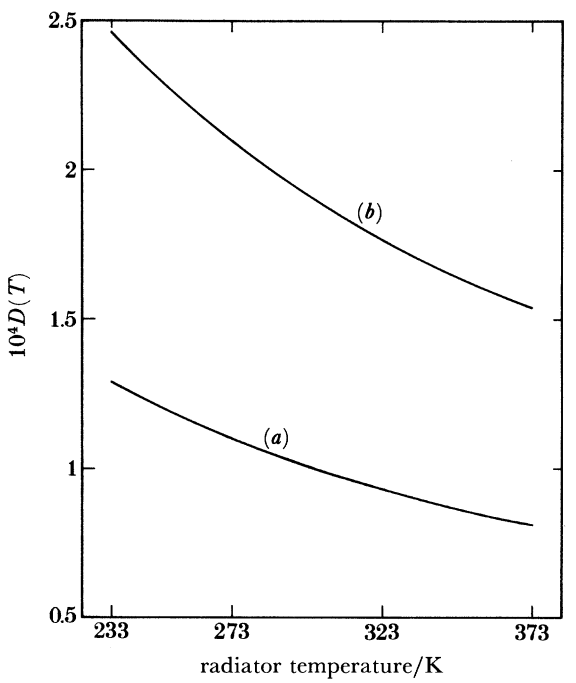

FIGURE 31. The fractional corrections, to be added to the measured radiant powers, due to diffraction losses, (*a*) for the large pair of apertures and (*b*) the small pair.

The uncertainties in $D(273\ \mathrm{K})$ shown above are the uncertainties used in the determination of the Stefan–Boltzmann constant. For the measurement of T we require the uncertainties in the change in the value of $D(T)$ between temperatures T_{tp} and T. In figure 31 it can be seen that the slope of $D(T)$ as a function of T becomes more negative as the absolute value of $D(T)$ increases. From these curves we can calculate the uncertainty in slope consequent upon a given uncertainty in the absolute value of $D(T)$. The uncertainties in $D(T)$ for both the large and small aperture pairs so deduced are shown in figure 32.

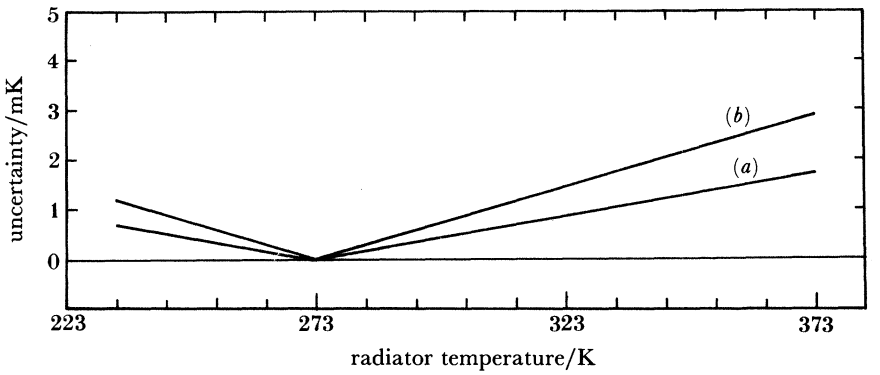

FIGURE 32. The uncertainties resulting from uncertainties in the change in the diffraction correction between 273 K and T, (*a*) for the large pair of apertures and (*b*) for the small pair of apertures, calculated in terms of millikelvin.

8. GAS CONDUCTION AND PRESSURE MEASUREMENT

(*a*) *Conduction by residual water vapour and hydrogen*

The pressure in the whole apparatus must be kept sufficiently low for energy transfer from the radiator by gas conduction to be only a very small fraction of the total energy absorbed by the calorimeter. This requires not only that the system be free of leaks, but also that the outgassing rate of the internal surfaces of the radiator be extremely low. A study of the outgassing rate of 3M black as a function of temperature was made by Compton *et al.* (1974). The results showed that, provided adequate baking was achieved, 3M-C 401 has an outgassing rate that ranges from 1.3×10^{-7} to 1.3×10^{-6} Pa m^3 s^{-1} (10^{-10} to 10^{-9} Torr l cm^{-2} s^{-1}). To achieve these figures, the painted surface must be heated in a vacuum to 250 °C for at least two days. During this operation considerable quantities of greasy matter are given off. In making these measurements and in the present calculations concerning energy transfer, it was assumed that, after bake-out, the predominant residual gases in the system are water vapour and hydrogen.

Pressures were measured with a nude Bayard–Alpert type ion gauge placed inside the radiator, as shown in figure 1. The gauge was calibrated for nitrogen by the NPL Division of Mechanical and Optical Metrology. Measurements were made at the beginning and at the end of each run, but not during a run, because the heat produced by the filament would cause too great a disturbance to the thermal conditions in the radiator. Pressures ranged from about 1.5×10^{-7} Pa (1×10^{-9} Torr) for radiator temperatures of about 10 °C and below, to 9×10^{-6} Pa (7×10^{-8} Torr) for a radiator temperature of 100 °C.

To estimate the energy transfer between the radiator at a temperature T and the calorimeter at a low temperature T_c we proceed in the following way. From kinetic theory we have the

following relations (see, for example, Tabor 1979); the number, n, of molecules per unit volume in a gas at a pressure P and temperature T is given by

$$n = P/kT.$$

The average velocity $\bar{v}$ of such molecules having a molecular mass m is given by

$$\bar{v} = (8kT/\pi m)^{\frac{1}{2}}, \tag{96}$$

where $m = Mm_u$, in which M is the relative molecular mass and m_u is the atomic mass unit equal to about 1.66×10^{-27} kg. The number, ϕ, of molecules striking unit area of the walls of the container per second is given by

$$\phi = \tfrac{1}{4}n\bar{v} = \tfrac{1}{4}P(kT)^{-1}(8kT/\pi m)^{\frac{1}{2}} = 2.6 \times 10^{24} P(MT)^{-\frac{1}{2}}. \tag{97}$$

The kinetic energy per degree of freedom per molecule is $\frac{1}{2}kT$. For water vapour, $M = 18$, having three rotational and three translational degrees of freedom, this gives a kinetic energy per molecule

$$E_k = 3kT. \tag{98}$$

At temperatures below about 130 °C vibrational degrees of freedom are not significantly excited in water molecules.

In addition to the kinetic energy, the energy of adsorption must also be taken into account. For adsorption of H_2O and H_2 at liquid-helium temperatures we need consider only physisorption, since the temperature is too low for chemisorption to take place. We have adopted a value of 17 kJ mol^{-1} for the energy of adsorption of H_2O on surfaces at liquid-helium temperatures. This figure is uncertain to the extent of about 50 % of its value. Thus the energy absorbed is given by

$$E_a = 2.9 \times 10^{-20} \text{ J per molecule.} \tag{99}$$

The sum of the kinetic and adsorption energies for water vapour, E_K, is obtained by substituting (97), (98) and (99) in the relation

$$E_K = (E_k + E_a)\,\phi g, \tag{100}$$

where g is the geometrical throughput, which is identical to that for thermal radiation. Thus the fractional correction for energy transfer by gas molecules is given by

$$p(T) = \frac{E_K}{E'(T)} = \frac{(E_k + E_a)\,\phi}{\sigma T^4} \tag{101}$$

$$= \frac{(3kT/\text{J} + 2.9 \times 10^{-20})\, 2.6 \times 10^{24}\, P}{\sigma T^4 \sqrt{MT}}. \tag{102}$$

For $M = 18$, this equation gives the fraction of the energy absorbed by the calorimeter that is due to conduction by water vapour. The uncertainty in the correction is due mainly to the uncertainty of 50 % in the adsorption energy of water vapour and uncertainty in the species of gas present. The uncertainty in the pressure measurement is estimated to be about ± 20 %. Overall, we estimate the uncertainty in this correction to be ± 60 % of its value. For hydrogen, the effect is rather smaller because the adsorption energy is very much smaller, only 0.2×10^{-20} J per molecule.

Figure 33 shows (102) evaluated for a range of pressures and temperatures encompassing those found in this work. The corrections made are always small and the uncertainties associated with them contribute very little to the final overall uncertainties of the results.

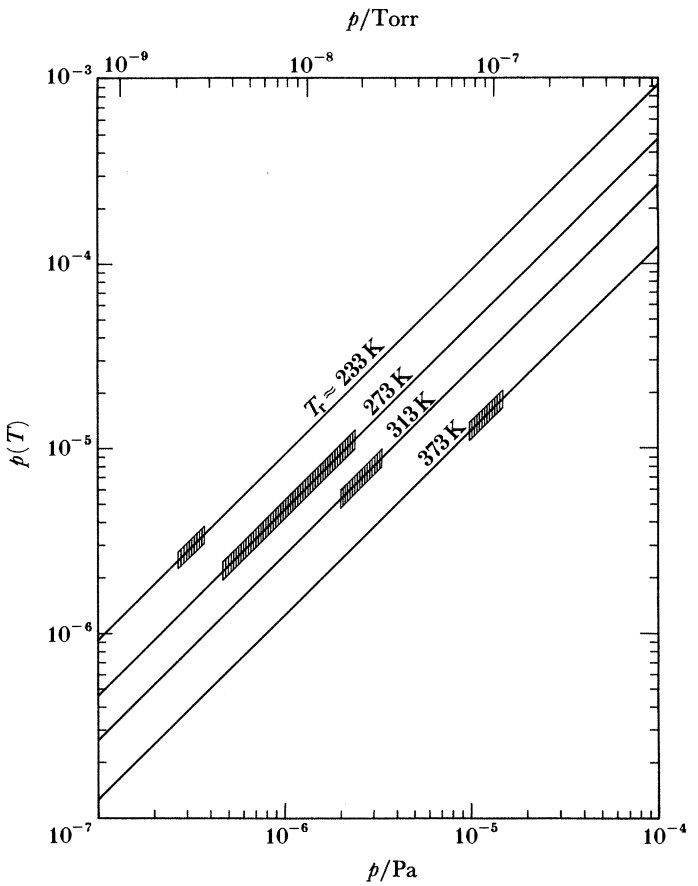

FIGURE 33. The fractional corrections, which must be subtracted from the measured radiant powers, due to gas conduction. The ranges of pressures observed are indicated by hatched areas.

(*b*) *The effects of hydrogen at low temperatures*

There are special problems due to the presence of hydrogen gas that arise only when the calorimeter temperature is below about 3.5 K. This only occurs with the small pair of apertures and for radiator temperatures below about 333 K. In the previous section we assumed that molecules follow only those paths followed by thermal radiation and that molecules entering the radiation trap are wholly adsorbed on the internal surfaces of the radiation trap, except for those that pass directly through the top aperture. This is a valid assumption for every gas except hydrogen and helium. While there is very little gaseous helium present, considerable quantities of hydrogen are outgassed from the copper radiator assembly, and together with water vapour it is one of the principal residual gases in the vacuum system. The vapour pressure of hydrogen at the temperature of the radiation trap, about 6 K, is of the order of 0.1 Pa (*ca.* 10^{-3} Torr). At the pressures existing in the apparatus, condensation will not, therefore, take place. Instead, a dynamic equilibrium will be established between the gas molecules entering the radiation trap and those leaving it. This can be expressed by

$$\frac{P_{\mathrm{r}}}{T_{\mathrm{r}}^{\frac{1}{2}}} = \frac{P_{\mathrm{rt}}}{T_{\mathrm{rt}}^{\frac{1}{2}}} = \frac{P_{\mathrm{c}}}{T_{\mathrm{c}}^{\frac{1}{2}}}, \tag{103}$$

where the subscripts r, rt and c signify, for the purposes of this discussion, the radiator, radiation trap and calorimeter, respectively. Molecules entering the radiation trap will come to thermal equilibrium with it before leaving. Monte Carlo calculations (Levinson *et al.* 1961) of the number of collisions with the walls undergone by gas molecules on passing through passages of various shapes show that for the geometry of the radiation trap an average of about seven collisions take place. What happens to a hydrogen molecule on leaving the radiation trap and entering the calorimeter depends critically upon the temperature of the calorimeter. If T_c is above about 4 K, at which the vapour pressure of hydrogen is still above 6.5×10^{-5} Pa (5×10^{-7} Torr), condensation will not take place and (103) fully describes the situation. A dynamic equilibrium will be established between the molecules entering and leaving the calorimeter. The energy transfer depends upon $(T_{rt} - T_c)$, which for the large pair of apertures is only about 1 K, but for the small pair of apertures can reach 8 K. This leads to significant kinetic energy transfer by hydrogen molecules for the small pair of apertures, but not for the large pair.

If, however, the temperature of the calorimeter is below about 3.5 K, which it is when the small pair of apertures are being used and T_r is below about 50 °C, the situation is very different. At 3 K, for example, the vapour pressure of hydrogen is below 2×10^{-8} Pa (*ca.* 1×10^{-10} Torr) (Mullins *et al.* 1961) and every molecule entering the calorimeter will remain and liberate its heat of adsorption. We estimate the effect of this hydrogen adsorption in the following way.

A quantitative evaluation of the effects of hydrogen adsorption is difficult because we do not have sufficient information on the amount of hydrogen present in the system. Measurements of the relative proportions of water vapour and hydrogen made by connecting a mass spectrometer to the system indicate that most of the residual gas in the outer, hotter, unbaked regions of the vacuum system was water vapour and the remainder was hydrogen. This is, of course, only a poor indication of the situation in the inner, cold, baked regions. Nevertheless, an estimate can be made of the order of magnitude of the effects due to hydrogen. We can show that the observed differences between the values of $(T - T_{68})$ measured for the small pair of apertures, in the presence of hydrogen condensation, and those measured without it are in qualitative agreement.

If the calorimeter temperature T_c is below the dew point of hydrogen, the number of molecules entering the calorimeter is greater than that leaving it by an amount that is proportional to $(P_r/T_r^{\frac{1}{2}} - p(T_c/T_c^{\frac{1}{2}}))$, where $p(T_c)$ is the vapour pressure of hydrogen at a temperature T_c. At very low temperatures all the molecules that enter are condensed and $P_r/T_r^{\frac{1}{2}} \gg p(T_c)/T_c^{\frac{1}{2}}$. Since $p(T_c)$ rises exponentially with T_c, there is a narrow range of temperature, T_c, over which $p(T_c)/T_c^{\frac{1}{2}}$ becomes comparable with, and then exceeds, $P_r/T_r^{\frac{1}{2}}$ despite the fact that P_r is increasing as T_r increases. This takes place in a range of temperature between about 3.2 and 3.6 K, equivalent to a range of radiator temperature between 30 and 60 °C. The error, ΔT, in the measured values of thermodynamic temperature is given by

$$\Delta T = T_r - T_{tp}\left[\frac{\sigma T_r^4 + \dot{Q}_c(T_r)}{\sigma T_{tp}^4 + \dot{Q}_c(T_{tp})}\right]^{\frac{1}{4}},$$

where $\dot{Q}_c(T_r)$ and $\dot{Q}_c(T_{tp})$ are the rates of energy transfer per square metre by hydrogen condensation for radiator temperatures of T_r and T_{tp}, respectively. ΔT will reach a maximum just before $p(T_c)/T_c^{\frac{1}{2}}$ exceeds $P_r/T_r^{\frac{1}{2}}$ and thereafter falls rapidly to zero. This maximum occurs for radiator temperatures in the range 30–40 °C. Estimates of the magnitude of ΔT(max) are

critically dependent upon the vapour pressure of hydrogen and the pressure of hydrogen in the system. Using the vapour pressure data of Mullins *et al.* (1961), and taking half the measured total pressure in the radiator to be due to hydrogen, we estimated a maximum value of ΔT of between 5 and 10 mK, occurring at $T_r \approx 40$ °C. The measured value of T obtained under these conditions for $T_r = 40$ °C with the small pair of apertures was, indeed, some 12 mK above that found with the large pair of apertures.

To obtain further support for the hypothesis that the difference was indeed due to the effects of condensed hydrogen, a second series of measurements was made for $T_r \approx 40$ °C. During the second series a constant background current was passed through the calorimeter heater to maintain T_c near 5 K, i.e. above the range in which hydrogen condensation takes place. The results of this series of measurement led to a value of T that was 12 mK below that of the first series, and in consequence the value of $(T - T_{68})$ agreed with the value obtained with the large pair of apertures.

The effect of kinetic energy transfer by hydrogen molecules between the radiation trap and calorimeter remains to be considered. This is proportional to both T_{rt} and the difference $(T_{rt} - T_c)$, and also to the overall pressure of hydrogen in the system. For the large pair of apertures the effect is negligible, but this is not the case for certain series of measurements made with the small pair. For the measurements made at $T_r = 109$ °C, the measured pressure was relatively high, 1.2×10^{-5} Pa, and $(T_{rt} - T_c)$ was about 8 K ($T_{rt} \approx 12$ K). This led to a calculated correction of 3 mK, by no means negligible, but subject to considerable uncertainty due to lack of knowledge of the real pressure of hydrogen in the system. For the measured value of $(T - T_{68})$ of this series to agree with that obtained with the large-aperture series a correction of 5.5 mK would be required.

In view of the uncertainty surrounding these corrections because of the effects of hydrogen, we have concluded that the only reliable series of measurements of $(T - T_{68})$ made with the small pair of apertures is that at 40 °C, in which T_c was maintained near 5 K. The measurements at 60 °C, 80 °C and 109 °C, although in approximate agreement after correction with those made with the large pair of apertures (they differ by between 5 and 8 mK), are subject to uncertainties that are difficult to evaluate, but which must be between 5 and 10 mK. They do not, therefore, contribute useful weight to the final set of values of $(T - T_{68})$ and we do not include them.

The values of $M'(T_{tp})$ obtained with the small pair of apertures are also subject to the effects of hydrogen condensation. For radiation temperatures near 273 K, however, the total pressure in the system was sufficiently low for the hydrogen effects to be small. From estimating $\dot{Q}_c(T_{tp})$ we deduced a rate of energy transfer of the order of 4 nW, only 2 parts in 10^5 of the measured radiant power. In applying this correction we associate with it an uncertainty equal to its value, namely ± 2 parts in 10^5 of σ. This correction and its uncertainty are both small compared with the other corrections and uncertainties listed for the small apertures in table 16. In calculating our final value for σ, therefore, measured values of $M'(T_{tp})$ obtained with the small pair of apertures are taken into account, along with those obtained for the large pair.

9. Electrical measurements and control systems

The general scheme of the electrical and control systems is shown in figure 34. The most critical measurements are those of the resistance of the platinum resistance thermometers, the calorimeter temperature and the electrical power supplied to the calorimeter. The details of

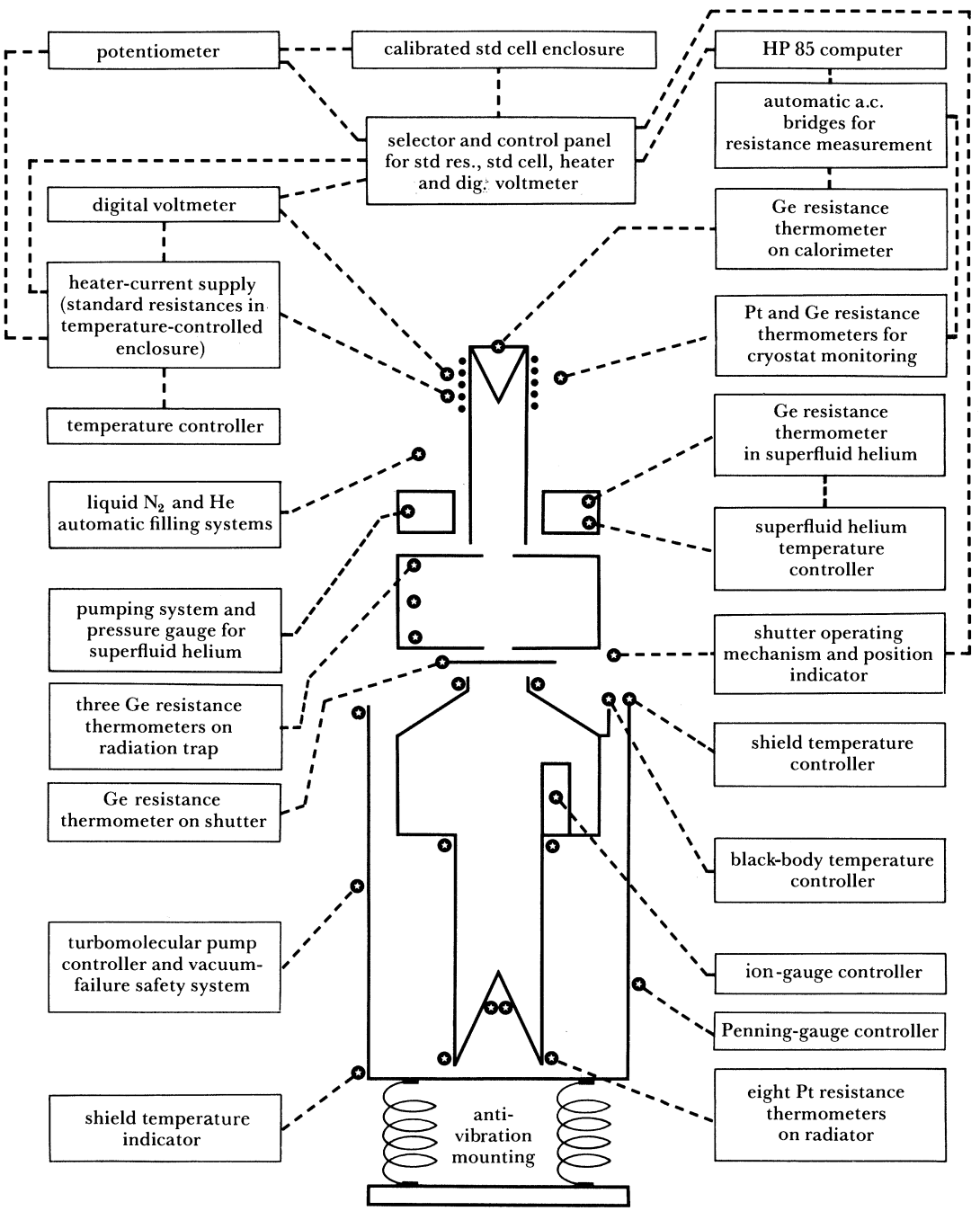

FIGURE 34. A schematic outline of the overall systems of the experiment.

how these are made have already been described in the relevant sections dealing with these aspects of the experiment.

The cryogenic system included provision for automatic filling of both the liquid-nitrogen and liquid-helium reservoirs. During a run these automatic systems were switched off, since the overall thermal stability of the low-temperature part of the apparatus would otherwise be disturbed. No effects related to the level of the liquid nitrogen or liquid helium in the reservoirs

could be detected. The proper functioning of the whole assembly was monitored by the germanium resistance thermometers and industrial platinum resistance thermometers at the locations indicated in figure 34.

10. Mechanical design

The overall size of the apparatus was fixed, as we have already seen, by the size and separation of the apertures. One of the principal requirements that had to be met in the design was that of mechanical rigidity and alignment of the apertures, radiator and calorimeter. For example, in figure 1 the shutter, attached to the bottom of the radiation trap and at liquid-helium temperature, must be aligned with the top of the radiator, which is at room temperature or above, to within 2 mm both vertically and horizontally. The shutter and radiator are independently supported from the top plate; that is to say through a total distance of some three metres, passing through temperature zones from 4 K up to room temperature. To achieve such small tolerances it was necessary first to use a manufacturing process that included full stress-relief by heat treatment of all welded parts before final machining and, second to have a design and assembly procedure that allowed the dimensions and positions of all internal components to be checked during assembly. Without proper stress relief, considerable deformation would take place in large components on cooling from room temperature to 77 or 4.2 K.

The top plate is made of stainless steel 2.5 cm thick and provides the reference plane and common axis for all the components. Two reference surfaces, to which are bolted the liquid-nitrogen and liquid-helium reservoirs, were machined on the lower surface of this plate. The nitrogen reservoir is of welded annular construction and is made entirely of stainless steel. On the lower flange of this a reference surface is machined to which a copper can is bolted. From the lower flange of this can, the radiator is accurately suspended with reference to the top plate by using eight 1 mm diameter stainless-steel wires.

The helium reservoir has a stainless-steel top flange and walls, but the lower flange, which has an upward pointing central well (see figure 1), is made from o.f.h.c. copper, vacuum-brazed to the wall. This copper flange has two reference surfaces machined on its lower face. The first provides location for another copper can, which has an accurately machined inside diameter that acts as an axial reference surface into which the radiation trap slides. The mating reference surface on the radiation trap is marked J in figures 12 and 28. As well as locating the radiation trap, this copper can also supports the shutter, which means that the length of this can is critical because it is one of the determiming dimensions fixing the separations of the lower aperture, shutter and radiator. The second reference surface on the lower flange of the helium reservoir locates six thin-walled stainless-steel tubes. Three of these serve simply to provide the location and support of the 2 K reservoir (one of these is marked S in figure 12), while the other three, in addition, pass up through the helium reservoir to the top plate (one of these is marked P in figure 12). These three provide means of pumping, pressure sensing and operation of the needle valve for filling of the 2 K reservoir, and are connected to the 2 K reservoir by indium-wire seals. The final reference surface to be mentioned here is that machined on the inner lower surface of the 2 K reservoir (K in figure 12), to which is bolted the copper tube that supports the stainless-steel heat link and calorimeter. The length of this copper tube is such that the lower aperture of the calorimeter is just 1 mm above the upper aperture in the radiation trap.

11. Results

(*a*) *Measurement procedure*

A total of 297 measurements were made with the large pair of apertures. The majority (270) were for the measurement of thermodynamic temperature at fifteen temperatures between about −40 and +100 °C and the remainder were for the measurement of the Stefan–Boltzmann constant. With the small pair of apertures, 100 measurements were made, again the majority were for the determination of four temperatures between +40 and +109 °C, with 20 measurements being used for the Stefan–Boltzmann constant.

Figures 35 and 36 illustrate the way a typical set of results were obtained for the measurement of $M'(T_{tp})$ and $M'(T)$ with the large pair of apertures. Consider first the measurement of $M'(T_{tp})$: the radiator is adjusted to obtain a suitable drift rate at a temperature within about two degrees of 273.16 K and its temperature distribution is measured with the shutter closed. The shutter is opened and the calorimeter allowed to come into equilibrium. About thirty minutes after the opening of the shutter, equilibrium is reached and the measurements illustrated in figure 35 are begun. The radiator temperature is measured by using the thermometers on the middle flange (T_1, T_8), lower flange (T_4, T_6) and the cone (T_2, T_3). At the same time, the resistance of the calorimeter thermometer is measured so that a series of

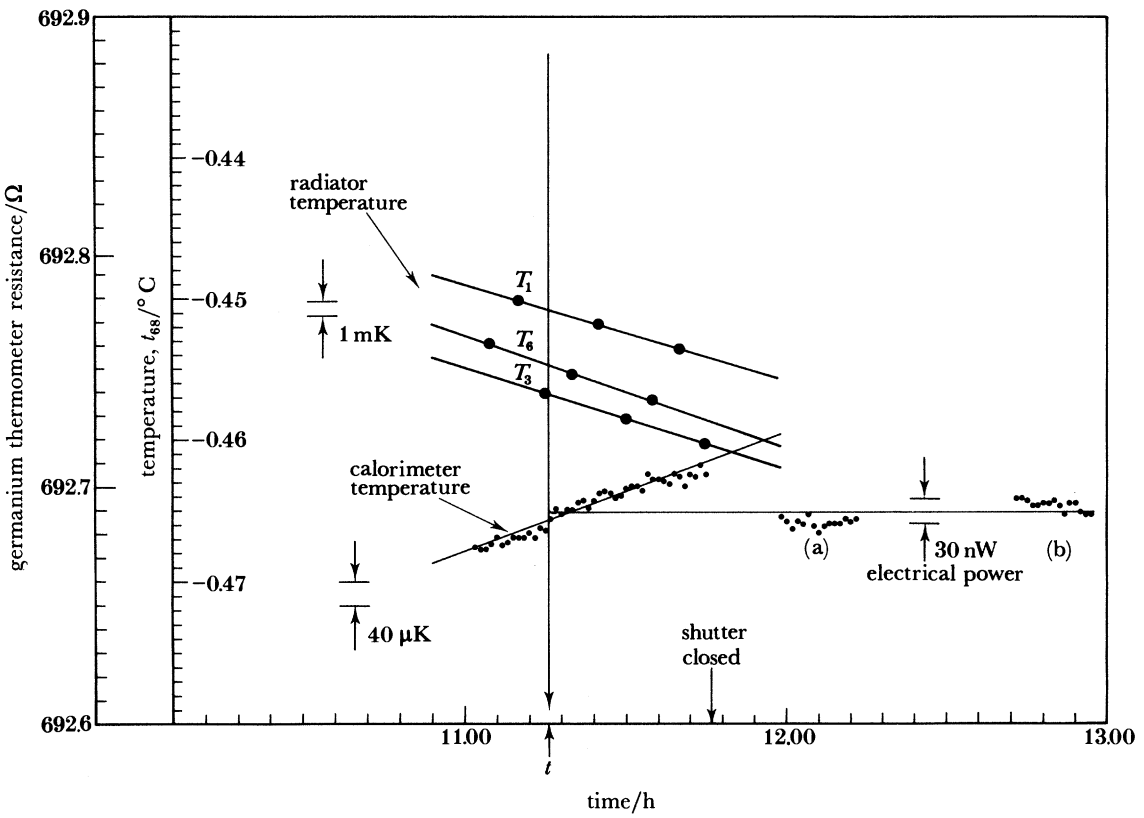

FIGURE 35. Data obtained during a run at a radiator temperature of 273 K using the large pair of apertures. The radiator temperature, t_{68}, at time t from the three temperatures, read from platinum resistance thermometers, T_3 (−0.4568 °C), T_6 (−0.4546 °C) and T_1 (−0.4507 °C) is −0.4556 °C for a drift rate of −0.6 mK/5 min. The calorimeter temperature is obtained from the resistance of the germanium thermometer. The electrical power, obtained from the average of (a) forward, and (b) reverse, current values is 1.339730 mW. Data from run number 8 at 102 °C (T_{tp}) (see table 19).

values of radiator temperature and calorimeter thermometer resistance are obtained. After such measurements have been made for about 40 min, all of which are made in a strict time sequence, the shutter is closed and electrical power applied to the calorimeter. The power is adjusted until the calorimeter temperature is within the range previously observed when the shutter was open. After a suitable series of power measurements have been made, as shown in the figure, the current is reversed and a second series made. From these measurements, taking account of the time constant of the calorimeter, a temperature of the radiator can be associated with the measured power on the calorimeter. The temperature of the three thermometers mounted in the radiation trap and the thermometer attached to the shutter are also recorded both for the open and closed positions of the shutter. The pressure inside the radiator is measured about three times during a series of measurements.

For the determination of the Stefan–Boltzmann constant with the large pair of apertures, three series were made, each comprising about ten measurements, and two similar series with the small pair. Between each series the whole apparatus was warmed to room temperature and pumped for periods of between one and four weeks. In addition, for the second series made with the small pair of apertures, the calorimeter was maintained at temperatures above about 5 K to avoid the effects of hydrogen condensation.

The measurement procedure for radiator temperatures away from 273.16 K is the same as just described, but the use to which the measured power is put is, of course, different. Instead

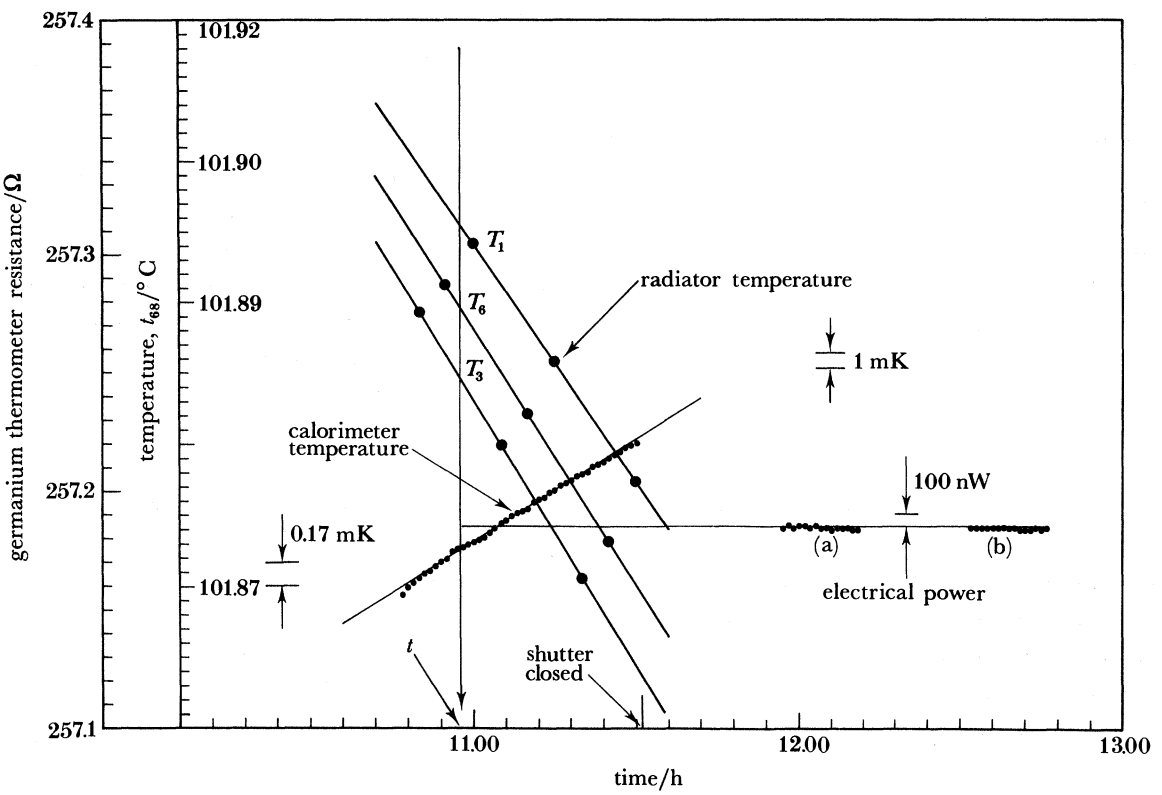

FIGURE 36. Data obtained during a run at a radiator temperature near 373 K with the large pair of apertures. The radiator temperature, t_{68}, at time t from the three temperatures, read from platinum resistance thermometers, T_3 (101.8844 °C), T_6 (101.8891 °C) and T_1 (101.8954 °C) is 101.8864 °C for a drift rate of −2.8 mK/5 min. The calorimeter temperature is obtained from the resistance of the germanium thermometer. The electrical power, obtained from the average of (a) forward, and (b) reverse, current values is 4.791 526 mW. Data from run number 7 at 102 °C (see table 19 and figure 10).

of deducing a value for $M'(T_{tp})$, the measurements allow us to obtain $M'(T)$ and hence $(T-T_{68})$, where T_{68} is the effective temperature of the radiator in terms of the IPTS-68 calibrations of the platinum resistance thermometers. Figure 36 illustrates such a measurement for a radiator temperature of 102 °C. From each value of $M'(T)$, a value of thermodynamic temperature T can subsequently be obtained by using the mean of the values of $M'(T_{tp})$. For each of the fifteen temperatures between -40 and $+102$ °C measured with the large apertures, about ten values of $M'(T_{68})$, followed by ten values of $M'(T_{tp})$, were obtained.

Figure 37 shows the order in which the measurements of T were made with the large pair of apertures. This figure also shows the values of $M'(T_{tp})$ obtained after each measurement of $M'(T)$ and the occasions on which the whole apparatus was warmed to room temperature. As expected, the values of $M'(T_{tp})$ that immediately follow excursions of the radiator to high temperatures are depressed, but subsequently recover after the next warm-up to room temperature. We suppose that this is due to the effects of cryodeposited films on the mirror surfaces, M_2 and M_3, and on the lands. These films form when the pressure in the radiator rises, as a result of outgassing, during the heating of the radiator to high temperatures and are removed by warming these surfaces to room temperature. We have, therefore, generally taken as the reference value for $M'(T_{tp})$ in calculating T, the one measured immediately after $M'(T)$.

There is evidence, however, that even without warming to room temperature, some clean-up takes place during prolonged use at low radiator temperatures following a run at high temperatures (see figure 37, February and March 1982 and May and June 1982). For the measurements of T at $t_{68} = -11$, -21 and -31 °C and at 12 and 21 °C we have taken, therefore, the mean of the values, weighted with time, of $M'(T_{tp})$ before and after these sets of runs. These changes in $M'(T_{tp})$, although significant, are not very large and only exceed 7 parts in 10^5 for temperatures of 90 °C and above.

By using the small pair of apertures, measurements were made at 40, 60, 80 and 109 °C. At 40 °C, two sets of measurements were made, during the second set the calorimeter was maintained near 5 K to avoid the effects of hydrogen condensation. For this set the values of $M'(T_{tp})$ used in the calculation of T were those of the second series of measurements with the small pair of apertures used for the calculation of σ, and during which T_c was also maintained near 5 K. As we have already seen in §8(*b*), only those measurements of T not subject to the effects of hydrogen condensation are included in our final results.

(*b*) *Corrections and uncertainties*

The principal measured quantities in both the Stefan–Boltzmann and thermodynamic-temperature work are the temperatures on IPTS-68 given by the platinum resistance thermometers and the electrical power applied to the calorimeter given by $V_c V_s/R_s$. In addition there are various small measured or calculated corrections. As explained in earlier sections, the relations between the thermodynamic temperature of the radiator (which we now revert to calling T or T_{tp}) and these measured and calculated quantities are thus:

$$M'(T) = M'(T_{68}+\Delta T) = F(\epsilon, a)\, g(1-D(T))\,(1-L(T))\,(1+s)\,(1+p(T))\,\sigma T^4 \quad (104)$$

and

$$M'(T) = (V_c V_s/R_s)\, T - \delta M'(T), \quad (105)$$

where $\Delta T = T - T_{68}$ and the other quantities are:

$F(\epsilon, a)$, the thermal radiation transfer function, which has no significant dependence upon the radiator temperature (§4(*b*));

T_{68}, the effective temperature of the radiator given by (34) (§§2(*c*) and 4(*a*));

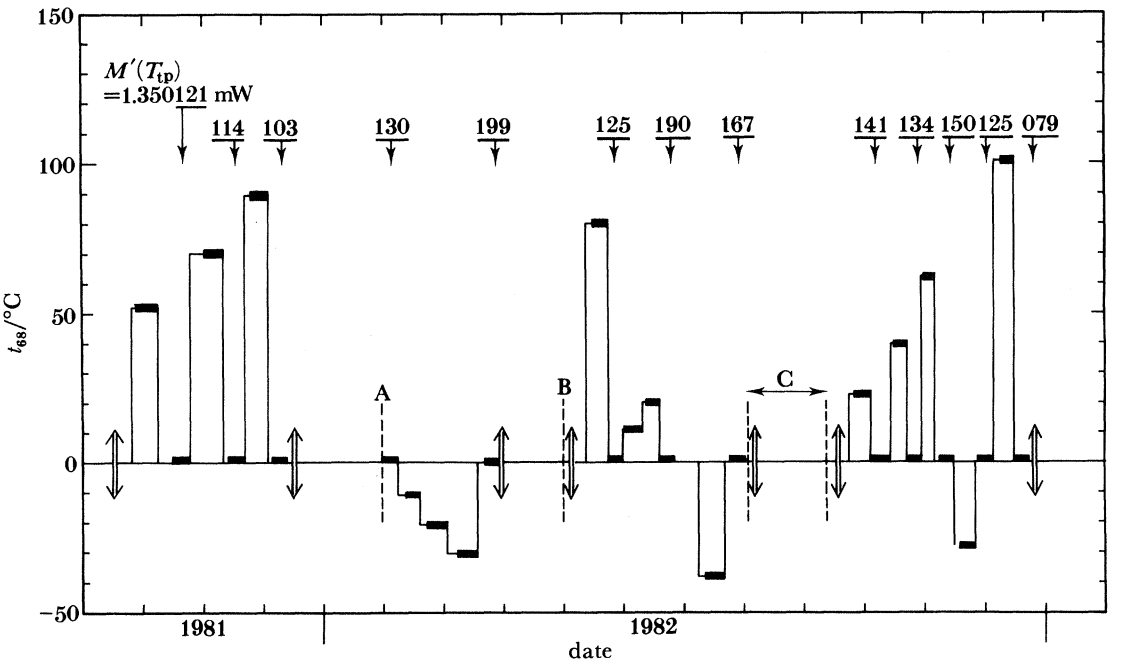

FIGURE 37. This figure shows the order in which measurements of T were made with the large pair of apertures. Also given are the values of $M'(T_{tp})$ obtained after each measurement of T (after the first value only the last three figures of the subsequent values are given). The value of $M'(T_{tp})$ equivalent to the final value for σ (large apertures) is 1.350200 mW. The double-headed arrows indicate the occasions on which the whole apparatus was warmed to room temperature: A, a failure of the turbomolecular pump; B, breakage of the shutter control wire; C, a period during which leaks appeared in a top-plate seal of the liquid-nitrogen reservoir.

g, the throughput (§6(*c*));

$D(T)$, the diffraction correction, which is a function of effective wavelength and hence a function of T (§7 and figures 31 and 32);

$L(T)$, the land scattering correction, which has a small wavelength dependence and is thus also a function of T (§5(*e*) and figure 27);

s, the radiation-trap scattering correction, which has a negligible wavelength dependence (§6(*d*) and table 11);

$p(T)$, the pressure correction, which depends upon radiator temperature (§8(*a*) and figure 33);

$\delta M'(T)$, the change in radiant power entering the calorimeter from the radiation trap on opening and closing the shutter (this depends upon T (§6(*d*))).

For the determination of the Stefan–Boltzmann constant, T is made sufficiently close to 273.16 K, the triple point of water, for the measured radiator temperature T_{68} to be equivalent to the thermodynamic temperature with negligible error, i.e. $\Delta T \approx 0$ (this difference between T and T_{68} deduced from our measurements at 274 K, for example, is about 0.3 mK).

For the measurement of T, which we write as $(T_{68}+\Delta T)$, the relation between measured quantities is given by

$$\frac{M'(T)}{M'(T_{tp})} = \frac{M'(T_{68}+\Delta T)}{M'(T_{tp})} = \frac{[1-D(T)]\,[1-L(T)]\,[1+p(T)]}{[1-D(T_{tp})]\,[1-L(T_{tp})]\,[1+p(T_{tp})]}\left(\frac{T}{T_{tp}}\right)^4 \tag{106}$$

and

$$\frac{M'(T)}{M'(T_{tp})} = \frac{[V_c V_s/R_s - \delta M'(T)]_T}{[V_c V_s/R_s - \delta M'(T_{tp})]_{T_{tp}}}, \tag{107}$$

where we assume that $M'(T_{tp})$ is measured immediately after $M'(T)$. From these relations, T can be determined in terms of the measured voltages and resistance and the small corrections. Since for each value of T the equivalent value of T_{68} is already known, the difference $(T-T_{68})$ is also obtained.

A summary of the corrections and their associated uncertainties of both type A and type B (see §1 (*e*)) given in terms of one standard deviation is given in tables 13 and 14 (*a*) and (*b*). The combination of these uncertainties is straightforward since, with the exception of $F(\epsilon, a)$ and s, they are all considered to be independent and can therefore simply be combined in quadrature.

TABLE 13. SUMMARY OF CALCULATED CORRECTIONS AND UNCERTAINTIES IN THE DETERMINATION OF THE STEFAN–BOLTZMANN CONSTANT σ

	large pair of apertures			small pair of apertures		
quantity	calculated correction $10^4\,(\Delta\sigma/\sigma)$	relative uncertainty $10^4\,(\Delta\sigma/\sigma)$		calculated correction $10^4\,(\Delta\sigma/\sigma)$	relative uncertainty $10^4\,(\Delta\sigma/\sigma)$	
$F(\epsilon, a)$	6.1	1.4[a]	type B	2.7	1.0[a]	type B
$D(T)$	1.1	0.7		2.1	1.2	
$L(T)$	2.4	0.2		1.8	0.15	
s	−0.8	0.2[a]		−0.8	0.2[a]	
$\Delta T(H_2)$[b]	nil	nil		−0.2[b]	0.2[b]	
$V_c V_s/R_s$	—	0.2		—	0.2	
T_{68}	—	0.1		—	0.1	
$p(T)$[c]	—	⩽ 0.01		—	⩽ 0.01	
$\Delta M'(T)$[c]	—	⩽ 0.01		—	⩽ 0.01	
g	—	0.9		—	1.6	
std deviation of n measured values	—	$(n = 27)$ 0.12[d]	type A	—	$(n = 20)$ 0.5[d]	type A
combined corrections and uncertainties	8.8	1.7		5.6	2.2	

[a] These uncertainties are strongly correlated because they both stem from uncertainties in surface reflectance. The combined uncertainties of $F(\epsilon, a)$ and s are thus 1.2×10^{-4} and 0.8×10^{-4} for the large and small apertures, respectively.

[b] This correction applies only to the first set of measurements made with the small pair of apertures, which are given in table 16.

[c] Each individual measurement of σ is subject to small corrections $p(T)$ and $\delta M'(T)$, which are listed in tables 15 and 16; here only the uncertainties in these corrections are given.

[d] Values taken from tables 15 and 16.

Rewriting (106) and (107), substituting $(T_{68}+\Delta T)$ for T and writing $D(T-T_{tp})$, $L(T-T_{tp})$ and $p(T-T_{tp})$ for the differences between the diffraction, land and pressure corrections at temperatures T and T_{tp}, we find

$$T_{68}+\Delta T = T_{tp}\left[\frac{[V_c V_s/R_s-\delta M'(T_{rt})]_T}{[V_c V_s/R_s-\delta M'(T_{tp})]_{T_{tp}}[1-\{D(T-T_{tp})+L(T-T_{tp})+p(T-T_{tp})\}]}\right]^{\frac{1}{4}}. \tag{108}$$

(*c*) *The Stefan–Boltzmann constant*

Tables 15 and 16 show the results of all the measurements made for the determination of the Stefan–Boltzmann constant with the large and small pair of apertures respectively. In each table the first five columns refer to the radiator temperature, giving values of T_1, T_6 and T_3 by difference from the effective temperature t_{68} (given in column 5) and the drift rate. Column

TABLE 14. SUMMARY OF CALCULATED CORRECTIONS AND UNCERTAINTIES IN THE DETERMINATION OF THERMODYNAMIC TEMPERATURE FOR BOTH THE LARGE AND SMALL PAIR OF APERTURES

(*a*) large pair of apertures*

quantity	$T = 233$ K calculated correction, ΔT/mK	$T = 233$ K relative uncertainty, ΔT/mK		$T = 375$ K calculated correction, ΔT/mK	$T = 375$ K relative uncertainty, ΔT/mK	
$D(T-T_{tp})$	1.1	0.7	type B	−2.8	1.7	type B
$L(T-T_{tp})$	−0.6	0.2		2.1	0.4	
$V_c V_s/R_s$	—	0.3		—	0.5	
T_{68}	—	0.6		—	1.0	
$p(T)$**	—	0.1		—	0.1	
$\delta M'(T)$**	—	0.05		—	0.1	
std deviation of n measured values	—	($n = 20$) 0.8	type A	—	($n = 20$) 1.4	type A
combined corrections and uncertainties	0.5	1.3		−0.7	2.5	

(*b*) small pair of apertures

quantity	$T = 313$ K calculated correction, ΔT/mK	$T = 313$ K relative uncertainty, ΔT/mK	
$D(T-T_{tp})$	3.2	1.0	type B
$L(T-T_{tp})$	−0.8	0.2	
$\Delta T(H_2)$ $T_c \leqslant 4$ K	X***	X	
$\Delta T(H_2)$ $T_c \approx 5$ K	nil***	—	
$V_c V_s/R_s$	—	0.4	
T_{68}	—	0.8	
$p(T)$**	—	0.5	
$\delta M'(T)$**	—	0.5	
std deviation of n measured values	—	($n = 20$) 5.4	type A
combined corrections and uncertainties			
$T_c \leqslant 4$ K	(difficult to evaluate)		
$T_c \approx 5$ K	2.4	5.6	

* The values given in this table are intended to give an overall view of the magnitude of these corrections and their uncertainties for values of T at the extremes of the measured range. The corrections and type A uncertainties for each individual measurement are given in tables 19 and 20 in terms of radiant power. The type B uncertainties for intermediate temperatures are given in table 18.

** The corrections to each individual measurement are given in tables 19 and 20.

*** X represents the correction and its associated uncertainty, each of the order of 10 mK, due to hydrogen condensation (§8(*b*)) present only for $T_c \leqslant 4$ K.

TABLE 15. STEFAN–BOLTZMANN CONSTANT, σ (LARGE APERTURES)

first set (29 April 1981 to 8 May 1981)

T_1/mK	T_6/mK	T_3/mK	$\frac{dT/5\text{ min}}{mK}$	t_{68}/°C	$M'(T)$/mW	$\frac{\delta M'(T)}{nW}$	$\frac{p(T)}{nW}$	$\frac{[D(T)+L(T)]}{nW}$	$\frac{[F(\epsilon,a)+s]}{nW}$	$\frac{10^8\,\sigma}{(W\,m^{-2}\,K^{-4})}$
+15.9	−0.2	−3.6	+1.8	−0.7547	1.334015	−18	−4	468	707	5.67002
+12.1	+0.2	−2.8	+0.7	0.1628	1.352091	−19	−4	474	717	5.67006
−2.2	+1.2	+0.5	−2.0	−0.7232	1.334610	−19	−4	468	708	5.66991
+0.4	+0.7	−0.1	−1.6	−0.6795	1.335493	−18	−4	468	708	5.67003
+2.1	+0.5	−0.5	−1.3	−0.7017	1.335044	−18	−4	468	708	5.66998
+0.4	+0.6	−0.1	−1.6	−0.6504	1.336065	−18	−4	469	708	5.67004
+1.4	+0.8	−0.3	−1.3	−0.6852	1.335360	−18	−4	468	708	5.66994
−1.2	+0.9	+0.2	−1.9	−0.5127	1.338764	−19	−4	470	710	5.67002

mean Stefan–Boltzmann constant = $(5.67000 \pm 0.00005) \times 10^{-8}$ W m^{-2} K^{-4}

TABLE 15. (*continued*)

second set (21 May 1981 to 2 June 1981)

T_1/mK	T_6/mK	T_3/mK	$\frac{dT/5\ min}{mK}$	t_{68}/°C	$M'(T)$/mW	$\frac{\delta M'(T)}{nW}$	$\frac{p(T)}{nW}$	$\frac{[D(T)+L(T)]}{nW}$	$\frac{[F(\epsilon,a)+s]}{nW}$	$\frac{10^8\,\sigma}{(W\,m^{-2}\,K^{-4})}$
−12.9	+1.8	+2.9	−4.3	2.5031	1.398933	−20	−4	490	742	5.66979
−11.1	+1.6	+2.4	−4.0	2.3986	1.396828	−20	−4	489	741	5.66985
−12.3	+1.7	+2.7	−4.2	2.2363	1.393514	−20	−4	488	739	5.66974
−6.4	+1.6	+1.4	−3.1	0.2978	1.354715	−19	−4	475	718	5.66985
−3.6	+1.3	+0.8	−2.2	0.0538	1.349920	−19	−4	473	716	5.66999
−2.6	+1.1	+0.6	−2.1	−0.0508	1.347831	−19	−4	472	715	5.66990
−2.0	+1.0	+0.4	−2.0	−0.0997	1.346887	−19	−4	472	714	5.66999
−3.3	+0.9	+0.8	−2.2	0.0119	1.349070	−19	−4	473	715	5.66990
−2.9	+1.1	+0.6	−2.2	−0.1239	1.346379	−18	−4	472	714	5.66986
−2.1	+1.0	+0.5	−2.1	−0.1740	1.345381	−19	−4	472	713	5.66982

mean Stefan–Boltzmann constant = $(5.66987 \pm 0.00008) \times 10^{-8}$ W m^{-2} K^{-4}

third set (25 June 1981 to 2 July 1981)

−5.3	+1.0	+1.2	−2.7	0.1579	1.351938	−18	−4	474	717	5.66983
−3.5	+0.9	+0.8	−2.3	0.0909	1.350615	−18	−4	473	716	5.66984
−3.4	+1.2	+0.7	−2.4	0.1515	1.351791	−19	−4	474	717	5.66974
−2.0	+0.9	+0.4	−2.1	0.0830	1.350486	−18	−4	473	716	5.66995
−2.1	+0.9	+0.5	−2.0	0.0031	1.348862	−18	−4	473	715	5.66976
−1.2	+1.1	+0.2	−1.9	−0.0572	1.347695	−18	−4	472	715	5.66986
−1.4	+0.9	+0.3	−1.9	−0.1029	1.346790	−18	−4	472	714	5.66985
−0.5	+0.8	+0.1	−1.7	−0.1444	1.345967	−18	−4	472	714	5.66983
−0.6	+0.8	+0.2	−1.8	−0.2242	1.344435	−18	−4	472	713	5.67000

mean Stefan–Boltzmann constant = $(5.66985 \pm 0.00008) \times 10^{-8}$ W m^{-2} K^{-4}

TABLE 16. STEFAN–BOLTZMANN CONSTANT, σ (SMALL APERTURES)

first set (16 May 1983 to 20 May 1983)

T_1/mK	T_6/mK	T_3/mK	$\frac{dT/5\ min}{mK}$	t_{68}/°C	$M'(T)$/mW	$\frac{\delta M'(T)}{nW}$	$\frac{p(T)}{nW}$	$\frac{[D(T)+L(T)]}{nW}$	$\frac{[F(\epsilon,a)+s]}{nW}$	$\frac{10^8\,\sigma}{(W\,m^{-2}\,K^{-4})}$
−12.3	−0.6	+0.3	−3.1	2.1801	0.217144	−2	−5	84	41	5.66956
−10.7	−0.3	+0.2	−2.8	2.0618	0.216747	−2	−5	83	41	5.66893
−7.3	+0.1	+0.1	−2.2	1.6865	0.215560	−1	−5	83	41	5.66877
−6.8	+0.1	+0.1	−2.2	1.6179	0.215342	−3	−5	83	41	5.66865
−4.7	+0.3	+0.1	−1.8	1.2353	0.214162	−1	−5	83	41	5.66914
−4.5	+0.4	+0.1	−1.8	1.1811	0.213993	−3	−5	83	41	5.66909
−3.6	+0.4	+0.1	−1.6	0.9330	0.213207	−3	−5	82	41	5.66875
−2.9	+0.5	+0.0	−1.5	0.8737	0.213031	−3	−5	82	40	5.66898
−2.5	+0.6	+0.0	−1.4	0.6528	0.212340	−3	−5	82	40	5.66885
−2.4	+0.5	+0.0	−1.4	0.6065	0.212191	−2	−5	82	40	5.66873

mean Stefan–Boltzmann constant = $(5.66894 \pm 0.00027) \times 10^{-8}$ W m^{-2} K^{-4}

second set (18 October 1983 to 26 October 1983)

+3.8	+1.6	−0.2	−0.3	0.3703	0.211485	−1	−1	82	40	5.66954
+7.0	+1.9	−0.3	+0.2	0.3709	0.211483	+0	−1	82	40	5.66946
+6.3	+1.9	−0.2	+0.1	0.7618	0.212693	−1	+0	82	40	5.66940
+5.8	+1.9	−0.2	−0.0	0.7661	0.212708	−1	+0	82	40	5.66944
+6.3	+1.9	−0.2	+0.1	0.9073	0.213166	−1	+0	82	41	5.66995
+6.2	+1.8	−0.2	+0.0	0.9134	0.213170	−1	+0	82	41	5.66955
+0.9	+1.2	−0.1	−0.8	−0.0842	0.210112	+0	+0	81	40	5.67036
+0.9	+1.3	−0.1	−0.9	−0.1169	0.209992	−1	+0	81	40	5.66981
+2.0	+1.4	−0.1	−0.6	−0.0814	0.210116	−1	+0	81	40	5.67021
+2.3	+1.5	−0.1	−0.6	−0.1024	0.210021	−1	+0	81	40	5.66939

mean Stefan–Boltzmann constant = $(5.66971 \pm 0.00035) \times 10^{-8}$ W m^{-2} K^{-4}

TABLE 17. FINAL RESULTS OF THE RADIOMETRIC DETERMINATION OF THE STEFAN–BOLTZMANN CONSTANT

	$10^8\,\sigma/(\mathrm{W\,m^{-2}\,K^{-4}})$	std deviation of n measurements[a], $10^8\,\sigma/(\mathrm{W\,m^{-2}\,K^{-4}})$	std deviation of type B uncertainties[b], $10^8\,\sigma/(\mathrm{W\,m^{-2}\,K^{-4}})$
large pair of apertures			
1st series	5.67000	0.00005 ($n = 8$)	0.00096
2nd series	5.66987	0.00008 ($n = 10$)	
3rd series	5.66985	0.00008 ($n = 9$)	
mean value	5.66991	0.00007 ($n = 27$)	0.00096
small pair of apertures			
1st series	5.66894	0.00027 ($n = 10$)	0.0012
2nd series	5.66971	0.00035 ($n = 10$)	
mean value	5.66933	0.00031 ($n = 20$)	0.0012
		(combined uncertainty)	
weighted mean	5.66967	0.00076	

[a] Type A uncertainties; values obtained from tables 15 and 16.
[b] Values taken from table 13.

6 shows the measured power equivalent to this value of t_{68}, columns 7 to 10 show the corrections which are made to this measured power and column 11 shows the resulting value for σ. The mean value of σ is given for each series together with the standard deviation of the measured values. The mean values of the three series of table 15 and two series of table 16 are given together with their associated standard deviation in table 17. The overall relative uncertainties for these two mean values of σ are obtained from table 13. These are 1.7 parts in 10^4 and 2.2 parts in 10^4 for the large and small aperture series, respectively. We thus find that the value of σ obtained from the measurements made with the large pair of apertures is

$$\sigma = (5.66991 \pm 0.00096) \times 10^{-8}\ \mathrm{W\,m^{-2}\,K^{-4}},$$

and for the small pair of apertures:

$$\sigma = (5.66933 \pm 0.00125) \times 10^{-8}\ \mathrm{W\,m^{-2}\,K^{-4}}.$$

Our final value for σ, which we have chosen to obtain by combining these two results with a weighting inversely proportional to the square of their respective standard deviations, is thus

$$\sigma = \mathbf{(5.66967 \pm 0.00076) \times 10^{-8}}\ \mathrm{W\,m^{-2}\,K^{-4}}.$$

Other ways of combining the data do not lead to final results differing by more than a small fraction of the standard deviation of the value given here.

This new measured value, the uncertainty of which is equivalent to 1.3 parts in 10^4 of σ, differs by 1.3 parts in 10^4 from the value calculated from fundamental physical constants given in §1 (*a*), namely

$$\sigma = 5.67042 \pm 0.00019) \times 10^{-8}\ \mathrm{W\,m^{-2}\,K^{-4}}.$$

The difference between these two values is thus a little less than their combined standard deviations and cannot, therefore, be considered significant (see figure 38). The previous best

measured value of σ, that of Blevin & Brown (1971), differed from the calculated value by about 1 part in 10^3, although this difference was not at the time considered significant, owing mainly to uncertainties related to the radiator at 1337 K. Our new result has, therefore, reduced by about a factor of ten the possible inconsistency between the measured and calculated values for σ.

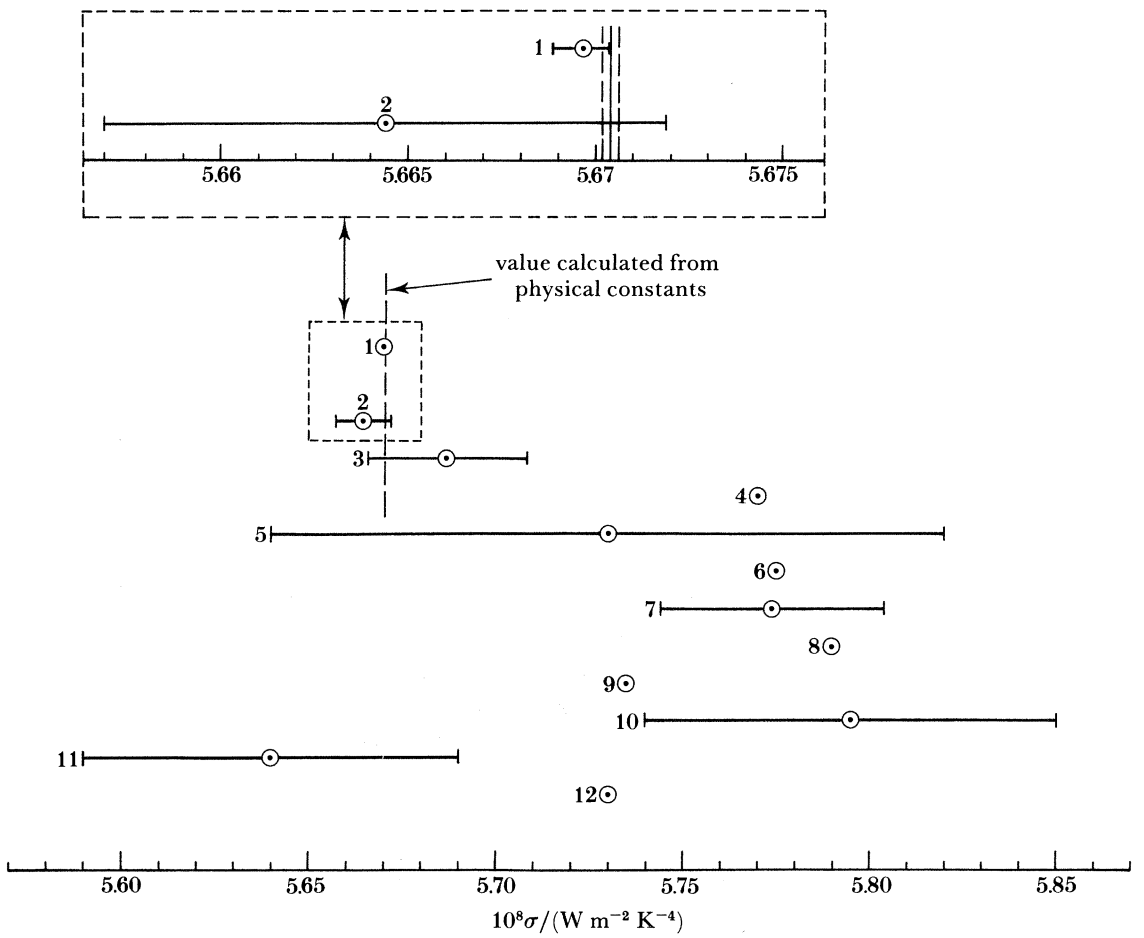

FIGURE 38. Experimental values for the Stefan–Boltzmann constant obtained since 1921. Note the long period, 1924 to 1965, during which all measurements apparently led to values, on average, 1.8% too high. The uncertainties are the authors' own estimates, and for Blevin & Brown (1971) represent a 99% confidence level. For the present work and for the calculated value the uncertainties are shown as ± 1 standard deviation. For bibliographic references to all the work before 1971, see Blevin & Brown (1971). The value calculated from physical constants is $(5.67042 \pm 0.00019) \times 10^{-8}$ W m^{-2} K^{-4}. The values or references, or both, for the other points are: (1) present work, $(5.66967 \pm 0.00076) \times 10^{-8}$ W m^{-2} K^{-4}; (2) Blevin & Brown (1971), $(5.6644 \pm 0.0075) \times 10^{-8}$ W m^{-2} K^{-4}; (3) Kendall (1968); (4) Gilham (1965); (5) Faure (1965); (6) Eppley & Karoli (1957); (7) Muller (1933); (8) Mendenhall (1929); (9) Hoare (1928); (10) Kaussmann (1924); (11) Hoffman (1923); (12) Wachsmuth (1921).

It has, in addition, brought the uncertainty of radiometric measurements of σ down to within nearly a factor of three of that of the value calculated from fundamental physical constants. Indeed, the repeatability of the measurements is already rather better than this (12 parts in 10^6 for the large pair of apertures (see table 17)) and thus holds out the possibility of a further substantial improvement provided that some of the other sources of uncertainty can be reduced.

This is discussed further in the last section of this paper. The final value for σ given here does not differ significantly from the preliminary value given by Quinn & Martin (1984).

The value of the gas constant, which can be deduced from our result by using the relation for σ given in (1) and (2) and on the basis of the values of h and N_A given in §1(*a*), is $R = 8.31420 \pm 0.00027\ \mathrm{J\ K^{-1}\ mol^{-1}}$. This is 33 parts in 10^6 different from the value of Colclough *et al.* (1979) obtained from measurements of the speed of sound (see also Colclough (1981) and Quinn *et al.* (1976)). However, the uncertainty (32 parts in 10^6) is more than three times larger than that of the acoustic value. Nevertheless, it is a striking example of the unity of physics: a value for the gas constant determined from measurements of the thermal radiative power of a black body by using the quantum theory of radiation deduced for an ideal, infinite, lossless closed cavity being indistinguishable from one obtained from measurements of the speed of sound in argon, by using a theory based upon classical dynamics of a continuous fluid. This result could also be interpreted as providing an experimental verification, to 1.3 parts in 10^4, of the Planck radiation law for 273 K radiation.

(*d*) *Thermodynamic temperatures*

The thermodynamic temperatures and the differences $(T - T_{68})$ resulting from this work are shown in figure 39 and table 18. For each of the fifteen temperatures measured with the large pair of apertures and the single temperature obtained without the effects of hydrogen

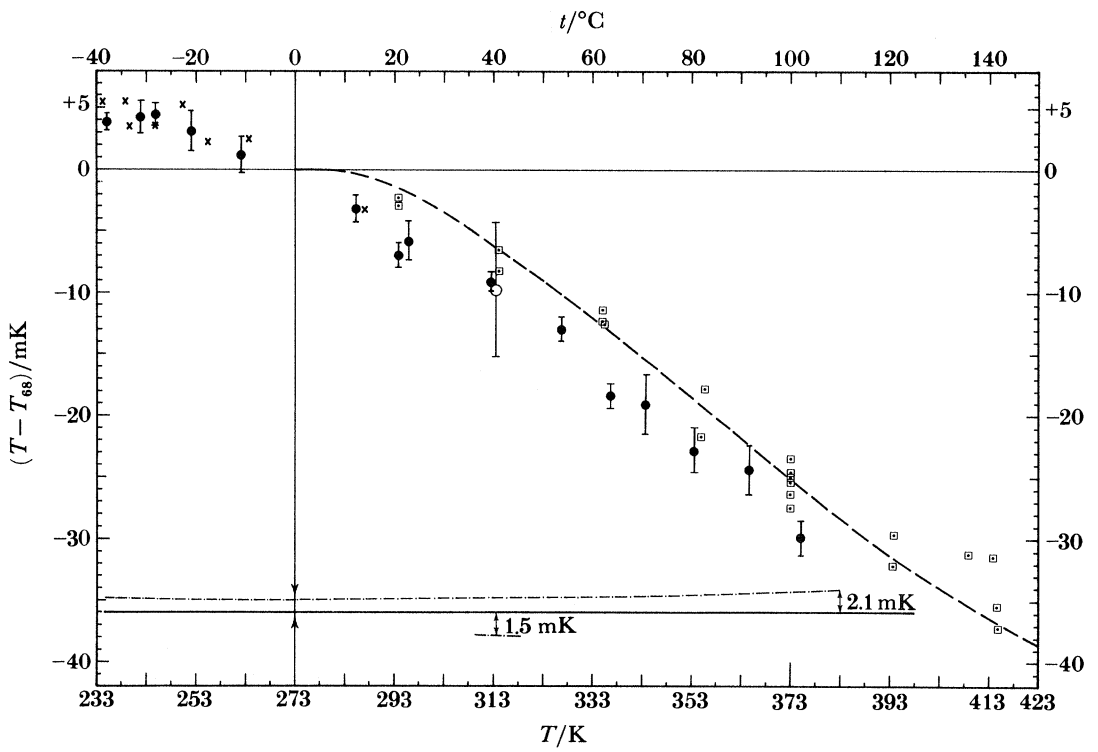

FIGURE 39. Results of radiometric measurements of $(T - T_{68})$ between 233 K and 373 K: ●, large pair of apertures; ○, small pair of apertures. The bars on each point represent ± 1 standard deviation of the measured values (type A uncertainty). At the bottom of the figure the chained line indicates one standard deviation of the type B uncertainty for the large pair (upper line) and the small pair (lower line). Also shown are the measured values of $(T - T_{68})$ of Guildner & Edsinger (1976), ⊡, together with their fitted curve, ——, and values from Kemp *et al.* (1984), ×.

condensation by using the small pair of apertures, the results are given in full in tables 19 and 20. These results do not differ significantly from the preliminary values for $t_{68} \approx 50$, 70 and 90 °C given by Quinn & Martin (1982). For each temperature in tables 19 and 20 the results are given in two parts, first the results of the series of about ten measurements of $M'(T_{tp})$, from which a mean value of $M'(T_{tp})$ is deduced, and second the results of the series of measurements of $M'(T)$. By using the mean value of $M'(T_{tp})$, a value of T is calculated from each of these values of $M'(T)$. The layout of the tables follows closely that of tables 15 and 16; columns 1 to 5 give the temperature distribution, drift rate and effective temperature, t_{68}, of the radiator, column 6 gives the measured value of $M'(T)$, columns 7 to 10 give the corrections that are applied to the measured power and column 11 gives either the calculated value of $M'(T_{tp})$ or T. A final column in the second part gives $(T-T_{68})$. Below each part of the table is the mean value of $M'(T_{tp})$ or $(T-T_{68})$. Each of these means has an uncertainty, which is the standard deviation of the individual values about the mean.

TABLE 18. FINAL RESULTS FOR $(T-T_{68})$

		uncertainties (1 std deviation)/mK		
t_{68}/°C	$(T-T_{68})$/mK	type A[a]	type B[b]	combined
−37.97	3.8	0.8	1.0	1.3
−30.75	4.2	1.3	1.0	1.6
−27.75	4.4	0.9	1.0	1.3
−20.87	3.1	1.6	1.0	1.9
−10.86	1.2	1.5	1.0	1.8
12.12	−3.2	1.1	1.0	1.6
20.75	−7.0	1.0	1.2	1.6
22.86	−5.8	1.6	1.2	2.0
39.69	−9.1	0.8	1.4	1.6
40.22[c]	−9.8	5.4	1.5	5.6
53.85	−13.0	1.0	1.4	1.7
63.66	−18.4	1.0	1.5	1.8
70.91	−19.1	2.4	1.6	2.9
80.57	−22.8	1.8	1.8	2.5
91.63	−24.3	1.9	1.9	2.7
102.03	−29.9	1.4	2.1	2.5

[a] Taken from tables 19 and 20.
[b] Interpolated values based upon those given in tables 14(*a*), (*b*).
[c] This measurement was made with the small pair of apertures.

The uncertainties of these means are then combined to give a standard deviation of the mean value of $(T-T_{68})$. This is a type A uncertainty and is given for each temperature in the tables and shown in figure 39 by the bar that is attached to each point. In addition, each value of $(T-T_{68})$ is subject to a type B uncertainty, which is the combination of the other uncertainties given in tables 14*a* and 14*b*. These are the uncertainties that stem mainly from uncertainties in the difference between the diffraction and land corrections at temperatures T and T_{tp}. They increase from about 1 mK at and below 273 K to 2.1 mK at 373 K, and are given in table 18 and shown by the chained lines at the bottom of figure 39. The combined type A and type B uncertainties are also given in table 18.

The differences $(T-T_{68})$ shown in figure 39 are in very close agreement with those deduced from gas thermometry by Guildner & Edsinger (1976) and which are also shown in the figure. The measurements of Guildner & Edsinger extended to much higher temperatures than ours (730 K), but did not extend below 273 K. More recently, gas thermometry by

TABLE 19. VALUES OF $T - T_{68}$

temperature: −38 °C (13 *July* 1982 *to* 28 *July* 1982)

T_1/mK	T_6/mK	T_3/mK	dT/5 min / mK	t_{68}/°C	$M'(T)$/mW	$\delta M'(T)$ / nW	$p(T)$ / nW	$[D(T)+L(T)]$ / nW	$[F(\epsilon,a)+s]$ / nW	$M'(T_{tp})$ / mW
+8.0	+0.2	−1.7	+0.2	−0.1698	1.345420	+12	−3	472	713	1.350165
+5.6	−0.0	−1.1	−0.4	−0.1931	1.344967	+12	−3	472	713	1.350172
+1.1	+2.3	−0.5	−1.3	−0.6827	1.335328	+12	−3	468	708	1.350156
+0.8	+2.2	−0.4	−1.4	−0.7463	1.334087	+12	−3	468	707	1.350161
+15.1	−0.6	−3.3	+1.8	−0.4734	1.339438	+12	−3	470	710	1.350160
+14.8	−0.5	−3.2	+1.7	−0.4384	1.340158	+12	−3	470	711	1.350191
+14.0	−0.6	−3.0	+1.6	−0.2474	1.343902	+12	−3	471	713	1.350177
+13.8	−0.5	−3.0	+1.5	−0.2247	1.344339	+12	−3	472	713	1.350167
+13.2	−0.5	−2.9	+1.3	−0.1562	1.345690	+12	−3	472	713	1.350169
+12.9	−0.4	−2.8	+1.3	−0.1349	1.346090	+12	−3	472	714	1.350147

mean $M'(T_{tp}) = 1.350167 \pm 0.000012$ mW

T_1/mK	T_6/mK	T_3/mK	dT/5 min / mK	t_{68}/°C	$M'(T)$/mW	$\delta M'(T)$ / nW	$p(T)$ / nW	$[D(T)+L(T)]$ / nW	$[F(\epsilon,a)+s]$ / nW	t/°C	$(T-T_{68})$ / mK
+1.4	+2.5	−0.7	−0.6	−37.3300	0.749335	+4	−2	269	397	−37.3270	+3.0
+2.4	+2.4	−0.9	−0.3	−37.5299	0.746798	+4	−2	268	396	−37.5269	+3.0
+2.3	+2.4	−0.9	−0.4	−37.5511	0.746548	+4	−2	268	396	−37.5466	+4.5
+2.9	+2.4	−1.1	−0.3	−37.7660	0.743811	+4	−2	267	394	−37.7628	+3.2
+2.6	+2.3	−0.9	−0.2	−37.7838	0.743591	+4	−2	267	394	−37.7802	+3.5
+2.9	+2.3	−1.0	−0.2	−37.9794	0.741136	+4	−2	266	393	−37.9748	+4.6
+2.7	+2.4	−1.0	−0.2	−37.9960	0.740917	+4	−2	266	393	−37.9921	+3.9
+4.0	+2.2	−1.3	+0.1	−38.5652	0.733767	+4	−2	264	389	−38.5615	+3.7
+4.2	+2.2	−1.4	+0.1	−38.5746	0.733656	+4	−2	264	389	−38.5704	+4.3
+4.7	+2.1	−1.4	+0.2	−38.6657	0.732515	+4	−2	263	388	−38.6616	+4.0

mean $(T - T_{68}) = +3.8 \pm 0.6$ mK

combining the uncertainties: $(T - T_{68}) = +3.8 \pm 0.8$ mK at $t_{68} = -37.97$ °C

temperature: −28 °C (22 *November* 1982 *to* 3 *December* 1982)

T_1/mK	T_6/mK	T_3/mK	dT/5 min / mK	t_{68}/°C	$M'(T)$/mW	$\delta M'(T)$ / nW	$p(T)$ / nW	$[D(T)+L(T)]$ / nW	$[F(\epsilon,a)+s]$ / nW	$M'(T_{tp})$ / mW
−9.9	+1.4	+2.3	−3.5	−1.1008	1.327149	−18	−5	465	704	1.350122
−9.5	+1.4	+2.2	−3.5	−1.1730	1.325742	−17	−5	465	703	1.350125
+5.5	+0.5	−1.3	−0.3	−1.0277	1.328600	−18	−4	466	704	1.350149
+5.3	+0.4	−1.2	−0.2	−1.0079	1.328975	−18	−4	466	705	1.350137
+4.8	+0.5	−1.0	−0.4	−0.7013	1.334966	−18	−4	468	708	1.350128
+5.3	+0.3	−1.2	−0.4	−0.6887	1.335207	−18	−4	468	708	1.350123
+2.8	+0.8	−0.6	−0.9	−0.3831	1.341210	−18	−4	470	711	1.350124
+2.7	+0.4	−0.5	−0.9	−0.3868	1.341123	−18	−4	470	711	1.350110
+2.7	+0.6	−0.6	−0.9	−0.2234	1.344351	−18	−4	472	713	1.350122
+3.3	+0.5	−0.7	−1.0	−0.2219	1.344366	−19	−4	472	713	1.350106

mean $M'(T_{tp}) = 1.350125 \pm 0.000012$ mW

T_1/mK	T_6/mK	T_3/mK	dT/5 min / mK	t_{68}/°C	$M'(T)$/mW	$\delta M'(T)$ / nW	$p(T)$ / nW	$[D(T)+L(T)]$ / nW	$[F(\epsilon,a)+s]$ / nW	t/°C	$(T-T_{68})$ / mK
+6.1	+1.5	−1.6	+0.3	−28.3263	0.870511	−10	−3	311	462	−28.3216	+4.7
+6.5	+1.7	−1.7	+0.4	−28.2978	0.870919	−10	−3	311	462	−28.2929	+4.9
+6.8	+1.6	−1.8	+0.4	−27.8558	0.877210	−10	−3	313	465	−27.8519	+3.9
+7.1	+1.7	−1.9	+0.4	−27.8271	0.877632	−10	−3	313	465	−27.8224	+4.7
+5.6	+1.5	−1.5	+0.2	−27.4886	0.882491	−10	−2	315	468	−27.4835	+5.1
+5.7	+1.8	−1.6	+0.1	−27.4701	0.882747	−10	−2	315	468	−27.4657	+4.4
+5.3	+1.6	−1.5	+0.0	−27.4538	0.882986	−10	−2	315	468	−27.4490	+4.8
+1.9	+2.0	−0.7	−0.6	−27.2996	0.885181	−10	−2	316	469	−27.2965	+3.1

mean $(T - T_{68}) = +4.4 \pm 0.6$ mK

combining the uncertainties: $(T - T_{68}) = +4.4 \pm 0.9$ mK at $t_{68} = -27.75$ °C

TABLE 19. (*continued*)

$M'(T_{tp})$ (1 *February* 1982 *to* 8 *February* 1982)

T_1/mK	T_6/mK	T_3/mK	dT/5 min / mK	t_{68}/°C	$M'(T)$/mW	$\delta M'(T)$ / nW	$p(T)$ / nW	$[D(T)+L(T)]$ / nW	$[F(\epsilon,a)+s]$ / nW	$M'(T_{tp})$ / mW
−6.3	+1.9	+1.3	−2.8	0.4717	1.358082	−20	−10	476	720	1.350097
−5.7	+1.9	+1.1	−2.8	0.4051	1.356814	−19	−10	476	719	1.350152
−9.3	+1.9	+2.0	−3.5	0.5415	1.359452	−19	−11	477	721	1.350081
−9.1	+1.9	+2.0	−3.5	0.4561	1.357823	−19	−11	476	720	1.350147
−8.9	+1.8	+1.9	−3.4	0.0420	1.349579	−19	−12	473	716	1.350104
−8.1	+1.8	+1.7	−3.2	−0.0333	1.348135	−19	−12	472	715	1.350147
+2.7	+0.3	−0.6	−1.0	−0.0092	1.348629	−19	−12	473	715	1.350166
+4.1	+0.3	−0.9	−0.7	−0.0184	1.348435	−19	−12	473	715	1.350153
−1.8	+1.7	+0.3	−1.9	0.8481	1.365594	−19	−13	479	724	1.350118
−1.3	+1.7	+0.2	−1.8	0.8145	1.364941	−19	−13	479	724	1.350135

mean $M'(T_{tp}) = 1.350130 \pm 0.000028$ mW

temperature: −31 °C (8 *March* 1982 *to* 16 *March* 1982)

T_1/mK	T_6/mK	T_3/mK	dT/5 min / mK	t_{68}/°C	$M'(T)$/mW	$\delta M'(T)$ / nW	$p(T)$ / nW	$[D(T)+L(T)]$ / nW	$[F(\epsilon,a)+s]$ / nW	t/°C	$(T-T_{68})$ / mK
−8.3	+1.6	+1.8	−2.7	−30.1005	0.845567	−10	−2	302	448	−30.0969	+3.5
−5.9	+1.7	+1.2	−2.3	−30.4282	0.841010	−10	−2	301	446	−30.4251	+3.1
−5.3	+1.4	+1.1	−2.2	−30.4922	0.840143	−10	−2	300	445	−30.4877	+4.5
−3.2	+1.3	+0.6	−1.7	−30.8132	0.835691	−10	−1	299	443	−30.8100	+3.2
−3.1	+1.3	+0.6	−1.7	−30.8429	0.835291	−10	−1	298	443	−30.8390	+3.9
−2.3	+1.2	+0.4	−1.5	−30.9344	0.834039	−10	−1	298	442	−30.9300	+4.4
−2.0	+1.2	+0.3	−1.5	−30.9705	0.833556	−10	−1	298	442	−30.9651	+5.4
−2.9	+1.3	+0.5	−1.6	−31.0581	0.832348	−10	−1	297	441	−31.0529	+5.2
−2.6	+1.2	+0.5	−1.6	−31.0955	0.831820	−10	−1	297	441	−31.0913	+4.1

mean $(T-T_{68}) = +4.2 \pm 0.8$ mK

combining the uncertainties: $(T-T_{68}) = +4.2 \pm 1.3$ mK at $t_{68} = -30.75$ °C

temperature: −21 °C (23 *February* 1982 *to* 2 *March* 1982)

T_1/mK	T_6/mK	T_3/mK	dT/5 min / mK	t_{68}/°C	$M'(T)$/mW	$\delta M'(T)$ / nW	$p(T)$ / nW	$[D(T)+L(T)]$ / nW	$[F(\epsilon,a)+s]$ / nW	t/°C	$(T-T_{68})$ / mK
+1.7	+1.1	−0.5	−0.8	−21.4651	0.972297	−12	−5	345	515	−21.4607	+4.4
+3.1	+1.2	−0.8	−0.5	−21.4637	0.972285	−12	−5	345	515	−21.4615	+2.2
+3.5	+1.3	−0.9	−0.4	−20.8981	0.981067	−12	−5	348	520	−20.8952	+2.9
+3.5	+1.2	−1.0	−0.4	−20.8908	0.981170	−12	−5	348	520	−20.8886	+2.3
+1.3	+1.3	−0.5	−0.8	−20.7309	0.983655	−12	−5	349	522	−20.7290	+1.9
+2.1	+1.4	−0.6	−0.9	−20.7345	0.983591	−12	−5	349	521	−20.7331	+1.3
−0.4	+1.2	−0.1	−1.3	−20.6493	0.984959	−12	−3	349	522	−20.6455	+3.9
−0.2	+1.4	−0.1	−1.2	−20.6649	0.984733	−13	−3	349	522	−20.6600	+4.8
+0.2	+1.3	−0.2	−1.1	−20.6022	0.985681	−12	−3	350	523	−20.5993	+2.9
+0.8	+1.4	−0.4	−1.1	−20.6199	0.985422	−13	−3	350	522	−20.6160	+4.0

mean $(T-T_{68}) = +3.1 \pm 1.2$ mK

combining the uncertainties: $(T-T_{68}) = +3.1 \pm 1.6$ mK at $t_{68} = -20.87$ °C

temperature: −11 °C (11 *February* 1982 *to* 19 *February* 1982)

T_1/mK	T_6/mK	T_3/mK	dT/5 min / mK	t_{68}/°C	$M'(T)$/mW	$\delta M'(T)$ / nW	$p(T)$ / nW	$[D(T)+L(T)]$ / nW	$[F(\epsilon,a)+s]$ / nW	t/°C	$(T-T_{68})$ / mK
−3.3	+1.4	+0.6	−1.8	−11.0880	1.142763	−15	−10	403	606	−11.0875	+0.5
+8.4	+0.6	−2.0	+0.5	−10.7129	1.149340	−15	−9	405	609	−10.7113	+1.6
−4.7	+1.5	+0.9	−2.3	−10.4635	1.153736	−15	−8	407	612	−10.4608	+2.7
−4.4	+1.4	+0.9	−2.3	−10.6401	1.150590	−15	−8	406	610	−10.6402	−0.1
−3.6	+1.6	+0.7	−2.2	−10.6877	1.149775	−15	−8	405	610	−10.6867	+1.0
−3.3	+1.5	+0.6	−2.0	−10.8305	1.147275	−15	−8	404	608	−10.8295	+1.0
−3.0	+1.4	+0.6	−1.9	−10.8683	1.146606	−15	−8	404	608	−10.8678	+0.5
−3.1	+1.5	+0.6	−1.9	−10.9877	1.144563	−15	−7	403	607	−10.9848	+2.9
−3.2	+1.4	+0.6	−2.0	−11.1399	1.141872	−15	−7	402	605	−11.1390	+0.9
−2.8	+1.5	+0.5	−1.9	−11.1729	1.141298	−15	−7	403	605	−11.1719	+1.0

mean $(T-T_{68}) = +1.2 \pm 1.0$ mK

combining the uncertainties: $(T-T_{68}) = +1.2 \pm 1.5$ mK at $t_{68} = -10.86$ °C

TABLE 19. (*continued*)

$M'(T_{tp})$[a] (19 *March* 1982 *to* 26 *March* 1982)

T_1/mK	T_6/mK	T_3/mK	dT/5 min mK	t_{68}/°C	$M'(T)$/mW	$\delta M'(T)$ nW	$p(T)$ nW	$[D(T)+L(T)]$ nW	$[F(\epsilon,a)+s]$ nW	$M'(T_{tp})$ mW
+6.7	+2.2	−1.9	−0.3	0.5775	1.360293	−20	−13	477	721	1.350203
+4.8	+2.3	−1.4	−0.7	0.5974	1.360701	−20	−13	477	721	1.350214
+0.0	+0.3	+0.1	−1.4	−0.4138	1.340686	−19	−12	470	711	1.350196
−0.3	+0.9	+0.1	−1.6	0.0023	1.348877	−19	−12	473	715	1.350186
+0.4	+0.6	−0.1	−1.4	−0.0190	1.348459	−19	−12	473	715	1.350190
−1.1	+0.8	+0.3	−1.8	0.0159	1.349141	−19	−11	473	715	1.350182
−0.8	+0.8	+0.2	−1.9	−0.0024	1.348833	−19	−11	473	715	1.350236
−1.0	+0.7	+0.2	−1.7	0.0381	1.349583	−19	−11	473	716	1.350187
−0.7	+0.7	+0.2	−1.7	0.0184	1.349198	−19	−11	473	715	1.350190
−0.5	+0.8	+0.1	−1.6	0.0614	1.350037	−19	−11	473	716	1.350180
−0.2	+0.7	+0.1	−1.7	0.0460	1.349780	−19	−11	473	716	1.350226

mean $M'(T_{tp}) = 1.350199 \pm 0.000019$ mW

[a] $M'(T_{tp})$ was measured before and after the measurements were taken at temperatures of −11, −21, and −31 °C. The values of $M'(T_{tp})$ used to evaluate T at these temperatures were the interpolated values between the two.

temperature: 23 °C (28 *September* 1982 *to* 12 *October* 1982)

T_1/mK	T_6/mK	T_3/mK	dT/5 min mK	t_{68}/°C	$M'(T)$/mW	$\delta M'(T)$ nW	$p(T)$ nW	$[D(T)+L(T)]$ nW	$[F(\epsilon,a)+s]$ nW	$M'(T_{tp})$ mW
+4.6	+0.7	−1.0	−0.6	1.6132	1.380935	−20	−3	484	732	1.350151
+8.2	+0.4	−1.9	+0.2	1.6323	1.381322	−20	−3	484	732	1.350155
+8.7	+2.2	−2.3	+0.3	2.1514	1.391779	−20	−3	487	738	1.350144
+9.0	+1.9	−2.3	+0.3	2.1901	1.392564	−20	−3	488	738	1.350146
−6.0	+0.9	+1.4	−2.8	1.6271	1.381177	−20	−3	484	732	1.350115
−4.9	+1.4	+1.0	−2.7	1.5672	1.379991	−20	−3	484	732	1.350133
−4.2	+1.4	+0.9	−2.5	1.3808	1.376254	−20	−3	482	730	1.350137
−3.9	+1.2	+0.8	−2.4	1.3418	1.375472	−20	−3	482	729	1.350137
−3.3	+1.4	+0.7	−2.4	1.2945	1.374536	−21	−3	482	729	1.350147

mean $M'(T_{tp}) = 1.350141 \pm 0.000012$ mW

										t/°C	$(T-T_{68})$ mK
+4.6	+0.4	−0.9	−1.1	22.6429	1.854533	−30	−7	645	983	22.6336	−9.3
+2.4	+0.4	−0.4	−1.6	22.6408	1.854556	−31	−7	645	983	22.6345	−6.3
−4.3	+0.2	+1.2	−3.0	22.4665	1.850192	−31	−7	643	981	22.4603	−6.2
−4.1	+0.2	+1.1	−3.0	22.4201	1.849073	−31	−7	643	980	22.4156	−4.5
+5.1	+0.1	−1.0	−0.9	22.6040	1.853672	−31	−7	644	983	22.5992	−4.8
+5.4	−0.0	−1.0	−0.8	22.6162	1.853982	−32	−7	644	983	22.6115	−4.7
−6.9	+0.1	+1.8	−3.6	23.5170	1.876640	−32	−7	652	995	23.5111	−5.9
−5.8	+0.3	+1.5	−3.4	23.4478	1.874909	−32	−7	651	994	23.4426	−5.1
−5.3	+0.3	+1.4	−3.2	23.3753	1.873071	−31	−7	651	993	23.3700	−5.3

mean $(T-T_{68}) = -5.8 \pm 1.5$ mK

combining the uncertainties: $(T-T_{68}) = -5.8 \pm 1.6$ mK at $t_{68} = 22.86$ °C

temperature: 12 °C *and* 21 °C (25 *May* 1982 *to* 25 *June* 1982)

T_1/mK	T_6/mK	T_3/mK	dT/5 min mK	t_{68}/°C	$M'(T)$/mW	$\delta M'(T)$ nW	$p(T)$ nW	$[D(T)+L(T)]$ nW	$[F(\epsilon,a)+s]$ nW	$M'(T_{tp})$ mW
−6.0	+1.2	+1.4	−2.2	−1.1440	1.326265	+12	−6	465	703	1.350109
−1.1	+1.4	+0.2	−1.6	−1.2266	1.324671	+12	−6	465	702	1.350126
+1.6	+1.1	−0.4	−0.9	−1.2788	1.323656	+12	−6	465	702	1.350128
+19.6	−0.6	−4.3	+2.6	−0.6360	1.336232	+12	−5	469	708	1.350142
+10.3	+0.9	−2.4	+0.7	−0.5742	1.337434	+12	−5	469	709	1.350132
+10.2	+1.0	−2.4	+0.5	−0.5718	1.337478	+12	−4	469	709	1.350129
+7.7	+0.3	−1.7	+0.4	−0.7229	1.334516	+12	−4	468	708	1.350132
+8.8	+0.7	−2.1	+0.4	−0.7288	1.334369	+12	−4	468	707	1.350101

mean $M'(T_{tp})$[b] $= 1.350125 \pm 0.000013$ mW

TABLE 19. (*continued*)

temperature: 12 °C *and* 21 °C (25 *May* 1982 *to* 25 *June* 1982)

T_1/mK	T_6/mK	T_3/mK	dT/5 min / mK	t_{68}/°C	$M'(T)$/mW	$\delta M'(T)$ / nW	$p(T)$ / nW	$[D(T)+L(T)]$ / nW	$[F(\epsilon,a)+s]$ / nW	t/°C	$(T-T_{68})$ / mK
+17.6	+0.1	−4.0	+1.8	11.9589	1.600836	+16	−4	558	849	11.9553	−3.6
+15.0	+0.3	−3.4	+1.4	11.9837	1.601406	+16	−4	558	849	11.9807	−3.0
+14.4	+0.8	−3.4	+1.3	11.9665	1.601031	+16	−3	558	849	11.9638	−2.7
+13.9	+0.8	−3.2	+1.1	11.9805	1.601356	+16	−3	558	849	11.9783	−2.3
+13.8	+0.7	−3.2	+1.2	12.1965	1.606184	+15	−2	560	852	12.1925	−4.0
+13.9	+0.8	−3.3	+1.1	12.2126	1.606566	+16	−2	560	852	12.2095	−3.0
+13.5	+0.8	−3.1	+1.1	12.2316	1.606989	+16	−2	560	852	12.2282	−3.4
+13.4	+0.8	−3.1	+1.1	12.2426	1.607273	+15	−2	561	852	12.2408	−1.8
+13.7	+0.6	−3.2	+1.1	12.2064	1.606408	+16	−2	560	852	12.2023	−4.1
+13.5	+0.9	−3.2	+1.0	12.2171	1.606656	+15	−2	560	852	12.2132	−3.8

mean $(T-T_{68}) = -3.2 \pm 0.7$ mK

combining the uncertainties: $(T-T_{68}) = -3.2 \pm 1.1$ mK at $t_{68} = 12.12$ °C

+7.6	+0.4	−1.7	−0.5	20.8500	1.810021	+17	−5	630	960	20.8430	−6.9
+10.2	+0.4	−2.2	+0.2	20.6050	1.804000	+19	−5	627	956	20.5982	−6.9
+10.2	+0.4	−2.3	+0.3	20.5774	1.803297	+17	−5	627	956	20.5695	−7.9
+15.5	−0.1	−3.4	+1.3	20.4751	1.800804	+17	−5	626	955	20.4678	−7.3
+15.3	+0.2	−3.5	+1.2	20.4871	1.801119	+17	−5	626	955	20.4806	−6.4
+23.2	+0.1	−5.3	+2.9	20.7304	1.807107	+18	−5	629	958	20.7243	−6.1
+22.9	+0.2	−5.2	+2.8	20.7939	1.808653	+18	−5	629	959	20.7871	−6.8
+22.1	+0.2	−5.0	+2.6	21.1089	1.816412	+18	−5	631	963	21.1017	−7.2
+21.4	+0.3	−4.9	+2.5	21.1583	1.817617	+18	−5	632	964	21.1505	−7.8

mean $(T-T_{68}) = -7.0 \pm 0.6$ mK

combining the uncertainties: $(T-T_{68}) = -7.0 \pm 1.0$ mK at $t_{68} = 20.75$ °C

										$M'(T_{tp})$ / mW
+0.3	+1.9	−0.3	−1.4	−1.3873	1.321589	+12	−2	464	701	1.350179
+1.5	+1.7	−0.5	−1.0	−1.4406	1.320552	+12	−2	463	700	1.350178
+9.7	+2.1	−2.5	+0.6	−1.5873	1.317708	+12	−2	462	699	1.350183
+9.8	+2.0	−2.6	+0.6	−1.5870	1.317713	+12	−2	462	699	1.350184
+13.0	+1.9	−3.3	+1.4	−1.7368	1.314848	+12	−2	461	697	1.350225
+12.2	+1.8	−3.0	+1.2	−1.7322	1.314912	+12	−2	461	697	1.350198
+11.9	+1.6	−3.0	+1.1	−1.7175	1.315183	+12	−2	461	697	1.350185

mean $M'(T_{tp})$[(b)] = 1.350190 ± 0.000016 mW

(b) $M'(T_{tp})$ was measured before and after the measurements were taken at temperatures 12 °C and 21 °C. The values of $M'(T_{tp})$ used to evaluate T at these temperatures were interpolated values between the two.

temperature: 40 °C (15 *October* 1982 *to* 28 *October* 1982)

T_1/mK	T_6/mK	T_3/mK	dT/5 min / mK	t_{68}/°C	$M'(T)$/mW	$\delta M'(T)$ / nW	$p(T)$ / nW	$[D(T)+L(T)]$ / nW	$[F(\epsilon,a)+s]$ / nW	$M'(T_{tp})$ / mW
+14.1	+1.4	−3.4	+1.3	−0.4119	1.340639	−18	−5	470	711	1.350118
−2.1	+1.2	+0.4	−1.9	−0.1699	1.345405	−19	−4	472	713	1.350121
−2.2	+1.2	+0.4	−1.9	−0.1969	1.344879	−18	−4	472	713	1.350129
−2.4	+1.0	+0.6	−2.0	−0.2228	1.344377	−19	−4	472	713	1.350135
−1.6	+1.1	+0.3	−1.8	−0.2726	1.343392	−18	−3	471	712	1.350133
−1.2	+1.2	+0.2	−1.8	−0.2993	1.342879	−19	−3	471	712	1.350145
−0.9	+1.2	+0.2	−1.6	−0.3266	1.342349	−19	−3	471	712	1.350151
−2.1	+1.1	+0.4	−1.9	−0.2852	1.343145	−19	−3	471	712	1.350134
−1.4	+1.3	+0.3	−1.8	−0.3205	1.342457	−19	−3	471	712	1.350140

mean $M'(T_{tp}) = 1.350134 \pm 0.000011$ mW

TABLE 19. (*continued*)

temperature: 40 °C (15 *October* 1982 *to* 28 *October* 1982)

T_1/mK	T_6/mK	T_3/mK	dT/5 min / mK	t_{68}/°C	$M'(T)$/mW	$\delta M'(T)$ / nW	$p(T)$ / nW	$[D(T)+L(T)]$ / nW	$[F(\epsilon,a)+s]$ / nW	t/°C	$(T-T_{68})$ / mK
+0.4	+1.9	−0.1	−2.3	39.1421	2.304239	−42	−13	797	1222	39.1322	−9.9
+3.0	+1.7	−0.8	−1.7	39.1247	2.303756	−42	−13	797	1221	39.1158	−8.8
+0.4	+1.6	−0.1	−2.3	39.9242	2.327445	−42	−12	805	1234	39.9156	−8.6
+1.3	+1.9	−0.4	−2.4	39.8782	2.326088	−42	−12	804	1233	39.8699	−8.3
+1.9	+1.9	−0.5	−2.0	39.8497	2.325214	−42	−12	805	1233	39.8405	−9.2
−3.3	+2.2	+0.7	−3.2	39.9256	2.327486	−42	−12	805	1234	39.9170	−8.7
−1.9	+2.2	+0.3	−2.9	39.8636	2.325616	−42	−12	804	1233	39.8541	−9.5
−2.0	+2.1	+0.3	−2.9	39.7920	2.323484	−42	−12	804	1232	39.7823	−9.6
−1.5	+2.0	+0.2	−2.8	39.7492	2.322238	−42	−12	804	1231	39.7403	−8.8

mean $(T-T_{68}) = -9.1 \pm 0.6$ mK

combining the uncertainties: $(T-T_{68}) = -9.1 \pm 0.8$ mK at $t_{68} = 39.69$ °C

temperature: 54 °C (29 *September* 1981 *to* 23 *October* 1981)

T_1/mK	T_6/mK	T_3/mK	dT/5 min / mK	t_{68}/°C	$M'(T)$/mW	$\delta M'(T)$ / nW	$p(T)$ / nW	$[D(T)+L(T)]$ / nW	$[F(\epsilon,a)+s]$ / nW	$M'(T_{tp})$ / mW
−3.1	+2.0	+0.5	−2.2	−1.0543	1.328054	−18	−5	466	704	1.350120
−2.7	+1.9	+0.5	−2.0	−1.1436	1.326304	−18	−5	465	703	1.350112
−3.4	+1.8	+0.6	−2.1	−1.1769	1.325675	−18	−5	465	703	1.350134
−2.0	+1.9	+0.2	−1.9	−1.4966	1.319426	−18	−4	463	700	1.350108
−1.7	+1.9	+0.2	−2.0	−1.5242	1.318925	−18	−4	463	699	1.350143
+3.8	+1.1	−0.9	−0.8	−1.3841	1.321617	−19	−4	464	701	1.350109
+0.9	+2.0	−0.4	−1.4	−1.2390	1.324432	−18	−4	465	702	1.350101
+1.6	+1.6	−0.6	−1.2	−1.2835	1.323592	−18	−4	465	702	1.350130
+1.0	+1.7	−0.4	−1.3	−1.2437	1.324364	−18	−4	465	702	1.350125
+0.5	+1.8	−0.3	−1.4	−1.2148	1.324927	−18	−4	465	702	1.350125

mean $M'(T_{tp}) = 1.350121 \pm 0.000013$ mW

T_1/mK	T_6/mK	T_3/mK	dT/5 min / mK	t_{68}/°C	$M'(T)$/mW	$\delta M'(T)$ / nW	$p(T)$ / nW	$[D(T)+L(T)]$ / nW	$[F(\epsilon,a)+s]$ / nW	t/°C	$(T-T_{68})$ / mK
+0.6	+2.9	−0.4	−2.9	54.0952	2.778215	−56	−50	959	1473	54.0824	−12.8
−0.4	+3.1	−0.1	−3.2	54.2384	2.783092	−56	−42	960	1475	54.2261	−12.3
+0.9	+3.1	−0.5	−2.9	54.1526	2.780150	−55	−42	959	1474	54.1396	−13.0
−1.7	+3.5	+0.1	−3.3	54.1344	2.779515	−58	−32	959	1474	54.1211	−13.3
−3.1	+2.9	+0.6	−3.3	53.6710	2.763824	−52	−20	954	1465	53.6588	−12.3
−0.8	+3.0	−0.0	−3.2	53.6895	2.764416	−54	−18	954	1466	53.6763	−13.3
+0.9	+2.9	−0.4	−2.9	53.6108	2.761749	−56	−18	953	1464	53.5974	−13.5
−2.1	+3.3	+0.2	−3.4	53.6916	2.764509	−53	−16	954	1466	53.6791	−12.5
−0.2	+3.0	−0.2	−3.0	53.6101	2.761716	−56	−15	953	1464	53.5965	−13.6
−0.1	+3.1	−0.3	−3.0	53.5767	2.760572	−52	−13	953	1464	53.5628	−13.9

mean $(T-T_{68}) = -13.0 \pm 0.6$ mK

combining the uncertainties: $(T-T_{68}) = -13.0 \pm 1.0$ mK at $t_{68} = 53.85$ °C

temperature: 64 °C (1 *November* 1982 *to* 12 *November* 1982)

T_1/mK	T_6/mK	T_3/mK	dT/5 min / mK	t_{68}/°C	$M'(T)$/mW	$\delta M'(T)$ / nW	$p(T)$ / nW	$[D(T)+L(T)]$ / nW	$[F(\epsilon,a)+s]$ / nW	$M'(T_{tp})$ / mW
−11.0	+1.1	+2.6	−3.7	−1.4436	1.320474	−18	−4	463	700	1.350125
−8.6	+0.8	+2.1	−3.2	−1.5077	1.319247	−18	−4	463	699	1.350144
−6.0	+0.9	+1.4	−2.7	−1.5829	1.317790	−18	−4	462	699	1.350148
+1.4	+1.7	−0.5	−1.2	−1.4560	1.320263	−18	−3	463	700	1.350157
+2.1	+1.5	−0.6	−1.0	−1.4667	1.320051	−18	−3	463	700	1.350152
+2.5	+1.4	−0.7	−1.1	−1.4762	1.319878	−18	−3	463	700	1.350164
+2.9	+1.4	−0.8	−0.9	−1.3485	1.322356	−18	−3	464	701	1.350159
+2.7	+1.5	−0.7	−0.9	−1.3486	1.322350	−18	−3	464	701	1.350154
+1.6	+1.6	−0.5	−1.1	−1.2176	1.324897	−18	−3	465	702	1.350151
+2.1	+1.5	−0.6	−1.1	−1.2337	1.324579	−18	−3	465	702	1.350147

mean $M'(T_{tp}) = 1.350150 \pm 0.000011$ mW

TABLE 19. (*continued*)

temperature: 64 °C (1 *November* 1982 *to* 12 *November* 1982)

T_1/mK	T_6/mK	T_3/mK	dT/5 min / mK	t_{68}/°C	$M'(T)$/mW	$\delta M'(T)$ / nW	$p(T)$ / nW	$[D(T)+L(T)]$ / nW	$[F(\epsilon,a)+s]$ / nW	t/°C	$(T-T_{68})$ / mK
−2.2	+3.4	+0.3	−3.7	63.7392	3.120307	−66	−24	1076	1654	63.7203	−18.9
−0.6	+3.1	−0.1	−3.6	63.6814	3.118178	−67	−23	1075	1653	63.6628	−18.5
−0.7	+3.2	−0.1	−3.5	63.7314	3.120051	−65	−20	1076	1654	63.7135	−17.8
+0.1	+3.3	−0.3	−3.4	63.6837	3.118263	−65	−19	1075	1653	63.6653	−18.4
+0.4	+3.2	−0.4	−3.4	63.6394	3.116638	−66	−19	1075	1652	63.6214	−18.0
−1.1	+3.2	+0.0	−3.6	63.6235	3.116056	−67	−18	1075	1652	63.6057	−17.8
−0.6	+3.3	−0.1	−3.4	63.5891	3.114750	−66	−18	1074	1651	63.5704	−18.7
−2.2	+3.5	+0.3	−3.8	63.6377	3.116548	−66	−15	1075	1652	63.6191	−18.7
−1.1	+3.5	−0.0	−3.6	63.5883	3.114704	−66	−15	1074	1651	63.5692	−19.1

mean $(T-T_{68}) = -18.4 \pm 0.5$ mK

combining the uncertainties: $(T-T_{68}) = -18.4 \pm 0.8$ mK at $t_{68} = 63.66$ °C

temperature: 71 °C (3 *November* 1981 *to* 20 *November* 1981)

T_1/mK	T_6/mK	T_3/mK	dT/5 min / mK	t_{68}/°C	$M'(T)$/mW	$\delta M'(T)$ / nW	$p(T)$ / nW	$[D(T)+L(T)]$ / nW	$[F(\epsilon,a)+s]$ / nW	$M'(T_{tp})$ / mW
−1.6	+1.2	+0.4	−1.5	−1.2276	1.324654	−13	−2	465	702	1.350107
+17.0	+0.3	−3.9	+2.0	−0.7303	1.334409	−13	−2	468	707	1.350146
+17.7	−0.0	−4.0	+2.1	−0.6310	1.336378	−14	−2	469	709	1.350168
−1.8	+0.2	+0.5	−1.9	−0.4522	1.339830	−14	−2	470	710	1.350110
−2.1	+0.5	+0.6	−2.0	−0.5006	1.338858	−13	−2	470	710	1.350088
−2.4	+0.4	+0.6	−2.0	−0.6952	1.335029	−14	−2	468	708	1.350078
−1.4	+0.3	+0.5	−1.9	−0.7491	1.333996	−13	−2	468	707	1.350100

mean $M'(T_{tp}) = 1.350114 \pm 0.000032$ mW

T_1/mK	T_6/mK	T_3/mK	dT/5 min / mK	t_{68}/°C	$M'(T)$/mW	$\delta M'(T)$ / nW	$p(T)$ / nW	$[D(T)+L(T)]$ / nW	$[F(\epsilon,a)+s]$ / nW	t/°C	$(T-T_{68})$ / mK
+8.0	+2.6	−1.9	−1.9	70.6622	3.384768	−64	−26	1167	1794	70.6444	−17.8
+11.3	+2.0	−2.6	−1.5	70.7035	3.386394	−66	−26	1167	1795	70.6856	−17.9
+11.3	+0.6	−2.4	−1.5	71.2859	3.409360	−67	−25	1175	1808	71.2671	−18.8
+0.4	+2.6	−0.1	−3.5	71.2613	3.408350	−66	−24	1174	1807	71.2417	−19.7
−3.0	+3.0	+0.6	−4.1	71.1471	3.403821	−65	−22	1173	1805	71.1273	−19.9
−2.6	+2.5	+0.6	−3.9	71.0821	3.401180	−64	−22	1172	1803	71.0605	−21.6
+2.3	+2.7	−0.6	−3.0	70.7492	3.388109	−60	−19	1168	1796	70.7295	−19.7
+3.2	+2.3	−0.8	−3.1	70.7213	3.387084	−61	−19	1167	1796	70.7034	−17.8
+3.7	+2.7	−1.0	−2.7	70.6912	3.385860	−61	−19	1167	1795	70.6724	−18.8
+2.9	+2.4	−0.7	−2.7	70.7689	3.388913	−58	−18	1168	1797	70.7500	−18.9

mean $(T-T_{68}) = -19.1 \pm 1.2$ mK

combining the uncertainties: $(T-T_{68}) = -19.1 \pm 2.4$ mK at $t_{68} = 70.91$ °C

temperature: 81 °C (13 *May* 1982 *to* 28 *May* 1982)

T_1/mK	T_6/mK	T_3/mK	dT/5 min / mK	t_{68}/°C	$M'(T)$/mW	$\delta M'(T)$ / nW	$p(T)$ / nW	$[D(T)+L(T)]$ / nW	$[F(\epsilon,a)+s]$ / nW	$M'(T_{tp})$ / mW
−6.0	+1.2	+1.4	−2.2	−1.1440	1.326265	+12	−6	465	703	1.350109
−1.1	+1.4	+0.2	−1.6	−1.2266	1.324671	+12	−6	465	702	1.350126
+1.6	+1.1	−0.4	−0.9	−1.2788	1.323656	+12	−6	465	702	1.350128
+19.6	−0.6	−4.3	+2.6	−0.6360	1.336232	+12	−5	469	708	1.350142
+10.3	+0.9	−2.4	+0.7	−0.5742	1.337434	+12	−5	469	709	1.350132
+10.2	+1.0	−2.4	+0.5	−0.5718	1.337478	+12	−4	469	709	1.350129
+7.7	+0.3	−1.7	+0.4	−0.7229	1.334516	+12	−4	468	708	1.350132
+8.8	+0.7	−2.1	+0.4	−0.7288	1.334369	+12	−4	468	707	1.350101

mean $M'(T_{tp}) = 1.350125 \pm 0.000013$ mW

TABLE 19. (*continued*)

temperature: 81 °C (13 *May* 1982 *to* 28 *May* 1982)

T_1/mK	T_6/mK	T_3/mK	dT/5 min mK	t_{68}/°C	$M'(T)$/mW	$\delta M'(T)$ nW	$p(T)$ nW	$[D(T)+L(T)]$ nW	$[F(\epsilon,a)+s]$ nW	t/°C	$(T-T_{68})$ mK
+8.5	+4.3	−2.3	−2.3	80.9829	3.809587	+16	−36	1312	2020	80.9594	−23.6
+7.2	+4.9	−2.1	−2.2	80.9223	3.807064	+14	−35	1311	2018	80.9007	−21.6
+14.3	+4.3	−3.8	−1.0	80.2525	3.778132	+22	−32	1301	2003	80.2264	−26.1
+13.4	+4.5	−3.6	−1.1	80.2133	3.776513	+21	−31	1301	2002	80.1885	−24.7
+30.6	+2.4	−7.2	+2.6	80.4978	3.788841	+47	−27	1305	2009	80.4772	−20.5
+27.3	+2.5	−6.4	+1.9	80.6664	3.796064	+53	−27	1308	2013	80.6458	−20.6
+27.0	+2.4	−6.3	+1.8	80.6858	3.796835	+52	−27	1308	2013	80.6637	−22.1
+28.1	+2.6	−6.7	+2.1	80.5333	3.790293	+59	−27	1306	2010	80.5114	−21.9
+27.2	+2.7	−6.4	+1.8	80.5466	3.790824	+60	−27	1306	2010	80.5238	−22.8
+27.9	+2.4	−6.5	+1.9	80.3512	3.782415	+64	−27	1303	2005	80.3276	−23.6

mean $(T-T_{68}) = -22.8 \pm 1.8$ mK

combining the uncertainties: $(T-T_{68}) = -22.8 \pm 2.0$ mK at $t_{68} = 80.57$ °C

temperature: 92 °C (25 *November* 1981 *to* 11 *December* 1981)

T_1/mK	T_6/mK	T_3/mK	dT/5 min mK	t_{68}/°C	$M'(T)$/mW	$\delta M'(T)$ nW	$p(T)$ nW	$[D(T)+L(T)]$ nW	$[F(\epsilon,a)+s]$ nW	$M'(T_{tp})$ mW
+2.2	+1.1	−0.5	−0.9	−0.3099	1.342603	−3	−7	471	712	1.350089
+10.2	+0.1	−2.3	+0.8	−0.2725	1.343326	−3	−6	471	712	1.350078
+10.7	+0.1	−2.4	+0.5	−0.2470	1.343862	−3	−6	471	712	1.350111
+9.0	+0.5	−2.1	+0.4	−0.1741	1.345299	−2	−5	472	713	1.350114
+9.2	+0.4	−2.1	+0.3	−0.1581	1.345614	−2	−5	472	713	1.350113
+6.9	+0.6	−1.6	−0.1	−0.2039	1.344678	−3	−4	472	713	1.350079
+6.6	+0.7	−1.6	−0.2	−0.2080	1.344621	−3	−4	472	713	1.350104
+7.3	+0.7	−1.7	+0.0	−0.2329	1.344149	−3	−4	472	713	1.350122
+7.2	+0.6	−1.6	−0.1	−0.2335	1.344130	−2	−4	472	713	1.350115

mean $M'(T_{tp}) = 1.350103 \pm 0.000017$ mW

T_1/mK	T_6/mK	T_3/mK	dT/5 min mK	t_{68}/°C	$M'(T)$/mW	$\delta M'(T)$ nW	$p(T)$ nW	$[D(T)+L(T)]$ nW	$[F(\epsilon,a)+s]$ nW	t/°C	$(T-T_{68})$ mK
+30.6	+2.4	−7.2	+1.7	91.2116	4.269123	−75	−43	1471	2263	91.1859	−25.7
+6.9	+4.3	−1.9	−2.8	91.9544	4.304172	−62	−40	1482	2282	91.9318	−22.6
+8.5	+4.3	−2.3	−2.6	91.9065	4.301849	−62	−39	1482	2281	91.8825	−24.0
+10.9	+3.5	−2.7	−2.2	91.8907	4.301095	−51	−37	1481	2280	91.8668	−23.9
+12.1	+3.7	−3.0	−1.9	91.8542	4.299371	−53	−37	1481	2279	91.8302	−24.0
+14.0	+3.1	−3.4	−1.2	91.4189	4.278959	−24	−32	1474	2269	91.3969	−21.9
+15.4	+3.3	−3.7	−1.2	91.3864	4.277377	−20	−32	1474	2268	91.3633	−23.1
+24.8	+3.3	−5.9	+0.7	91.6591	4.290142	−14	−32	1478	2275	91.6351	−24.0
+24.2	+3.3	−5.8	+0.6	91.6897	4.291490	−15	−32	1479	2275	91.6637	−26.0
+12.9	+3.5	−3.2	−1.5	91.4858	4.281897	−7	−31	1475	2270	91.4599	−25.9
+15.7	+3.6	−3.8	−1.2	91.4220	4.278870	−8	−32	1474	2269	91.3954	−26.7

mean $(T-T_{68}) = -24.3 \pm 1.5$ mK

combining the uncertainties: $(T-T_{68}) = -24.3 \pm 1.9$ mK at $t_{68} = 91.63$ °C

temperature: 102 °C (8 *December* 1982 *to* 21 *December* 1982)

T_1/mK	T_6/mK	T_3/mK	dT/5 min mK	t_{68}/°C	$M'(T)$/mW	$\delta M'(T)$ nW	$p(T)$ nW	$[D(T)+L(T)]$ nW	$[F(\epsilon,a)+s]$ nW	$M'(T_{tp})$ mW
−5.2	+0.7	+1.2	−2.5	−1.0465	1.328136	−6	−7	466	704	1.350059
+10.7	+1.1	−2.6	+0.6	−0.9859	1.329333	−6	−7	466	705	1.350073
+10.8	+1.0	−2.6	+0.6	−0.9614	1.329833	−6	−7	466	705	1.350094
+9.2	+0.8	−2.2	+0.3	−0.7165	1.334609	−5	−6	468	708	1.350080
+9.9	+1.5	−2.5	+0.3	−0.6998	1.334920	−5	−6	468	708	1.350063
+5.3	+0.8	−1.2	−0.4	−0.5099	1.338675	−6	−4	470	710	1.350092
+5.9	+0.9	−1.4	−0.3	−0.5160	1.338552	−5	−4	470	710	1.350091
+4.9	+1.0	−1.2	−0.6	−0.4556	1.339730	−6	−4	470	710	1.350082
+4.9	+0.8	−1.1	−0.6	−0.4712	1.339421	−5	−4	470	710	1.350079

mean $M'(T_{tp}) = 1.350079 \pm 0.000012$ mW

TABLE 19. (*continued*)

temperature: 102 °C (8 *December* 1982 *to* 21 *December* 1982)

T_1/mK	T_6/mK	T_3/mK	dT/5 min / mK	t_{68}/°C	$M'(T)$/mW	$\delta M'(T)$ / nW	$p(T)$ / nW	$[D(T)+L(T)]$ / nW	$[F(\epsilon,a)+s]$ / nW	t/°C	$(T-T_{68})$ / mK
+5.1	+2.7	−1.1	−3.6	102.2242	4.808957	−96	−63	1657	2550	102.1956	−28.5
+6.2	+2.9	−1.4	−3.6	102.1988	4.807618	−96	−62	1657	2549	102.1695	−29.3
+7.1	+2.7	−1.6	−3.2	102.1316	4.804255	−97	−62	1656	2547	102.1038	−27.7
+5.0	+2.8	−1.0	−3.6	102.1385	4.804475	−74	−58	1656	2547	102.1087	−29.9
+7.6	+2.9	−1.8	−3.4	102.0493	4.799856	−74	−58	1654	2545	102.0184	−30.8
+7.7	+2.6	−1.7	−3.1	102.0075	4.797739	−76	−58	1653	2544	101.9770	−30.5
+9.0	+2.7	−2.0	−2.8	101.8864	4.791526	−56	−53	1651	2540	101.8560	−30.4
+9.8	+2.9	−2.2	−2.8	101.8294	4.788613	−56	−53	1651	2539	101.7990	−30.4
+10.3	+2.9	−2.4	−2.7	101.7722	4.785651	−57	−53	1650	2537	101.7410	−31.2

mean $(T-T_{68}) = -29.9 \pm 1.1$ mK

combining the uncertainties: $(T-T_{68}) = -29.9 \pm 1.4$ mK at $t_{68} = 102.03$ °C

TABLE 20

temperature: 40 °C (10 *October* 1983 *to* 26 *October* 1983)

T_1/mK	T_6/mK	T_3/mK	dT/5 min / mK	t_{68}/°C	$M'(T)$/mW	$\delta M'(T)$ / nW	$p(T)$ / nW	$[D(T)+L(T)]$ / nW	$[F(\epsilon,a)+s]$ / nW	$M'(T_{tp})$ / mW
+3.8	+1.6	−0.2	−0.3	0.3703	0.211485	−1	−1	82	40	0.210492
+7.0	+1.9	−0.3	+0.2	0.3709	0.211483	+0	−1	82	40	0.210490
+6.3	+1.9	−0.2	+0.1	0.7618	0.212693	−1	+0	82	40	0.210487
+5.8	+1.9	−0.2	−0.0	0.7661	0.212708	−1	+0	82	40	0.210489
+6.3	+1.9	−0.2	+0.1	0.9073	0.213166	−1	+0	82	41	0.210508
+6.2	+1.8	−0.2	+0.0	0.9134	0.213170	−1	+0	82	41	0.210493
+0.9	+1.2	−0.1	−0.8	−0.0842	0.210112	+0	+0	81	40	0.210523
+0.9	+1.3	−0.1	−0.9	−0.1169	0.209992	−1	+0	81	40	0.210503
+2.0	+1.4	−0.1	−0.6	−0.0814	0.210116	−1	+0	81	40	0.210517
+2.3	+1.5	−0.1	−0.6	−0.1024	0.210021	−1	+0	81	40	0.210487

mean $M'(T_{tp}) = 0.210499 \pm 0.000013$ mW

										t/°C	$(T-T_{68})$ / mK
+6.1	+2.4	−0.3	−0.4	40.2494	0.364470	−1	−3	134	69	40.2358	−13.5
+6.7	+2.6	−0.3	−0.3	40.2382	0.364429	−1	−3	134	69	40.2270	−11.2
+7.2	+2.7	−0.3	−0.2	40.2201	0.364349	−1	−3	134	69	40.2099	−10.2
+7.2	+2.7	−0.3	−0.2	40.2147	0.364325	−1	−3	134	69	40.2047	−10.0
+5.1	+2.5	−0.3	−0.6	40.2859	0.364653	+0	−3	134	69	40.2755	−10.4
+5.5	+2.5	−0.3	−0.5	40.2691	0.364598	−1	−3	134	69	40.2634	−5.6
+5.7	+2.5	−0.3	−0.5	40.2566	0.364518	−1	−2	134	69	40.2463	−10.3
+5.0	+2.5	−0.3	−0.5	40.1373	0.363974	+0	−2	133	69	40.1296	−7.7
+5.2	+2.3	−0.2	−0.6	40.1195	0.363886	−1	−2	133	69	40.1104	−9.1

mean $(T-T_{68}) = -9.8 \pm 2.2$ mK

combining the uncertainties: $(T-T_{68}) = -9.8 \pm 5.4$ mK at $t_{68} = 40.22$ °C

Kemp *et al.* (1984) has given values of $(T-T_{68})$ from 30 K up to 280 K. Their preliminary results above 233 K, also shown in figure 39, are clearly in very good agreement with our radiometric values. This good agreement between the radiometric and gas thermometric values for $(T-T_{68})$ not only confirms the discovery by Guildner & Edsinger that substantial differences exist between T_{68} and thermodynamic temperatures in this range, but also gives us confidence that the values of $(T-T_{68})$ resulting from all of the work are substantially correct. It also shows that total radiation thermometry can equal the accuracy of the best gas thermometry.

The agreement between our values of T and those of gas thermometry can also be taken as providing by far the most sensitive test yet, to a few parts in 10^5, of the fourth-power dependency of radiant power upon T.

(*e*) *Future improvements in radiometric measurements of* σ *and* T

In the light of the experience gained during the course of the present work, it is possible to foresee ways in which significant improvements in accuracy might be achieved. In the absolute measurement of thermal radiative power, that is to say in the determination of σ, the most significant uncertainties (see table 13) are those related to the emissivity and absorptivity of the radiator–calorimeter, the measurement of g, diffraction and scattering. Significant improvements have been made in the production of low-reflectance surfaces since this work was begun (Smith 1984; Pompea *et al.* 1983). It should now be possible to design a radiator–calorimeter assembly for which the radiation transfer function departs from unity by less than one fifth of that used here. In addition, the knowledge of the optical properties of these surfaces should be better than that for 3M Nextel. Overall, taking into account also minor changes in calorimeter design, the uncertainty in the radiation transfer function might be expected to reduce by nearly a factor of ten. Modifications to the design of the apertures, in particular an increase in the aperture diameters and separation and a significant increase in the angle of the conical entrance to the aperture, and the experience gained in the metrology of the radiation trap should all contribute to a reduction in the uncertainties due to diffraction and scattering and the measurement of g by a factor of about four. It should be remembered that the random scatter of the results is already quite small. In the best series of measurements of σ (see table 17) the standard deviation of the measured values is equivalent to only 9 parts in 10^6 in the measured power.

If all of these improvements could be made, an overall uncertainty in the determination of σ approaching 2 parts in 10^5 could be expected. This would lead to an uncertainty in the Boltzmann constant of 5 parts in 10^6, which is better than can be achieved by any other method at present. Similar improvements could also be expected in the measurement of thermodynamic temperature. In particular, by taking further precautions with regard to temperature uniformity in the radiator, uncertainties in the measured values of T might be expected to fall to a few tenths of a millikelvin. To achieve this improvement in accuracy in T, some reduction would be required in the random scatter of the measured values. The best that has been achieved here can be found at three temperatures, namely 40, 60 and -40 °C, where the standard deviation of the twenty measured values of T was 0.8 mK. This is equivalent to a standard deviation in the measurements of thermal radiative power of 1 part in 10^5, very similar to that of the best measurements of σ. We believe that most of this scatter comes from the measurement of the resistance of the germanium thermometer on the calorimeter. Improvements in technique here should lead to a reduction in this scatter of more than a factor of ten. If such reduction in uncertainty in the measured values of T could be obtained, we would find that the uncertainty in the measured values of $(T - T_{68})$ would be limited by the reproducibility and non-uniqueness of T_{68} rather than by uncertainties in T.

The authors are very pleased to acknowledge the part played in the early stages of this work by John Compton, without whose contribution it is unlikely that the cryogenic radiometer would have worked so well. Among those who took part in the construction of the radiometer in the NPL workshops, we must acknowledge especially Ernie Pinn (who made the apertures) and Eric Charles and Mick Rogers. For the measurements of the dimensions of the radiation trap and apertures we are grateful for the help given by Stan Poole, Gary Severn,

Peter Kelley and David Flack of the NPL Division of Mechanical and Optical Metrology. Among the many calibrations and other measurements made for us during the course of the work we must mention the measurements of the thermal expansion of Cu–Be, for which we thank Clayton Swenson of Iowa State University; the reflectance of the model of the calorimeter, by Edward Zalewski of the National Bureau of Standards; the reflectance of Cu–Be samples, by George Freeman of NPL; and the calibrations of the platinum resistance thermometers by Maurice Chattle of NPL. Christine Barker assisted in many of the measurements made with the radiometer. In addition, we are grateful to Ronald Bedford of the National Research Council and Chu Zaixiang of the Harbin Institute of Technology, who made calculations for us of the absorptivity of the calorimeter. We must also acknowledge the help and advice given on many occasions by members of the NPL Temperature Section and, finally, Peter Coates, John Cox, Ralph Hudson, Jörge Müller, John Redgrove and Richard Rusby, who read the manuscript of this article and made many helpful comments.

One of us (T.J.Q.) wishes also to thank the Directors of BIPM and NPL for encouraging him to continue with this work after his move to BIPM and the Director of BIPM for facilities provided there.

Appendix A. Derivation of an expression for $T(x)$

In this Appendix we derive an expression for the temperature, $T(x)$, of an element on the cylindrical wall of the radiator a distance x from the aperture (see figure A 1). In doing so, we assume that the radiator is drifting in temperature at a rate $\partial T/\partial t$, which is small, constant over the period of interest and uniform over the whole of the radiator. This corresponds with that observed in practice. It is also assumed that, because of efficient external radiation screening, the only significant net heat loss from the cylindrical and conical parts of the radiator takes place by thermal radiation through the aperture.

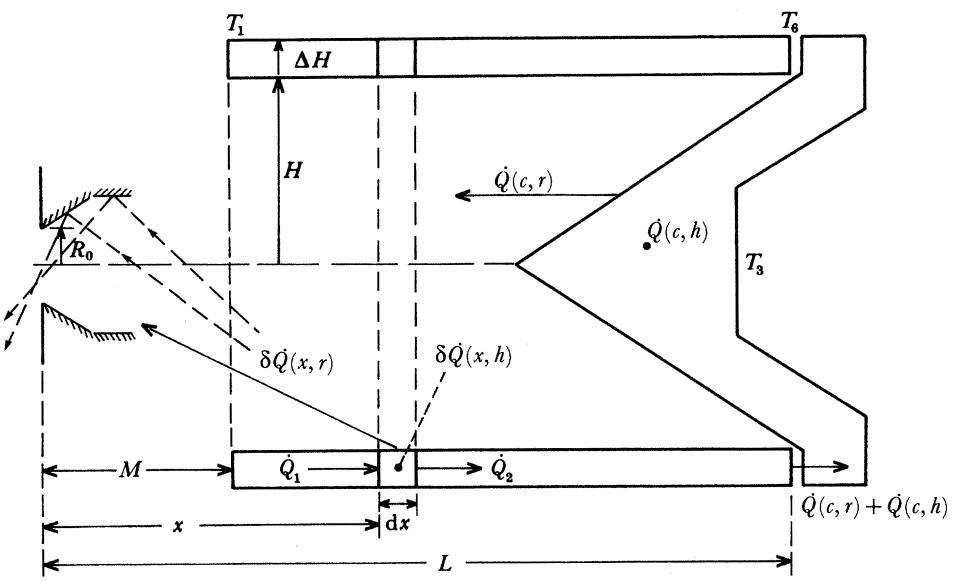

Figure A 1. Schematic drawing of radiator showing parameters used in the derivation of the heat-flow equation.

The net heat loss from an element of the cylindrical wall of the radiator depends upon the solid angle subtended at the element by the aperture and by its images in the reflecting conical entrance to the aperture and in the cylindrical mirror attached to the top of the radiator. In addition, we must take into account the absorption of the cold surfaces of the aperture and its surroundings, which result from the presence of the condensed gas. This absorption is estimated to be 0.25 on the basis of diffraction experiments described in §7. The overall heat loss from these lower regions of the radiator is, therefore, considerably larger than would be expected by taking simply the direct heat loss through the aperture, and it is evaluated in the following way.

We take first the large pair of apertures, for which the radius of the lower aperture $R_{\mathrm{L}} = 0.9$ cm and the angle of the entrance cone is 60°. The radius of the virtual image of the aperture in the entrance cone is 1.7 cm, which we denote by R_{L1}. This image is itself visible by reflection in the cylindrical mirror of radius R_{M} at the top of the radiator (see figure A 1). The shape of this reflected image varies when viewed from elements over the length of the cylindrical part of the radiator from $x = 23$ cm to $x = 60$ cm, but direct observation allowed us to estimate an average area of about one half that of the virtual image of the aperture in the cone. Thus we assign an effective radius R_{L2} to this image, given by $R_{\mathrm{L2}} = R_{\mathrm{L1}}/\sqrt{2}$. Absorption also takes place in the annular region between the outside rim of the aperture and its housing, indicated by N in figure 12. Since about four reflections are required before a ray entering this region can return to the radiator, a surface reflectance of 0.75 leads to an effective absorptance of 0.7. This annular region is equivalent to a completely absorbing disc of radius $R_{\mathrm{L3}} = 1$ cm. The remaining cold surfaces, in which an image of the aperture is not seen, are taken to have an absorption of 0.25, and to have a surface area equivalent to a disc of radius R_{M} less the sum of the areas of all the aperture images and annular ring. We can thus deduce the radius, R_0, of an absorbing disc having an absorption equivalent to the sum of the various components described above:

$$R_0^2 = 0.25R_{\mathrm{M}}^2 + (1-0.25)\,(R_{\mathrm{L1}}^2 + R_{\mathrm{L2}}^2 + R_{\mathrm{L3}}^2). \tag{A 1}$$

From this we find that $R_0 = 2.4$ cm, which we subsequently use as an effective radius of the aperture and with which we associate an uncertainty of 5% (not a significant contributing uncertainty in the final result).

For the small pair of apertures, the radius of the equivalent absorbing disc is rather smaller. The cone angle of the aperture is 90°, with the result that there is no virtual image of the aperture visible in the cone, so $R_{\mathrm{L1}} = R_{\mathrm{L}}$. Taking $R_{\mathrm{L}} = 0.5$ cm, we find that $R_0 = 1.7$ cm.

Having found an expression for the effective area of the aperture viewed from elements along the cylindrical wall and on the surface of the cone, we can write down an expression for the radiant heat loss, $\delta\dot{Q}(xr)$, from a cylindrical element a distance x from the aperture (see figure A 1). We show in (C 4) of Appendix C that the fraction $\mathrm{d}F_{H-L}$ of the thermal radiation emitted by a cylindrical element that reaches a coaxial disc of radius R_0 at a distance x from the element is given by

$$\mathrm{d}F_{H-L} = xR_0^2 H/(x^2+H^2)^2. \tag{A 2}$$

Since here x is always much greater than H, the radius of the cylinder, we can approximate this by

$$\mathrm{d}F_{H-L} \approx R_0^2 H/x^3. \tag{A 3}$$

Thus the heat loss from the cylindrical element through the aperture R_0 is given by

$$\delta\dot{Q}(x,r) = 2\pi\epsilon R_0^2 H^2 \sigma T^4 x^{-3}\,\mathrm{d}x, \tag{A 4}$$

where ϵ is the emittance of the surface and T is its temperature.

The heat required to change the temperature of the element at a rate $\partial T/\partial t$ we call $\delta\dot{Q}(x,h)$, and it is given by

$$\delta\dot{Q}(x,h) = 2\pi H \Delta H \rho s(\partial T/\partial t)\,\mathrm{d}x. \tag{A 5}$$

The radiant heat loss from the whole of the cone, $\dot{Q}(c,r)$, is given by

$$\dot{Q}(c,r) = \pi H^2 R_0^2 \sigma T^4/L^2. \tag{A 6}$$

The heat required to change the temperature of the cone at a rate $\partial T/\partial t$ is given by

$$\dot{Q}(c,h) = ms\,\partial T/\partial t, \tag{A 7}$$

where m is the mass of the cone. The heat balance equation for the cylindrical element $\mathrm{d}x$ is

$$\dot{Q}_1 - \dot{Q}_2 = \delta\dot{Q}(x,r) + \delta\dot{Q}(x,h), \tag{A 8}$$

where

$$\dot{Q}_1 = -\kappa A\,\partial T/\partial x$$

and

$$\dot{Q}_2 = -\kappa A\left(\frac{\partial T}{\partial x} + \frac{\partial^2 T}{\partial x^2}\,\mathrm{d}x\right),$$

in which κ is the thermal conductivity of the material and A is the cross sectional area of the element given by $A = 2\pi H \Delta H$. Thus

$$\dot{Q}_1 - \dot{Q}_2 = 2\pi H \Delta H \kappa(\partial^2 T/\partial x^2)\,\mathrm{d}x, \tag{A 9}$$

so that combining (A 8) and (A 9) and substituting for $\delta\dot{Q}(x,r)$ and $\delta\dot{Q}(x,h)$ from (A 4) and (A 5) and simplifying we find

$$\frac{\partial^2 T}{\partial x^2} = \frac{\epsilon H R_0^2 \sigma}{\kappa \Delta H}\,T^4\,\frac{1}{x^3} + \frac{\rho s}{\kappa}\,\frac{\partial T}{\partial t}. \tag{A 10}$$

This we write as

$$\frac{\partial^2 T}{\partial x^2} = \frac{N}{x^3} + J(t), \tag{A 11}$$

where

$$N \equiv \epsilon H R_0^2 \sigma T^4/\kappa \Delta H$$

and

$$J(t) \equiv \frac{\rho s}{\kappa}\,\frac{\partial T}{\partial t},$$

remembering that $\partial T/\partial t$ is independent of x and t. Integrating with respect to x, we have

$$\frac{\partial T}{\partial x} = -\frac{N}{2x^2} + Jx + c_1. \tag{A 12}$$

The first boundary condition is that at $x = L$ we have

$$\left.\frac{\partial T}{\partial x}\right|_{x=L} = \frac{-[\dot{Q}(c,r) + \dot{Q}(c,h)]}{\kappa A},$$

so substituting for $\dot{Q}(c,r)$ and $\dot{Q}(c,h)$ from (A 6) and (A 7) and putting $m/2\pi H\Delta H\rho \equiv c$, we find

$$\left.\frac{\partial T}{\partial x}\right|_{x=L} = -\frac{N}{2L^2} - cJ. \tag{A 13}$$

Hence, substituting into (A 12), we find

$$c_1 = -J(c+L), \tag{A 14}$$

so that (A 12) becomes

$$\partial T/\partial x = -(N/2x^2) + Jx - J(c+L). \tag{A 15}$$

Integrating a second time with respect to x we find

$$T = (N/2x) + \tfrac{1}{2}Jx^2 - J(c+L)\,x + c_2. \tag{A 16}$$

The second boundary condition is that for $x = M$

$$T(M,t) = T_1, \tag{A 17}$$

so that (A 16) becomes

$$T_1 = (N/2M) + \tfrac{1}{2}JM^2 - J(c+L)\,M + c_2,$$

whence

$$c_2 = T_1 - (N/2M) - \tfrac{1}{2}JM^2 + J(c+L)\,M. \tag{A 18}$$

By substituting into (A 16) and simplifying we can finally write

$$T(x,t) = T_1 - \frac{N}{2}\left(\frac{1}{M} - \frac{1}{x}\right) - \frac{J}{2}(M^2 - x^2) - J(c+L)\,(x-M). \tag{A 19}$$

This is the required expression that is used in § 2 (*c*).

Appendix B. The evaluation of the view factors, $V(x)$ and $V_c(x)$

From figure 17*a*, we require the ratio of the area of the fraction of the upper aperture visible through the lower aperture to the area of the lower aperture viewed from dx ($V(x)$ if the element dx is situated on the cylindrical wall or $V_c(x)$ if it is on the cone). First, for $V(x)$, we can write

$$V(x) = (S_1 + S_2)/(\pi R_L^2). \tag{B 1}$$

Making use of the standard relation for the area of a segment of a circle, we can write for an element dx on the cylindrical wall

$$S_1 = R_L^2 \arccos(Y_1/R_L) - Y_1(R_L^2 - Y_1^2)^{\frac{1}{2}}, \tag{B 2}$$

$$S_2 = \left\{\frac{R_U^2\,x^2}{(x+D)^2}\arccos\left[\frac{(Y_2-Y_1)\,(x+D)}{R_U\,x}\right] - (Y_2-Y_1)\left[\frac{R_U^2\,x^2}{(x+D)^2} - (Y_2-Y_1)^2\right]^{\frac{1}{2}}\right\}, \tag{B 3}$$

where

$$Y_2 = H_1 D/(x+D) \tag{B 4}$$

and, to calculate $V_c(x)$ for the elements on the cone,

$$Y_2 = H_c D/(x+D),$$

where H_c is distance of the element dx from the axis given by

$$H_c = H_1 - (L-x)\tan\tfrac{1}{2}\gamma,$$

in which L is the length of the cylinder and γ the angle of the cone. Y_1 is the solution of

$$\left.\begin{aligned} X^2+Y^2 &= R_L^2, \\ X^2+(Y-Y_2)^2 &= R_U^2\,x^2/(x+D)^2 \end{aligned}\right\} \tag{B 5}$$

in the plane X–Y of figure 17*a*.

When $Y = Y_1$ we have

$$(Y_1-Y_2)-Y_1^2 = R_U^2\,x^2/(x+D)^2-R_L^2, \tag{B 6}$$

from which

$$Y_1 = \frac{-R_U^2\,x^2}{2Y_2(x+D)^2}+\frac{R_L^2}{2Y_2}+\frac{Y_2}{2}. \tag{B 7}$$

Figure (B 1) shows $V(x)$ evaluated for the large and small pairs of apertures for the ranges of x for which $V(x) \geqslant 0$.

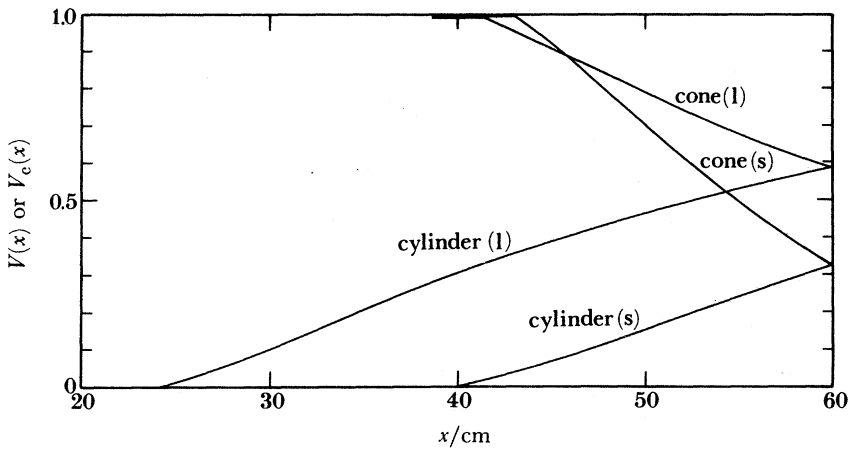

FIGURE B 1. The view factors from elements on the cylinder $V(x)$ and cone $V_c(x)$ for the large (l) and small (s) pairs of apertures; x is the distance of the element from the aperture.

APPENDIX C. THE EVALUATION OF $dE(T_x)$ AND $dE(T_{cx})$

In this Appendix we derive expressions for the fractions of the radiant flux leaving elements on the cylinder and cone of the radiator that pass through the lower aperture. The results are used in equation (25). The effective radius of the lower aperture is R_0, derived in Appendix A.

The fraction of radiant flux leaving a disc of radius R_0 that is intercepted by a parallel coaxial disc of radius H a distance x from R_0 is given by

$$F_{L-H} = H^2/(x^2+H^2). \tag{C 1}$$

This is an approximate form of (81), which is sufficient for $x > H$ and $x \gg R_0$.

Differentiating (C 1) with respect to x gives the fraction intercepted by the cylindrical element dx (see figure C 1),

$$dF_{L-H} = \frac{-2xH^2}{(x^2+H^2)^2}\,dx, \tag{C 2}$$

but from angle-factor algebra we know that for a pair of surfaces a, b of areas A and B, $dF_{a-b}\,A = dF_{b-a}\,B$, so that we can write

$$dF_{H-L} = \frac{-\pi R_0^2}{2\pi H\,dx}\,dF_{L-H} = \frac{xR_0^2\,H}{(x^2+H^2)^2}. \tag{C 3}$$

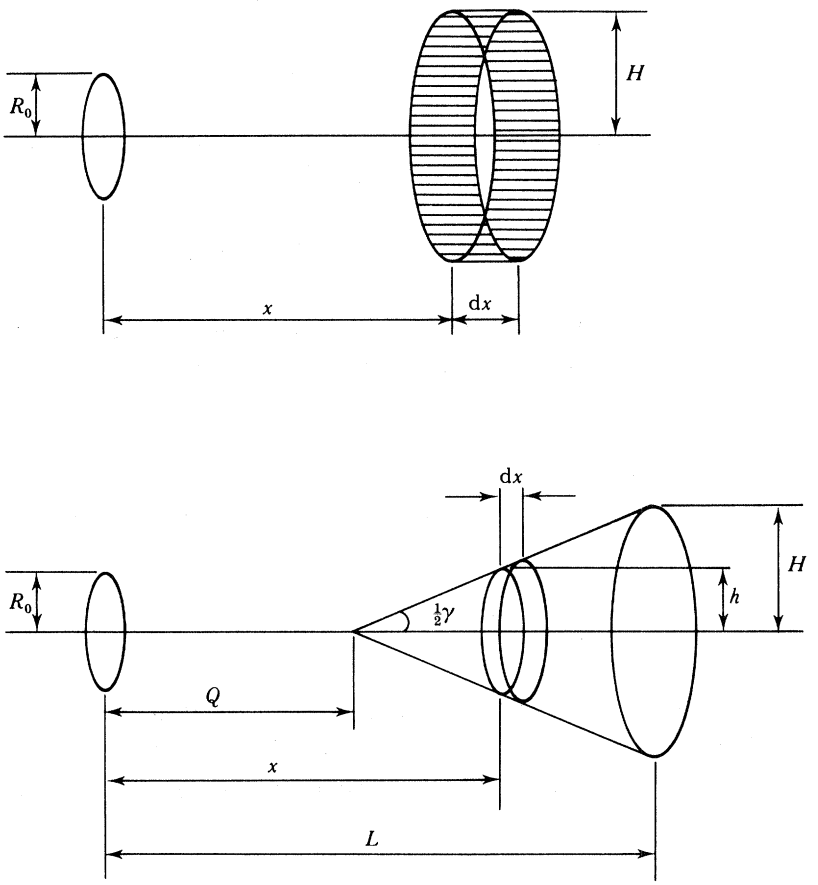

FIGURE C 1. Geometry used for calculating expressions for $dE(T_x)$ and $dE(T_{cx})$.

From figure C 1 we can write down an expression for the radiant power from the cylindrical element dx that passes through R_0:

$$dE(T_x)\,dx = 2\pi H\,dx\,\epsilon(x)\,E(T_x)\,dF_{H-L}, \tag{C 4}$$

where $E(T_x)$ is the total radiant exitance of the element dx at a temperature T_x, $\epsilon(x)$ is the emittance of the element and H is the radius of the cylindrical part of the radiator (equal to 6 cm), so that

$$dE(T_x)\,dx = \frac{2\pi\epsilon(x)\,H^2R_0^2\,E(T_x)\,x\,dx}{(x^2+H^2)^2}. \tag{C 5}$$

This is the required expression.

Coming now to an element dx on the cone, from figure C 1 we can write down

$$F_{L-h} = \frac{h^2}{x^2+h^2} = \frac{(x-Q)^2\tan^2\frac{1}{2}\gamma}{x^2+(x-Q)^2\tan^2\frac{1}{2}\gamma}, \tag{C 6}$$

where $Q = 36.5$ cm and $\gamma = 30°$, which is equal, with an error of less than 1 %, to

$$F_{L-h} = \frac{(x-Q)^2\tan^2\frac{1}{2}\gamma}{x^2} \tag{C 7}$$

$$= (1-2Qx^{-1}+Q^2x^{-2})\tan^2\tfrac{1}{2}\gamma, \tag{C 8}$$

so that $$dF_{L-h} = 2Q(x^{-2} - Qx^{-3}) \tan^2 \tfrac{1}{2}\gamma \, dx. \quad (C\ 9)$$

But $$dF_{h-L} = \frac{\pi R_0^2 \cos \tfrac{1}{2}\gamma}{2\pi h \, dx} dF_{L-h}. \quad (C\ 10)$$

From figure C 1 we can write down an expression for the radiant power $dE(T_{cx})$ from the element dx on the conical surface that passes through R_0:

$$dE(T_{cx}) \, dx = \frac{2\pi h \, dx \, \epsilon_c(x)}{\cos \tfrac{1}{2}\gamma} E(T_{cx}) \, dF_{h-L}, \quad (C\ 11)$$

where $E(T_{cx})$ is the total radiant exitance of the element dx at a temperature T_{cx} and $\epsilon_c(x)$ is the emittance of the element. Substituting for dF_{h-L} we arrive at

$$dE(T_{cx}) \, dx = 2\pi R_0^2 \epsilon_c(x) \, Q \tan^2 \tfrac{1}{2}\gamma (x^{-2} - Qx^{-3}) \, E(T_{cx}) \, dx, \quad (C\ 12)$$

which is the required expression.

As a check on the approximations made in deriving (C 7), we note that for $\epsilon(x) = \epsilon_c(x)$ and $T_x = T_{cx}$ = a constant,

$$\int_{x=60}^{\infty} \frac{2\pi H^2 R_0^2 \, x \, dx}{(x^2 + H^2)^2} \approx \int_{x=Q}^{60} 2\pi R_0^2 \, Q \tan^2 \tfrac{1}{2}\gamma (x^{-2} - Qx^{-3}) \, dx. \quad (C\ 13)$$

These two integrals should be identical because under these conditions they each represent the radiant power passing through R_0 from a diffusely radiating disc of radius H at a distance x from R_0. Since they in fact differ by only a small percentage, we consider that the approximations were adequate.

Appendix D. The evaluation of the angle factors and reflectances for scattering within the radiation trap

In this Appendix we evaluate the angle factors and reflectances of (84)–(89), which allow the scattering from the radiation trap to be calculated. We denote here the lower aperture by A1, the upper by A2, the side walls by S, the upper walls by U and the lower walls by L and adopt the convention that the fraction of the radiant flux passing from A1 to U, say, is written $F_{A1\text{–}U}$. Using standard angle-factor algebra and the geometry of figure 29, we can write down.

$F_{A1\text{–}U}$. This is the fraction of the radiation leaving A1 that is intercepted by U and is given by

$$F_{A1\text{–}U} = 2R^2/\{R^2 + R_L^2 + D^2 + [(R^2 + R_L^2 + D^2)^2 - 4R^2R_L^2]^{\frac{1}{2}}\}, \quad (D\ 1)$$

which we write as $$F_{A1\text{–}U} = 2R^2/M, \quad (D\ 2)$$

where R is the radius of the radiation trap.

$F_{A1\text{–}S}$. It follows that

$$F_{A1\text{–}S} = 1 - F_{A1\text{–}U}, \quad (D\ 3)$$

hence $$F_{A1\text{–}S} = 1 - 2R^2/M. \quad (D\ 4)$$

$F_{U\text{–}L}$. This is given by

$$F_{U\text{–}L} = 2R^2/\{2R^2 + D^2 + [(2R^2 + D^2)^2 - 4R^4]^{\frac{1}{2}}\}, \quad (D\ 5)$$

which we write as $$F_{U-L} = 2R^2/N. \tag{D 6}$$

F_{U-S}. It follows that

$$F_{U-S} = 1 - F_{U-L}, \tag{D 7}$$

hence $$F_{U-S} = 1 - 2R^2/N. \tag{D 8}$$

F_{S-A2}. From angle-factor algebra we know that

$$F_{S-A2} = \frac{(\text{area of A2})}{(\text{area of S})} F_{A2-S}, \tag{D 9}$$

but $$F_{A2-S} = 1 - F_{A2-L} \tag{D 10}$$

and $$F_{A2-L} = 2R^2/\{R^2 + R_U^2 + D^2 + [(R^2 + R_U^2 + D^2)^2 - 4R^2R_U^2]^{\frac{1}{2}}\}$$

$$= 2R^2/P. \tag{D 11}$$

Thus $$F_{S-A2} = \frac{R_U^2}{2RD}\left(1 - \frac{2R^2}{P}\right). \tag{D 12}$$

F_{L-A2}. As before, we can write

$$F_{L-A2} = \frac{(\text{area of A2})}{(\text{area of L})} F_{A2-L}, \tag{D 13}$$

so that $$F_{L-A2} = \frac{R_U^2}{R^2}\frac{2R^2}{P} = 2R_U^2/P. \tag{D 14}$$

F_{S-L}. In this case we can simply write

$$F_{S-L} = \frac{(\text{area of L})}{(\text{area of S})} F_{L-S} \tag{D 15}$$

$$= \frac{R^2}{2RD}(1 - F_{L-U}), \tag{D 16}$$

but $F_{L-U} = F_{U-L}$, so that $$F_{S-L} = \frac{R}{2D}\left(1 - \frac{2R^2}{N}\right). \tag{D 17}$$

$F_{A1-S'}$. This represents the fraction of the radiation from A1 that strikes the edges of the baffles ranged up the sides of the radiation trap. If the average thickness of these edges is δD and there are n of them

$$F_{A1-S'} = F_{A1-S}\, n\, \delta D/D \tag{D 18}$$

$$= (1 - 2R^2/M)\, n\, \delta D/D. \tag{D 19}$$

$F_{S'-A2}$. This represents the fraction of the radiation diffusely scattered from the edges of the baffles that reaches A2, for which

$$F_{S'-A2} = F_{S-A2} \tag{D 20}$$

$$= \frac{R_U^2}{2RD}\left(1 - \frac{2R^2}{P}\right). \tag{D 21}$$

$F_{A\,1\text{–}A\,2'}$. This represents the fraction of the radiant flux from A 1 striking the unpainted annular ring of width $t(\leqslant R_U)$ surrounding A 2,

$$F_{A\,1\text{–}A\,2'} = \frac{2R_U\,t}{D^2}. \tag{D 22}$$

$F_{A\,2'\text{–}L'}$. All of the radiant flux reaching the unpainted ring A_2' is reflected down towards the flat surface L' surrounding the lower aperture so that

$$F_{A\,2'\text{–}L'} = 1. \tag{D 23}$$

$F_{L'\text{–}A\,2}$. This represents the fraction of the radiant flux coming from A 2′ that is diffusely reflected from L′ back to A 2. It is given by

$$F_{L'\text{–}A\,2} = 2R_U^2/\{R_U^2 + R_{L'}^2 + D^2 + [(R_U^2 + R_{L'}^2 + D^2)^2 - 4R_U^2\,R_{L'}^2]^{\frac{1}{2}}\}, \tag{D 24}$$

where $R_{L'}$ is the radius of the illuminated area of L′, given approximately by $2R_U - R_L$.

It is now necessary to evaluate the reflectance factors.

The baffles were designed so that no surface directly irradiated by A 1 was visible from A 2. A minimum of two reflections from the 3M black paint is therefore required before a ray can pass from A 1 to A 2. Here we denote the diffuse reflectance of the black paint by $\rho_S = 0.057$. The only exceptions are the scattering from the sharp edges of the baffles and the reflection from the unpainted annular ring surrounding A 2. The three conditions of illumination for the lower, middle and upper baffles on the side walls S are shown in figure D 1. For the middle baffles, the incident flux is intercepted by the lower surface of the baffle marked A and is diffusely reflected downwards. From simple geometry about half of this reflected flux strikes the baffle just below in the region B visible from A 2. Of this about one half is reflected back to A and the other half is equally divided between an outward reflection and further reflections at the base of the V groove. Thus

$$\rho(\mathrm{A1, S, A2}) = \tfrac{1}{8}\rho_S^2 \tag{D 25}$$

for the middle baffles on the side walls.

In a similar way the reflectance can be estimated for the upper and lower baffles on the side walls. Since either the area illuminated by A1 or the area viewed from A2 is smaller than for the symmetrical middle baffles, we find rather lower values of reflectance, about $\frac{1}{24}\rho_S^2$. We shall, however, adopt a conservative estimate for the average reflectance and take

$$\rho(\mathrm{A1, S, A2}) = \tfrac{1}{12}\rho_S^2 \tag{D 26}$$

as representing the average reflectance of the baffles on the side walls S.

The remaining half from the first reflection at A is roughly equally divided between the outward reflection down towards L and inwards towards the base of the groove, where it undergoes further reflections so that we can deduce

$$\rho(\mathrm{A1, S, L}) = \tfrac{1}{4}\rho_S. \tag{D 27}$$

The reflectance of the sharp edges is treated differently. Each baffle during manufacture was first painted and baked to give a hard, relatively thick, layer of paint covering the sharp copper edge. The hardened paint was then filed to as sharp an edge as possible, as previously described. The final radius of curvature of the edge was estimated to be about 40 μm, leading to an effective

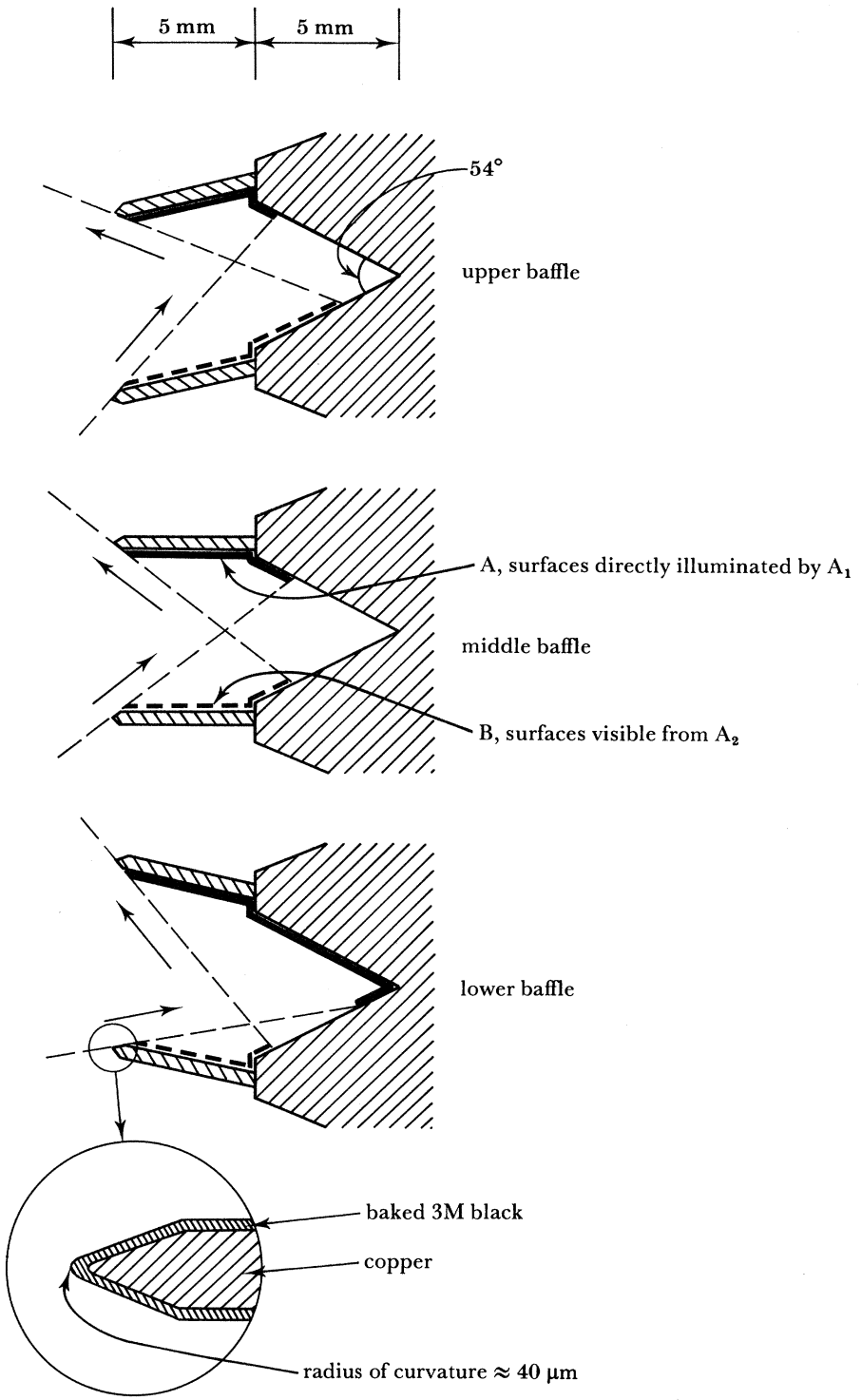

FIGURE D 1. Cross sections of examples of baffles on the side walls of the radiation trap. The baffles on the upper and lower walls are similar in cross section to the middle baffles shown here.

scattering width of about 60 μm. Since there were 19 baffles along the vertical height of S, $n\delta D/D = 0.01$ and the reflectance

$$\rho(\mathrm{A1}, \mathrm{S}', \mathrm{A2}) = 0.01\rho_{\mathrm{s}}.$$

The reflectance of the upper surface, U, of the radiation trap in the direction of the lower surface, L, is found by taking first the reflectance of the V groove and then modifying it with respect to the presence of baffles. The diffuse reflectance of a V groove is given by (Psarouthakis 1963)

$$\rho_{\mathrm{V}} = \frac{\rho_{\mathrm{s}} \sin \tfrac{1}{2}\theta}{1-\rho_{\mathrm{s}}(1-\sin \tfrac{1}{2}\theta)}, \tag{D 28}$$

which, for an included angle of 54°, leads to

$$\rho_{\mathrm{V}} = 0.45\rho_{\mathrm{s}}/(1-0.55\rho_{\mathrm{s}}). \tag{D 29}$$

The reflectance of the groove with baffles is less than this, since we need to consider only the radiant flux that passes out through the opening between the baffles, which is about half that coming from the V groove. We thus find

$$\rho(\mathrm{A1}, \mathrm{U}, \mathrm{L}) = \tfrac{1}{2}\rho_{\mathrm{V}}. \tag{D 30}$$

The reflectance of L for radiant flux coming from S, $\rho(\mathrm{S}, \mathrm{L}, \mathrm{A2})$, will be lower than the reflectance of L for radiant flux coming from U, since most of the surfaces illuminated directly by S are invisible from A2, and it can be taken to be equal to $\rho(\mathrm{A1}, \mathrm{S}, \mathrm{A2})$, which we have already calculated (equation (D 26)). The reflectance of S for radiant flux coming from U and reflected in the direction of A2, $\rho(\mathrm{U}, \mathrm{S}, \mathrm{A2})$, contributes very little to the final result and may be taken to be $\frac{1}{4}\rho_{\mathrm{V}}$. Similarly, the reflectance of U in the direction of S for radiant flux coming from A1 contributes very little and can be taken, by symmetry, to be equal to $\frac{1}{4}\rho_{\mathrm{V}}$.

Note added in proof (2 August 1985). The 1985 Least Squares Adjustment of the Fundamental Constants has not yet been finally approved by Codata. The values given here should, therefore, be checked against the eventual publication by Taylor & Cohen. It is not expected that the final values or their uncertainties will differ significantly from those given here.

References

Baltes, H. P. 1972 In Thermal radiation in finite cavities. Thesis. Swiss Federal Institute of Technology.

Baltes, H. P. 1973 *Appl. Phys.* **1**, 39–43.

Baltes, H. P. 1976 *Infrared Phys.* **16**, 1–8.

Baltes, H. P. & Hilf, E. R. 1976 In *The spectra of finite systems.* Mannheim: Wissenschaftsverlag Bibliographisches Institut.

BIPM 1980 Report of the BIPM enquiry on error statements. *BIPM Rapport* no. 80/3.

Blevin, W. R. 1970 *Metrologia* **6**, 39–44.

Blevin, W. R. & Brown, W. J. 1971 *Metrologia* **7**, 15–29.

Callendar, H. L. 1899 *Phil. Mag.* **48**, 519–547.

Case, K. M. & Chiu, S. C. 1970 *Phys. Rev.* A **1**, 1170.

Coates, P. B. & Andrews, J. W. 1982 In *Temperature: its measurement and control in science and industry*, vol. 5, pp. 109–144. Instrument Society of America.

Colclough, A. R. 1984 In *Proceedings of the 2nd Int. Conf. on Precision Measurement and Fundamental Constants 1981. Natn. Bur. Stand. Spec. Publ.* no. 617.

Colclough, A. R., Quinn, T. J. & Chandler, T. R. D. 1979 *Proc. R. Soc. Lond.* A **368**, 125–139.

Compton, J. P., Martin, J. E. & Quinn, T. J. 1974 *J. Phys.* D **7**, 2501–2510.

Garrett, K. W. & Rosenberg, H. M. 1974 *J. Phys.* D **7**, 1247–1258.

Giacomo, P. 1981 *Metrologia* **17**, 69–74.
Ginnings, D. C. & Reilly, M. L. 1972 *Temperature: its measurement and control in science and industry*, vol. 4, pp. 339–348. Instrument Society of America.
Guildner, L. A. & Edsinger, R. E. 1976 *J. Res. natn Bur. Stand.* A **80**, 703–738.
Hawks, K. H. & Cottingham, W. B. 1970 *Adv. cryogenic Engng* **16**, 467–474.
Heaney, J. B., Stewart, K. P. & Hass, G. 1983 *Appl. Opt.* **22**, 4069–4072.
Holmes, S., Mugman, A. & Kraatz, P. 1973 *Appl. Opt.* **12**, 1743–1745.
Holtz, R. L. & Swenson, C. A. 1983 *J. appl. Phys.* **54**, 2844–2846.
Hsia, J. J. & Richmond, J. C. 1976 *J. Res. natn Bur. Stand.* A **80**, 189–220.
James, G. L. 1976 In *Geometrical theory of diffraction for electromagnetic waves*. London: Peter Peregrinus Ltd.
Jung, H. J. 1984 *Metrologia* **20**, 67–69.
Keller, J. B. 1957 *J. appl. Phys.* **28**, 426–444.
Kemp, R. C., Besley, L. N. & Kemp, W. R. G. 1984 *BIPM Com. Cons. Thermometrie*, vol. 15.
Kendall, J. M. 1968 *JPL Tech. Rep.* no. 32, 1263.
King, R. W. P. & Wu, T. T. 1959 In *The scattering and diffraction of waves. Harvard monographs in physical science*, vol. 7. Harvard University Press.
Koike, C., Hasegawa, H. & Manabe, A. 1980 *Astrophys. Space Sci.* **67**, 495–502.
Kroeger, F. R. & Swenson, C. A. 1977 *J. appl. Phys.* **48**, 853–864.
Levinson, L. L., Milleron, N. & Davis, D. H. 1961 *Trans. 7th Am. Vacuum Symp.*, p. 372. Oxford: Pergamon Press.
Mullins, J. C., Ziegler, W. T. & Kirk, B. S. 1961 Thermodynamic properties of para-hydrogen from 1 K to 22 K. *Tech. Rep. no. 1.* Engineering Experimental Station, Georgia Institute of Technology.
Pompea, S. M., Bergener, D. W., Shepard, D. F. & Russak, S. 1983 *Proc. Soc. Photo-opt. Instr. Engng* **400**.
Preston-Thomas, H. & Kirby, C. G. M. 1968 *Metrologia* **4**, 30–40.
Psarouthakis, J. 1963 *AIA Aerospace Jl* **1**, 1879–1882.
Quinn, T. J. 1980 *High Temp.–High Pressures* **12**, 359–372.
Quinn, T. J. 1983 In *Temperature*, p. 302. London: Academic Press.
Quinn, T. J., Colclough, A. R. & Chandler, T. R. D. 1976 *Phil. Trans. R. Soc. Lond.* A **283**, 367–420.
Quinn, T. J. & Martin, J. E. 1982 In *Temperature: its measurement and control in science and industry*, vol. 5, pp. 103–107. New York: Am. Inst. Phys.
Quinn, T. J. & Martin, J. E. 1984 In *Proceedings of the 2nd Int. Conf. on Precision measurement and fundamental constants 1981. Natn. Bur. Stand. Spec. Publ.* no. 617.
Radcliffe, W. J., Gallop, J. C. & Dominique, J. 1983 *J. Phys.* E **16**, 1200–1202.
Shitzer, W. G. & Kleinman, D. A. 1961 *Phys. Rev.* **121**, 1324–1335.
Schmidt, C. 1979 *Rev. scient. Instrum.* **50**, 454–457.
Sievers, A. J. 1978 *J. opt. Soc. Am.* **68**, 1505–1516.
Smith, S. M. 1984 *Appl. Opt.* **23**, 2311–2326.
Stierwalt, D. L. 1966 *Appl. Opt.* **5**, 1911–1915.
Stierwalt, D. L. 1979 *Opt. Engng* **18**, 147–151.
Tabor, D. 1979 In *Solids liquids and gases*, 2nd edn. Cambridge University Press.
Taylor, B. N. & Cohen, E. R. 1985 (See note added in proof before reference list.)
Touloukian, Y. S., Powell, R. W., Ho, C. Y. & Klemens, P. G. 1970 In *Thermophysical properties of matter, vol. I. Thermal conductivity of metallic elements and alloys*. New York: Plenum Press.
Trowbridge, T. S. 1978 *J. opt. Soc. Am.* **68**, 1225–1242.
Tsujimoto, S., Kanda, M. & Tsujimoto, T. 1982*a* *Cryogenics* **22**, 591–597.
Tsujimoto, S., Konishi, A. & Kunimoto, T. 1982*b* *Cryogenics* **22**, 603–607.
Westcott, M. 1968 The measurement of solar absorptance and thermal emittance. *ESRO tech. Note* no. 23.
Weyl, H. 1913 In *Gesammette Abhardlungen* (ed. K. Chandrasekharan), vol. 1, paper nos 13, 16–19, 22. Berlin: Springer.

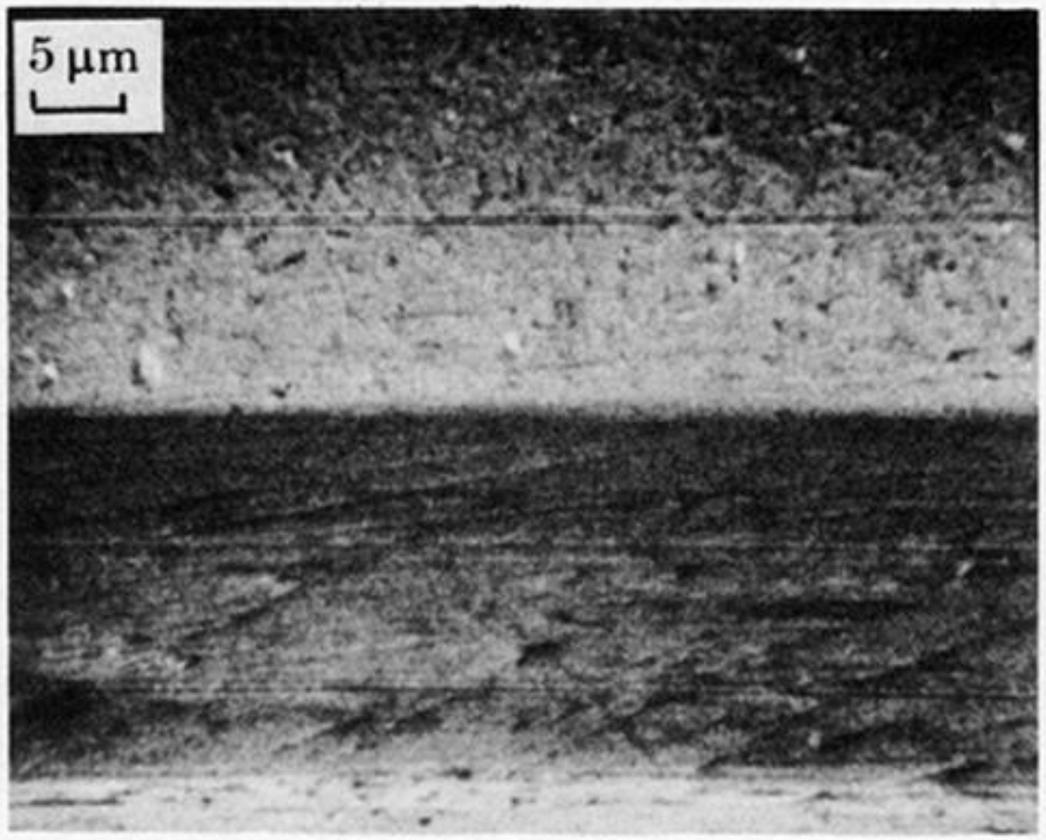

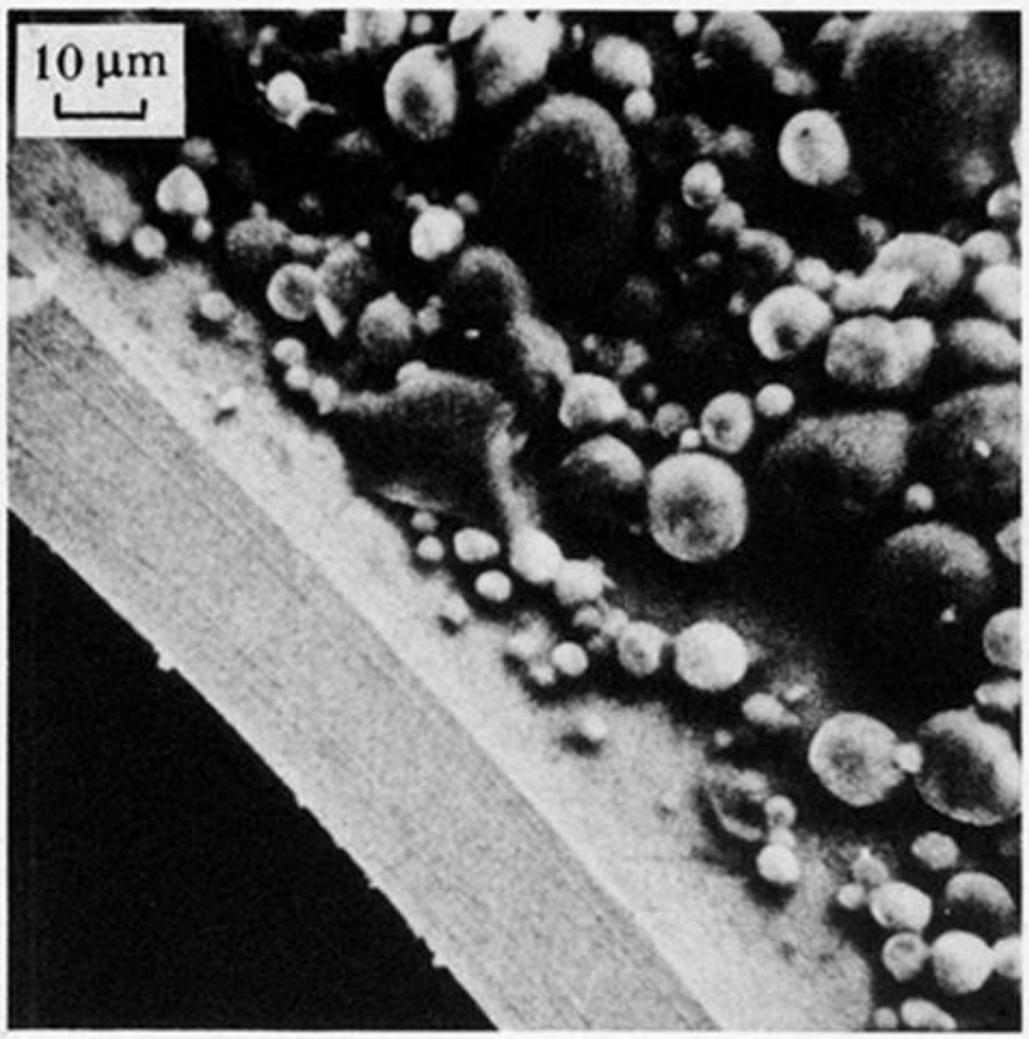

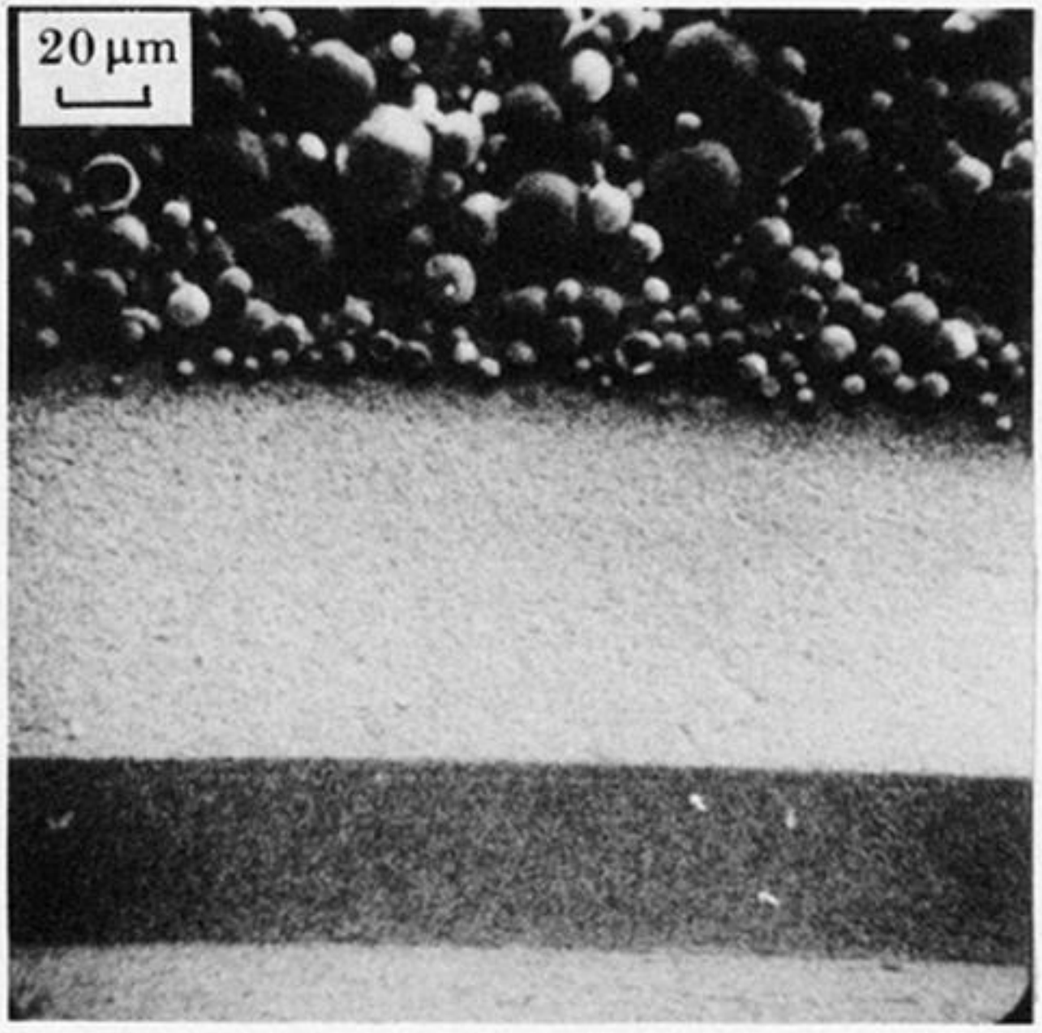

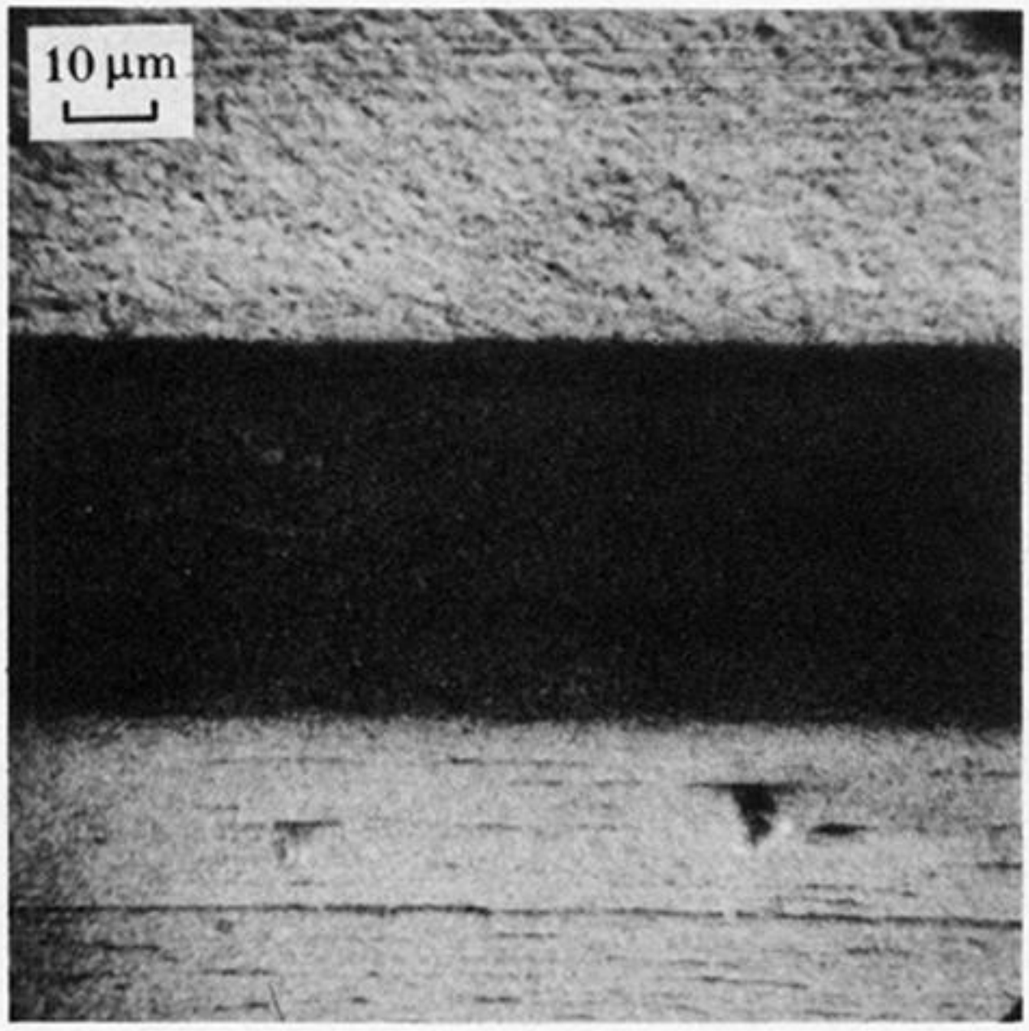

FIGURE 21. Representative views of the edges of the four apertures obtained by a scanning electron microscope. In some views the silica spheres of the 3M black paint are visible.